Elsevier Editorial System(tm) for
Experimental Thermal and Fluid Science
Manuscript Draft

Manuscript Number: ETFS-D-16-00791R1

Title: An experimental investigation and optimization of screen mesh heat pipes for low-mid temperature applications

Article Type: Research paper

Keywords: Heat pipe, experimental analysis, optimization, thermal resistance, maximum heat transport capability

Corresponding Author: Dr. Davoud jafari, Ph.D.

Corresponding Author's Institution: Università di Pisa

First Author: Davoud jafari, Ph.D.

Order of Authors: Davoud jafari, Ph.D.; Hamidereza Shamsi; Sauro Filippeschi; Paolo Di Marco; Alessandro Franco

Abstract: The perspectives of utilization of a screen mesh heat pipe (HP) for low to medium operating temperature applications are studied in this study. A two-dimensional mathematical model for heat and mass transfer of HPs is presented to define its performances under steady state operations. The model couples heat conduction in the wall with both liquid flow in the wick and vapor flow in the core. Experimental analysis is developed to evaluate the influence of operating parameters (the orientation and the cooling temperature) as well as the evaporator section length on the performance of the HP. Furthermore, a modeling approach to optimize the HP performance from a thermal point of view is presented. Using the heat transfer capability and total thermal resistance as the objective function and the structure parameters as the decision variable, the optimization design for the HP is performed using the Non-Dominated Sorting in Genetic Algorithms-II (NSGA-II). The results show that the optimal wick thickness and wick permeability to be a strong function of the heat flux. It is concluded that to have lower thermal resistance at lower heat fluxes for a screen mesh wick HP may have a large effective thermal conductivity, but have a small permeability. While at high heat transfer rate a small effective thermal conductivity, but a large permeability is recommended. The designer must always make trade-offs between these competing factors to obtain an optimal wick design. The investigations are aimed to determine working limits and thermal performance of HPs for low to medium operating temperature applications.

DESTEC
UNIVERSITÀ DI PISA

Dipartimento di Ingegneria dell'Energia, dei Sistemi, del Territorio e delle Costruzioni

Largo Lucio Lazzarino - 56122 Pisa (Italy)
Tel. +39 050 2217300 Fax + 39 050 2217333
Partita IVA 00286820501 VAT No. IT00286820501
Codice fiscale 80003670504

Pisa 18 of November 2016

Object: Submission of revision paper (**ETFS-D-16-00791**)

Dear Professor David Christopher,

Please find enclosed the revised version of our manuscript (ETFS-D-16-00791). We greatly appreciate the opportunity that we have been given to further revise the manuscript. We have deeply revised the original document submitted during the October 2016. After further step of revision, we hope that the scientific content and the clarity of the manuscript are improved.

We have accepted and considered all the comments of reviewers as explained in the "Detail response to reviewers" and we have produced a new version of the manuscript accordingly. For the sake of simplicity we have enclosed a revised version with marked correction in which are reported all the modifications introduced: in blue added or modified phrases and red the deleted phrases including all the minor corrections and other modifications.

We would like to express our gratitude to you and reviewers for the extremely helpful comments and guidance in the revision. We hope that our efforts have succeeded in addressing yours and reviewers concerns. We look forward to your decision.

Sincerely yours,

Davoud Jafari

Davoud Jafari
Department of Energy, Systems, Territory and Construction Engineering (DESTEC),
University of Pisa,
Largo Lucio Lazzarino, 56126 PISA, ITALY
Phone: +39 3472817717
e-mail: d.jafari@studenti.unipi.it, j.davoud@yahoo.com

Highlights for:

An experimental investigation and optimization of screen mesh heat pipes for low-mid temperature applications

- Thermal performances of screen mesh heat pipes are analytically and experimentally investigated.
- An optimization approach is presented to maximize the heat flux and minimize the thermal resistance.
- The effect of the cooling temperature, the orientation and the evaporator and condenser lengths is investigated.
- It is found that the optimal wick thickness and wick permeability are a strong function of the heat flux.

Corresponding Author:

Davoud Jafari

Department of Energy, Systems, Territory and Constructions Engineering (DESTEC), University of Pisa, Largo Lucio Lazzarino, 2, 56126 PISA, Italy

Phone: +393472817717

Email: d.jafari@studenti.unipi.it, jafariidavoud@gmail.com

An experimental investigation and optimization of screen mesh heat pipes for low-mid temperature applications

Davoud Jafari[1,*], Hamidereza Shamsi[2], Sauro Filippeschi[1], Paolo Di Marco[1], Alessandro Franco[1]

[1]*Department of Energy, Systems, Territory and Constructions Engineering (DESTEC), University of Pisa, Italy*

[2]*Department of Energy Engineering, Sharif University of Technology, Tehran, Iran*

Abstract

The perspectives of utilization of a screen mesh heat pipe (HP) for low to medium operating temperature applications are studied in this study. A two-dimensional mathematical model for heat and mass transfer of HPs is presented to define its performances under steady state operations. The model couples heat conduction in the wall with both liquid flow in the wick and vapor flow in the core. Experimental analysis is developed to evaluate the influence of operating parameters (the orientation and the cooling temperature) as well as the evaporator section length on the performance of the HP. Furthermore, a modeling approach to optimize the HP performance from a thermal point of view is presented. Using the heat transfer capability and total thermal resistance as the objective function and the structure parameters as the decision variable, the optimization design for the HP is performed using the Non-Dominated Sorting in Genetic Algorithms-II (NSGA-II). The results show that the optimal wick thickness and wick permeability to be a strong function of the heat flux. It is concluded that to have lower thermal resistance at lower heat fluxes for a screen mesh wick HP may have a large effective thermal conductivity, but have a small permeability. While at high heat transfer rate a small effective thermal conductivity, but a large permeability is recommended. The designer must always make trade-offs between these competing factors to obtain an optimal wick design. The investigations are aimed to determine working limits and thermal performance of HPs for low to medium operating temperature applications.

Keywords:

Heat pipe, experimental analysis, optimization, thermal resistance, maximum heat transport capability

Nomenclature

C	Specific heat (J/kg K)	x	axial coordinate (m)
D	Diameter (m)	***Greek symbols***	
d_w	Wire diameter (m)	θ	relative temperature (°C)
F_k	Nonempty front	E	Porosity
hfg	Heat of vaporization (J/kg K)	ν	Kinematic viscosity (m^2/s)
I	Individual	ρ	Density (kg/m^3)
I_e	Current (A)	μ	Dynamic viscosity (Pa s)
K	Permeability	σ	surface tension (N/m)
k	Thermal conductivity (W/mK)	α_c	Crowded comparison operator
L	Length (m)	η	Thermal efficiency
$\dot{m}$	Mass flow rate (kg/s)	***Subscripts***	
N	Mesh number	a	Adiabatic
n_o	Number of objectives	ave	Average
n_p	Size of population	b	Boiling
P	Pressure (Pa)	c	Condenser
P_c	Capillary pressure (Pa)	e	Evaporator
q	Heat flux (W/m^2)	eff	Effective
Q	Heat transfer rate (W)	I	Inner
R_{tot}	Total thermal resistance (K/W)	in	Inlet
R	Radius (m)	l	Liquid
r	radial coordinate (m)	out	Outlet
r_c	Effective capillary radius (m)	s	Solid
r_n	Critical nucleation site radius (m)	tot	Total
S	Crimping factor	v	Vapor
T	Temperature (K)	w	Wick
t	Thickness (m)		
u	Axial velocity (m/s)		
V	Voltage (V)		
v	Radial velocity (m/s)		

1. Introduction

Energy use has become a crucial concern in the last decades and the improvement of energy efficiency is very important in various sustainable renewable energy technologies. The majority of thermal energy in various energy conversion system applications is at low to medium operating temperature (50-120°C) [1]. With regard to heat transfer point of view, the magnitude of the temperature difference between the heat source and heat sink is an important factor on the thermal performance. The problems connected with the limitation on the maximum temperature, the temperature difference and the level of temperature uniformity must be solved for the thermal management of various heat exchanger systems. Heat pipes (HPs) as one of the excellent two-phase passive thermal transfer devices, have effective thermal conductivities orders of magnitude higher than those of similarly-dimensioned solid materials [2]. Thus, their integration into heat exchangers has been shown to have strong potential for energy saving. The field of application of HPs in low to medium operating temperature is wide enough [3,4], including, but not limited, heating, ventilation and air conditioning (HVAC) systems [5], automotive cooling systems [6], photovoltaic/thermal systems [7], power plant cooling tower systems [8], solar water heating [9,10] and thermal energy storage systems [11]. The advantage of using HPs in heat exchanger applications includes multiple redundancies (each HP operates independently so unit is not vulnerable to a single HP failure), low fouling, ease of cleaning and maintenance, isothermal operation (no hot or cold spots), low working pressure drop and highly scalable and configurable [12,13].

The design of HPs for a particular application needs of careful consideration. Several modeling approaches have been reported from a simple lumped model [14] to a transient multi-dimensional simulation [15]. However, a steady state thermal performance prediction is of significant value in the design of HPs [16,17]. Among others, Vafai and Wang [18] developed a modeling approach for the heat and mass transfer analyses in a flat HP. They applied Darcy's law to verify the liquid flow in the wick and assumed a parabolic vapor velocity profile to obtain the axial vapor pressure distribution. With the same approach, Vafai et al. [19] presented a numerical simulation in a disk shaped HPs. Zhu and Vafai [20] extended the work of Vafai et al. [19] considering inertial effects on the liquid flow in the HP wick section. As the most commonly operating limitation to the performance of a HP for low to medium temperature application appears to be capillary limit [2,12,13], researchers

investigated this problem. Among others, Lefevre and Lallemand [21] developed a steady state analytical model considering both liquid flow in the wick and vapor flow to analyze thermal behavior of a flat miniature HP as well as prediction of the maximum heat transfer capability. Rice and Faghri [22] developed a numerical model considering the liquid flow in the wick to investigate thermal performance of screen mesh HPs. They show that the capillary dryout limitations can be predicted for a given heating load in their simulations. Aghvami and Faghri [23] presented a steady state model including both liquid and vapor flows to investigate thermal and hydraulic behavior of flat HPs. They investigated capillary pressures for given heat inputs to determine the dryout limitations. Shabgard and Faghri [24] extended the above modeling approach to cylindrical HPs. They coupled two-dimensional heat conduction in the HP's wall with the liquid flow in the wick and the vapor hydrodynamics. Among above presented models Vafai and Wang [18], Vafai et al., [19] and Zhu and Vafai [20] did not considered axial heat conduction in the HP's wall while Shabgard and Faghri [24] found that neglecting the axial heat conduction through the wall resulting in overestimated pressure drops up to 10%.

In reviewing the recent experimental investigations on design variables and operating parameters of HPs, it is apparent that the geometric properties of the wick structure, such as the wick thickness and porosity should always be carefully considered [25-33]. Furthermore, operating parameters such as filling ratio, cooling temperature, input heat flux and orientating could be important factors affecting thermal performance of the HP [34-40] as well as its evaporation to condensation length ratio [41-43]. Brautsch and Kew [25] studied heat transfer process of stainless steel mesh HPs using water as working fluid. They showed that maximum heat flux increases with wick thickness but also increases thermal resistance. Li et al. [26] and Li and Peterson [27] investigated the influence of varying wick thicknesses, porosities, and pore sizes on thermal resistance and critical heat flux of a horizontal copper surface sintered with multiple layers of copper mesh. They illustrated that the evaporation/boiling is strongly dependent on the wick thickness, however, it is weakly dependent on porosity. Kempers et al. [28] investigated the effect of the wick thickness on the heat transfer performance of screen mesh wick HPs using water as the working fluid. They observed that there is a small increase in thermal resistance when increasing the wick thickness; however, the maximum heat transfer also increases. Wang and Peterson [29] investigated a sintered copper screen mesh flat HP to examine its maximum heat transport

capacity. They concluded that increasing the structural thickness increased the thermal resistance, but it enhanced heat transfer capacity. Wong and Kao [30] investigated screen mesh HPs using ether as working fluid at different mesh wicks, fluid charges and heat loads. They found a partial dryout at small filling ratio and boiling in the larger water/wick thickness. Weibel et al. [31] analyzed the dependence of thermal resistance on the thickness of sintered powder wicks surfaces. They showed a trade-off between the increased area for heat transfer and increased thermal resistance. Brahim et al. [32] investigated screen mesh HPs and showed that the mesh number is an important factor which affects the overall thermal performance of the system. Tsai and Lee [33] investigated the effects of structural parameters on the evaporation heat transfer in sintered wick HPs. They suggested thinner structural thickness to enhance evaporation heat transfer. Among operating parameters affection on thermal performance of HPs, the tilt angle have a considerable impact by assisting (the condenser section above the evaporator section, e.g. gravity-assisted) or suppressing (the evaporator section above the condenser section, e.g. gravity-opposed) the return of the working fluid. However, the sensitiveness to the orientation is much different for various wick structures [2]. A number of investigations have been shown that the thermal performance of groove type wick HPs significantly depend on the orientation [36] while a much smaller impact has found in sintered wick HPs [37]. Some other researchers [29] indicated that the maximum heat transport capacity of screen mesh wick is reduced by increasing the tilt angle while the performance of the sintered mesh wick is better than the screen mesh one because of the higher effective thermal conductivity. Kumaresan et al. [38] showed that the increasing of angle of inclination of the sintered wick HP improves the HP condensation heat transfer by 30% at 45° orientation in comparison of the horizontal position. However, tilt angles close to vertical position results in deterioration of performance. Sadeghinezhad et al. [39] recently showed the orientation of a sintered wick HP has a major influence on its thermal efficiency, in which gradually increases with the inclination angle up to 60° and then decreases, while Li and Lv [40] have not found a major influence of title angle on the thermal resistance of a flat HP from 45° to vertical position, however it was lower than horizontal position. With regard to impact of the ratio of the evaporator length to the condenser length on the thermal performance of HPs, Wang et al. [41] investigated the effect of evaporation and condensation length on thermal performance of flat HPs. They showed that dryout would occur at a lower heating power for a longer

condensation section length and thermal performance is better at equal lengths of the condensation and evaporation sections. Liang and Hung [42] found that the optimal evaporator length to condenser length ratio of the sintered HP depends on other geometrical parameters such as its diameter. Chen and Chou [43] investigated the effects of length (80 mm-300 mm) on the thermal performance of flat HPs. They showed that an increasing of the length from 80 mm to 300 mm increases the overall thermal resistance of the HP while the maximum heat transport capability decreases.

The above studies indicate that thermal performance and maximum heat transfer capacity of HPs strongly depending on the geometry and the capillary structure. A good HP is characterized by a low thermal resistance and a high dryout tolerance. Thus, optimization approaches help to better understand of optimal structural parameters in the design of HPs. To optimize the heat transfer performance of HPs, Kim et al. [44] proposed a one-dimensional mathematical model in a grooved wick HP to maximum heat transport rate and the overall thermal resistance. Their model included the effects of the liquid–vapor interfacial shear stress, the contact angle, and the amount of initial liquid charge. Sousa et al. [45] proposed generalized extremal optimization (GEO) approach to optimize the thermal performance of a HP for a space engineering application by minimizing its total mass. The method is a global search meta-heuristic, as the Genetic Algorithm (GA), but with a priori advantage of having only one free parameter to adjust. The results showed that the GEO algorithm is a good candidate to be incorporated to the designer's tools. With the same optimization approach (GEO), Vlassov et al. [46] optimized the mass characteristics for a grooved wick HP for space application for different operational modes. They concluded that the proposed optimization approach can be effectively applied to complex optimal design problems. Rao and More [47] presented an optimization algorithm, Teachinge Learning-Based Optimization (TLBO), to optimize Ω-shaped grooved HP. They considered the maximizing of the heat transfer rate and minimizing the resistance of a HP as objective functions. They compared results of application of TLBO algorithm for the design optimization of HPs with other optimization approaches (Niched Pareto Genetic Algorithm (NPGA), Grenade Explosion Method and GEO) and found that proposed algorithm produces better results in improvement of heat transfer rate and total thermal resistances. Zhang et al. [48] utilized the NPGA based approach to optimize an axial Ω-shaped micro grooves HP. They performed the HP optimization design

regarding the heat transfer capability and total thermal resistance as the objective function and the structure parameters as the decision variable. They concluded that the optimal set of solution can be used as an optimal design for a given application. To the best of authors' knowledge, although there are some papers presented on the optimization of grooved wick HPs, there is no study available in the literature on the optimal design of a screen mesh HP considering both the heat transfer capability and the total thermal resistance.

All in all, the paper review with respect to the experimental and analytical studies on screen mesh HPs, as well as relevant optimization methodologies is insufficient. The main concern of the proposed research is to verify the operation of a screen mesh HP under different operating conditions and design variables for a given wick size and to optimize its thermal performance by maximizing the heat transfer capability and minimizing the thermal resistance. In a first step, a steady state model of the HP is presented for a quick check on the estimated performance and to optimize their heat transfer capacity at horizontal position. In this model the two-dimensional variations of the wall temperature and the Darcian effects for the liquid flow through the porous wick are considered. Additionally, as the mathematical modeling could not predict the thermal performance and operating limitation of HPs at all the operating conditions (e.g. the orientation), a specific experimental setup has been designed to not only validate the HP model at medium operating temperature, but also to understand the combined effect of the orientation and the evaporator length. In order to optimize the thermal performance of the HP, a Non-dominated Sorting Genetic Algorithm NSGA-II approach is proposed. The design parameters are selected as the decision variables including the evaporator length, the condenser length, the wick thickness and the porosity. The optimization results are evaluated to verify how the wick thickness and the porosity as well as the evaporation length to the condensation length ratio impact on the thermal performance of screen mesh HPs at a heat input to operate at the lowest thermal resistance.

2. Description of the HP and design variables

As shown in **Fig. 1**, the components of a HP include pipe wall and end caps, a wick structure and a small amount of working fluid. The length of a HP is divided into three parts: the evaporator, the adiabatic and the condenser. A HP operates when heat externally is applied to the evaporator section, conducting through the

wall, which causes vaporization of the working fluid. The vapor pressure drives the vapor through the adiabatic section to the condenser, and then the vapor condenses, releasing its latent heat of vaporization to the heat sink. In a HP, the capillary pressure created in the wick pumps the condensed liquid back to the evaporator section. Therefore, the HP can transfer the latent heat of vaporization from the evaporator to the condenser section as long as there is a sufficient capillary pressure to drive the condensate back to the evaporator [2]. There are several important factors affecting HP performance: the working fluid, the wick structure, the material, the dimension, the orientation, the filling ratio, the operating temperature and the input heat flux. The diameter and the length need to be considered for designing HPs. Larger diameter of the HP allows higher vapor volume to be moved from the evaporator to the condenser which is direct function of the heat pipe limits e.g. sonic and entrainment. The ratio of the evaporation section to the condensation section is one of the geometric characteristics which affects on the thermal performance of HPs with controlling the resistance. The filling ratio, which defines as the ratio of the working fluid volume to the wick portion volume of the HP, also needs to be considered. Usually, the HP filling is over the optimum requirement (wick is completely saturated). A small filling ratio decreases the maximum heat transfer capacity while overfilling leads to a higher thermal resistance [12, 13]. A small filling ratio causes dryout at the evaporator while large filling ratios lead to flooding at the condenser [49]. Generally, it is better to overfill than to under-fill the HP [2].

The performance of a HP under specific orientations is directly related to its wick structure. The wick structure is the function of HPs as it is returned the condensate to the evaporator section. The appropriate selection of a screen mesh structure for a HP is based on material compatibility and performance. The effective capillary radius (r_c), the permeability (K), the effective thermal conductivity (k_{eff}) and the wick thickness are the most important parameters to select the wick structure and to determine the thermal performance of the HP. The relation of the screen mesh HP wick design is described in **Table 1.**

A screen mesh structure with a small effective capillary radius and a large effective thermal conductivity may have a small permeability. Therefore, the selection of these competing factors to obtain an optimal wick design is an important point of view. Another important parameter is the wick thickness. The thickness of the wick determines the cross sectional area for fluid transport from the condenser to the evaporator. A HP containing

thicker wick has a lower pressure drop in the condensate flow, but has a higher thermal resistance for the heat transfer between the wall and the pipe core. Based on above discussion, for applications involving low to medium operating temperature, the investigation of the screen mesh wick structural parameters of HPs is important in its design.

3. Methodology

The methodology applied in this study is based on both mathematical modeling and experimental analysis, as described in following subsections.

3.1. Mathematical model of the HP

The geometry of the cylindrical HP is shown in Fig. 2. The proposed model includes thermal-fluid phenomena occurring within a HP: (1) heat conduction in the wall, (2) liquid flow in the wick, (3) vapor flow in the core region and (4) interaction between the liquid and vapor flows. The wall of the HP has a material with thermal conductivity of k_s and its thickness is equal to t_w (r_o-r_i). The capillary structure is modeled by considering a porous medium of permeability K and heat conductivity k_w. The liquid along the porous medium has a dynamic viscosity μ_l, a heat conductivity k_l and a density ρ_l. The equivalent conductivity of both the liquid and the porous medium is equal to k_{eff}. The vapor space radius is equal to r_v, and kv and μ_v are the vapor heat conductivity and dynamic viscosity, respectively. Two-dimensional heat conduction in the wall is coupled with the one-dimensional heat conduction in the wick (radial) based on approach used in [21, 23, 24]. The assumptions in the analysis are steady state, incompressible and laminar flow, a saturated wick, constant properties and saturation temperature, and linear temperature profile across the thin wick structure [19-21, 23, 24].

Table 2 summarizes the governing equations of different sections of the HP and related boundary conditions. The two-dimensional steady state heat conduction equation considering constant thermal conductivity is applied in the wall (Eq. 5). Linear partial differential equations are solved for boundary condition proposing the separation-of-variable method [50]. To introduce homogeneous wall-wick boundary condition θ is considered as T-T_v. The boundary conditions at the end caps (Eq. 6) and at the outer wall include constant heat fluxes in the

evaporators (Eq. 7), convection in the condenser (Eq. 8) and the heat flux equal to zero in the adiabatic section (Eq. 9). Linear temperature profile across the wick structure and constant saturation temperature at the liquid-vapor interface is considered at wall-wick interface (Eq. 10). Concerning the method of separation of variables, the Eq. 5 is solved to determine the wall temperature (see Appendix A). The continuity equation for the incompressible liquid flow (Eq. 11) and Darcy's law (one-dimensional steady state conservation of momentum, Eq. 12) is used for the liquid flow in the porous wick. Where u_l is the average axial velocity of the liquid phase divided by the overall volume which is obtained by integrating the continuity equation with respect to r. One observation that can be made about this expression is that the pressure drop is inversely proportional to the product of the permeability and the wick thickness. If the permeability of the wick is increased, then the thickness can be reduced, and this in turn will reduce the temperature drop across the wick. The interfacial velocity (v_l) at wall-wick interface equal to zero and v_l at the wick-vapor interface is define by the heat flux at liquid-vapor interface (Eq. 13). The liquid pressure can be obtained by considering the solution obtained from heat conduction in the wall. The average liquid velocity can also be obtained according Darcy's law when the axial gradient of pressure is calculated. The governing equations for the continuity equation (Eq. 15) and the momentum equations (16) are described to determine vapor velocity and pressure in the vapor space of the HP. The boundary conditions include the no-slip condition for velocity at the end caps of the HP, (Eq. 17), and at the vapor-wick interface the no-slip condition is in effect (Eq. 19). At the centerline, the radial gradient of the axial velocity is equal to zero (Eq. 18). Details of using the method of separation of variables to solve the treatment of energy equations (Eq. 5) to verify the axial temperature distribution, the continuity equation (Eq. 11) and Darcy's law (Eq. 12) to obtain the axial gradient of pressure and the average liquid velocity along the wick portion and the conservation equations for mass (Eq. 15) and momentum (Eq. 16) to yield vapor velocity profile and the axial vapor pressure distribution describe in Appendix A.

A MATLAB platform is used to discretize the governing equations, the number of terms to solve the problem is considered as 300 points and independency of the analytical results from the number of terms was tested.

3.2. Experimental setup

A specific experimental setup is developed to analyze the thermal behavior and operating limitation of the HP at horizontal orientation. The tested HP is characterized using the experimental facility shown in **Fig. 3**. The HP has the outer/inner diameter of 35/33 mm and the length of 500 mm (the evaporator lengths of 75 mm, 150 mm, 225 mm and 300 mm and the condenser length of 150 mm). The HP is made by smooth copper pipe where it is closed at the ends with two 3 mm thick copper caps consisting of three layers of stainless steel screen mesh (100 mesh/inch) with a wire diameter of 0.114 mm. Experiments are performed with a fluid charge of 45 ml of degassed, ultra-pure water which this corresponded to a filling ratio of 115%. The amount of charged water is enough in order to ensure that the wick completely saturated. The evaporator section is uniformly heated using silicon type thermofoil heater (model MINCO HK5488R17.2L12A) clamped to the HP and the power input is supplied by a DC Power supply (Agilent DC6575A) which has an accuracy of ±1 percent of reading. In the condenser section, heat is convectively removed by water extracted from a cooling bath (HAKKE F-3C DIN 58966), by means of a 150 mm long copper manifold mounted around the HP. The constant-temperature bath is set to the required temperature and held at a constant-temperature (25 °C, 55 °C and 85 ˚C) through the tests. An electromagnetic flow meter (Siemens SITRANS F M MAGFLO5000) measures the mass flow rate of the cooling water with an accuracy of about 1%. Two thermocouples (K-type stainless steel probe) in the manifold inlet and the outlet and the mass flow measurement allow to calculate the power output from the condenser section, and to compare it to the input electrical power. All the HP wall temperatures are measured using eleven T-type thermocouples, which have been calibrated with an accuracy of ±0.2˚C. All the signals to monitor HP temperatures and cooling mass flow rates are acquired by the Agilent HP32790 data acquisition system, and stored in a computer. During the tests, heaters and blocks as well as adiabatic and condenser sections are covered with several layers of polymer insulation to minimize heat losses. Energy balances between the heat input by the electrical heaters and the heat removed by the sinks is monitored to ensure an energy balance within 90 percent in the worst case. Prior to the recording of any test data, the test facility allows to reach the steady state, defined as the point at which the temperature reading for any thermocouple varied by less than 0.5°C over a period of fifteen minutes.

3.3. Optimization modeling approach

The maximization of heat transfer capability and the minimization of temperature difference between the evaporator and the condenser of the HP are selected as the objective functions in this study. The wick thickness (t_w), porosity (ε), evaporator length (L_e) and condenser length (L_c) are selected as decision variables in the optimization process. **Table 3** and **Table 4** show the variable and fix design parameters chosen to perform the present analysis. Using these criteria, the optimization problem simply formulates as:

$Q=(t_w, \varepsilon, L_e, L_c)$ and $R_{tot}=(t_w, \varepsilon, L_e, L_c)$ (20)

The first real problem for designing a HP is to avoid operating limitation. HPs are very sensitive to their operational limitations such as capillary limit, boiling limit, entrainment limit, viscous limit and sonic limit. The capillary limit consists in the fact that, for a HP to operate properly, the net pressure drop must be greater than the capillary pressure which is derived from the Laplace-Young equation ($\Delta P_c=2\sigma_l/r_c$), where σ_l is liquid surface tension and r_c is effective capillary radius of the evaporator wick. Therefore, the capillary pumping capability of the wick is based on some average effective pore radius for the wick. The boiling limit means the initiation of bubble generation inside the wick structure, and it may result in a locally burn out if the bubbles are trapped inside the wick. At higher applied heat flux, nucleate boiling may appear in the wick structure. At steady state operations, an expression for the heat flux beyond which bubble growth will occur may be developed by [12]:

$$Q_b = \frac{2\pi L_{eff} k_{eff} T_v}{\rho_v h_{fg} \ln(r_i/r_v)}(2\sigma_l/r_n - \Delta P_c) \quad (21)$$

where L_{eff} is the effective length, T_v is the vapor temperature, and r_v and r_i are the vapor core and the inner HP radius, and r_n is the critical nucleation site radius, which according to [13] ranges from 0.1 to 25 μm for conventional metallic case materials. Therefore, to maximize heat transfer capability:

$$\begin{cases} Q < Q_b & (22) \\ \Delta P_{l+v} < \Delta P_c & (23) \end{cases}$$

With regard to the fact that only one objective (maximum heat transfer capacity) is not sufficient to optimize performance of a HP. Therefore, multi-objective evolutionary algorithms (the maximization of the heat flux and the minimization of temperature difference) are performed in order to find the Pareto optimal set of individuals.

In multi-objective optimal methodology, the set of all non-dominated solutions is considered as the Pareto optimal set, and the corresponding objective function values are named as the Pareto frontier. In the present investigation, the Pareto optimal set and the corresponding Pareto frontier are achieved using the evolutionary algorithm based on the NSGA-II proposed by Deb et al. [51]. Thanks to the fast HP mathematical model employed in this study, the large number of function evaluations usually required by the GA is not a limitation. The scheme of a NSGA-II approach is summarized in **Fig. 4**. The elements of the proposed approach includes: non-dominated sorting, crowding distance, selection and recombination and mating.

In this approach [51], solutions of the first non-dominated front in a population size (n_p) are defined by comparison of every other solution in the population to find if it is dominated. This requires ($n_p n_o$) comparisons for each solution, where n_o is the number of objectives. This process is continued to find all members of the first non-dominated level in the population which all individuals in the first non-dominated front are found. Here in n_p and n_o are 160 and 4, respectively (see **Table 5**). The individuals in the next non-dominated front can be found by discounting temporarily of the solutions of the first front and repeating the above procedure. The euclidian distance between each individual in a front based on their n_o objectives in the n_o dimensional space identifies by implementation of the crowing distance calculation. All the individuals in the population are assigned a crowding distance value as the individuals are selected based on rank and crowding distance. Crowding distance is assigned front wise as follow:

For all the individuals initialize the distance to be zero, $F_k(d_j) = 0$, where j corresponds to the j_{th} individual in k_{th} nonempty front (F_k). It should be noticed that for each objective function, sort the individuals in front based on objective and boundary values for each individual are assigned infinite value.

$$I(d_p) = I(d_p) + \frac{I(p+1)m - I(p-1)m}{f_m^{\max} - f_m^{\min}} \tag{24}$$

where $I(p)m$ is the value of the mth objective function of the pth individual in individuals *(I)*.

To do the selection and recombination, the selection is performed using a crowded comparison operator (α_c). The individuals in front F_k are firstly ranked as $p_{rank} = i$; afterward, from the crowding distance $F_k(dj)$, the ranks are compared using the comparison operator. The individuals are identified by using tournament selection with

crowed comparison-operator. In applied method, a combination of an extrapolation method with a crossover method is performed. It begins by randomly selecting a variable in the first pair of parents to be the crossover point.

4. Results and discussion

4.1. Results of analytical study

The experiments are performed with the HP in the horizontal position and the temperature measurements are taken in the axial length of HP at the steady state operation. In order to evaluate the thermal performance of the HP and validate the model at medium cooling temperature (85°C), the experiments are conducted for various heat loads (100 W, 200 W, 300 W, 350 W and 400 W). **Fig. 5** shows experimentally and analytically axial temperature distribution of the HP wall. The results indicate that the evaporator wall temperature rises with the increase of heat flux and the temperature distribution of the HP is uniform in the condenser and the evaporator sections. A comparison between the axial wall temperatures obtained from analytical model with the experimental data are in good agreement. It is evidenced that at an input heat transfer rate of 400 W, the evaporator wall temperatures dramatically increase. This phenomenon can be explained by capillary limit [22]. There is need to know the pressure drop in the wick to calculate the capillary limitations of a HP. For this deal the analytical methods used to determine the pressure drop, as presented in **Fig. 6**. It is evidenced that by increasing input heat transfer rate, the mass flow rate increases at the liquid-vapor interface by the increasing condensation of vapor, resulting the increase of pressure drop. **Fig. 7** shows the pressure drop predicted through HP by analytical model and the material properties of water which is substituted into ($\Delta P_c=2\sigma_l/r_c$) for several vapor temperatures. From the analysis of experimental data, it is observed that the reported maximum heat transfer capacity due to capillary limit (**Fig. 5)**, has good agreement with the analytical calculations (**Fig. 7**) in which the maximum heat transfer rate obtains (350 W). Therefore, it is evidenced that the analytical approach can predict the maximum heat transfer rate of the HP at mid-temperature operation (85°C).

4.2. Results of experimental analysis: effect of design variables

In this section, the effect of the evaporator length as well as operating parameters (the orientation and the cooling temperature) on thermal performance of the screen mesh HP is described. Several evaporation section lengths (75 mm, 150 mm, 225 mm and 300 mm) and orientations (horizontal, 45° orientation and vertical) are tested at the constant condenser length. It would be noted that in the oriented position as well as vertical one the condenser section of the HP places at the top and the evaporator at its lower end (gravity assisted orientation). **Figs. 8(a-c)** provide the axial wall temperature distributions of the HP for different evaporator lengths and orientations. As it is evidenced in all the orientations, the jumps in the maximum wall temperature occur in shorter evaporator length and more effect observed for vertical position. It is concluded that the ratio of the heat source length to the overall HP length is an important parameter controlling the resistance.

The heat transfer behavior of a HP can be described by the overall thermal resistance analysis (R_{tot}) in which lower thermal resistance indicates better overall thermal performance. This is obtained by evaluating the temperature drop along the longitudinal direction of a HP for a heat transfer rate:

$$R_{tot} = \frac{T_{e,ave} - T_{c,ave}}{Q_{ave}} \tag{25}$$

where $T_{,e,ave}$ and $T_{c,ave}$ are average evaporator wall temperature (depending on evaporator length) and average condenser wall temperature (T_{10} and T_{11}), respectively. The heat transport rate (Q_{av}) is calculated based on the principle of average of the heat dissipated from the condenser section (Q_{out}) and the input heat transfer rate by electrical heaters (Q_{in}):

$$Q_{out} = \dot{m} C_P (T_{out} - T_{in}) \tag{26}$$

$$Q_{in} = VI \tag{27}$$

where T_{in}, T_{out} and ṁ denote the inlet and outlet water temperatures and the mass flow rate of the cooling jacket mounted surround the condenser section, respectively, V is the voltage and I is the current. The thermal resistance versus the evaporator length at heat transfer rate of 200 W is shown in **Fig. 9** for different orientations (horizontal, 45° orientation and vertical). It is clear that different orientations show a similar qualitative trend; the thermal resistance decrease as the evaporator length increases. Its major impact observes as the evaporator

length increase from 75 mm to 150 mm at orientations of horizontal, oriented (45°) and vertical by decreasing of 31%, 44% and 48%, respectively. However, further increase of evaporator length has not significant effect on the thermal resistance of the HP at different orientations. Moreover, it is evidenced that effect of orientation is not significant at the same evaporator length. It could be concluded that the smaller heat source has the higher maximum wall temperature (see **Fig. 8**). As the heater size is reduced, the heat flux in the evaporator region increases and causes ~~to~~ a jump in the HP maximum wall temperature. It is because that the evaporation occurs in the evaporator section is more intense. This leads to increase the pressure difference between the evaporation and the condensation which is unbeneficial to assists the condensed liquid to flow back to the evaporation section. Thus, the temperature difference between evaporation and condensation increases and, therefore, the thermal resistance increases.

The thermal efficiency (η) of the HP at different orientations and evaporator lengths is evidenced in **Fig. 10**.

$$\eta = \frac{Q_{out}}{Q_{in}} \times 1000 \tag{28}$$

The lowest thermal efficiency observes for evaporator length of 75 mm (90.4%) and the highest thermal efficiency observes for evaporator length of 150 mm (98%). Based on experimental observations, it could be concluded that at the same operating condition (the cooling temperature, the orientation and the input heat transfer rate) with the increase of evaporation section length, the thermal resistance decreases while there is an optimal evaporator length in which the device shows a superior thermal efficiency.

In order to investigate the effect of cooling temperature, a horizontal HP with evaporator length of 225 mm and cooling temperature of 25 °C, 55 °C and 85 °C is tested. **Fig. 11** shows the total thermal resistances under changes of the cooling temperatures in the range of heat loads from 60 W to 350 W. According to the presented results, the thermal resistance decreases with an increase in the condenser cooling temperature. However, no significant difference is observed in the thermal resistance at higher heat transfer rate of cooling temperature of 55 °C and 85 °C. Such behavior could be explained by the fact that for a give heat flux, the vapor and liquid friction factor and simultaneously the vapor pressure drop and the liquid pressure drop along the wick portion decreases as the cooling temperature increases because of viscosity changes [~~32~~52].

Fig. 12 also shows the related heat transfer rate dependences of the temperature of the evaporator wall. It is observed that a change in the condenser cooling temperature of a certain magnitude (30°C) does not always load to equivalent changes in the operating temperature of the HP. It means that temperature deference of evaporator walls are lower than temperature differences of cooling temperatures from 25 °C to 55 °C and to 85 °C. With an increase in the cooling temperature from 25°C to 55°C and from 55 °C to 85 °C the average HP wall temperature increases by 26.8 °C and 24.7 °C. Therefore, decreasing of the thermal resistance with an increase in the condenser cooling temperature (see **Fig. 11**) could be also explained by the fact that an increase in cooling temperature leads to a decrease in the temperature drop between the evaporator and the condenser, according to the presented results in **Fig. 12**. This shows the advantage of the use of hotter medium (water, air, etc.) for cooling the HP condenser when lower values of its thermal resistance are required in a practical application.

Based on above experimental results, it is evidenced that the orientation has less effect on the thermal performance of the screen mesh HPs while the ratio of evaporator length and condenser length shows significant impact. Therefore, in this study the effect of the evaporator length to condenser length ratio at cooling temperature of 85 °C is considered for optimization.

4.3. Results of optimization approach

To find the best solution (the maximum heat transfer capability and the minimum temperature difference) for mid-operating temperature applications (85˚C), A NSGA-II approach performs to solve the optimization problem of a screen mesh HP with the conditions shown in **Tables 4** and **5**. Based on the optimization method, the initial and final population distributions are illustrated in **Fig. 13**. The Pareto-optimal solution sets are given in **Table 6**. As shown in **Fig. 13**, the random initial population is distributed throughout the search space, and the NSGA-II finds an apparent front after 120 generations. It is promising to see that in the final population there is a definite improvement. According to the different applications at mid-operating temperature, the designer must make a choice from the Pareto-optimal solution set as determined by the NSGA-II utilizing the requirements of the specific application. For example, as evidenced in **Table 6** for solution no. 12, there is no individual in the final population for which both Q>259.3W and R_{tot}<0.033 °K/W. It means that at selected heat

flux, solution no. 12 represents the optimized design which it could be practical to design a HP heat exchanger for mid-operating temperature.

Herein, a parametric study is presented based on obtained optimal set of solutions. **Fig. 14** shows the optimal wire diameter and porosity of wick structure at different heating power. As it is evidenced, the optimization results indicated that with increasing heat transfer rate the wire diameter decreases to have lower thermal resistance. In contrast, the porosity should be decreases with increasing heat transfer rate to have an optimal case depending heat transfer rate. These two parameters simultaneously change the conductive and permeability characteristics of the wick structure. For example, with increasing of the wick porosity, the effective thermal conductivity decreases while permeability increases. Moreover, increasing wire diameter leads to increase of permeability. Thus, the effective thermal conductivity and permeability of wick structure need to be analyzed in optimal cases. **Fig. 15** indicates the optimal permeability and effective thermal conductivity of the HP at various heating power. As it is observed, the optimal permeability increase with increasing of heat transfer rate to have a small liquid pressure drop, and thus, avoiding capillary limit (see Table 6) while the optimal effective thermal conductivity decreases as heat transfer rate increases. Therefore, it is concluded that to have optimal case at lower heat fluxes for a screen mesh wick HP may have a large effective thermal conductivity, but have a small permeability. While at high heat transfer rate a small effective thermal conductivity, but a large permeability is recommended. The designer must always make trade-offs between these competing factors to obtain an optimal wick design.

The wick thickness is also a parameter impact on the determination of the thermal resistance of the HP, thus an optimal thickness is important to reach maximum performance. **Fig. 16** shows optimum wick thickness for an applied heat flux and related liquid pressure drop along the wick. It is indicated that the wick thickness values increase with increasing of heat transfer rate. An increase of the layer of the mesh wick can reduce the liquid frictional pressure drop proportionally by increasing the liquid flow area, resulting in improved heat transfer capacity. However, the increase in the layer of the screen mesh results in significant increases in superheat through the wick layer, and therefore, in premature boiling limitations [29]. On the other hand, decreasing the

wick thickness decreases the radial thermal resistance of the wick while the working fluid cannot be supplied efficiently to the evaporator, which causes dryout.

Finally, the thermal resistance of a HP as well as maximum heat transfer capacity depends on the evaporator length to the condenser length, L_e/L_c ratio. The optimal L_e/L_c ratio and a function of wick permeability and wick thickness of the HP at various heating power are shown in **Fig. 17**. The motivation of presenting a function consisting both optimal wick permeability and wick thickness is that, as the wick thickness (See **Fig. 16**) and/or wick permeability (see **Fig. 15**) increase, the pressure drop decreases. Thus, an optimal relation of these two important parameters at a given heat flux could be useful to design a screen mesh wick structure for a particular application. It is evidenced that the optimal L_e/L_c ratio for HPs is constant as about 1 while the function of wick permeability and wick thickness increase with increasing heat flux. It could be concluded that the optimal wick thickness and wick permeability are a strong function of the heat flux. The obtained optimal cases at equal lengths of the condensation and evaporation sections also affirms by experimental results in which highest thermal efficiency is obtained (see **Fig. 10**).

5. Conclusions

For particular applications involving low to medium operating temperature, this study investigates the screen mesh wick HPs structural parameters as well as its operating parameters both analytically and experimentally. For this aim, a mathematical simulation, an experimental facility and optimization approach develop to measure and predict the maximum heat flux and thermal performance of HPs. A mathematical model is presented to study the steady state performance of the horizontal HP and also to predict its operating limitation and to optimize its thermal performance. The model involves coupling two-dimensional heat conduction in the HP's wall with the liquid flow in the wick and the vapor hydrodynamics. A series of experiments performs to evaluate the heat transfer performance of the HP at different heat transfer rates, orientations, cooling temperatures and evaporator lengths as well as validation of analytical model in horizontal position at medium operating temperature. A NSGA-II optimization approach is introduced to maximize the heat transfer capability and to minimize the overall thermal resistance of screen mesh HPs. A modeling approach is conducted to optimize the

structural parameters of screen mesh wick including wick thickness and porosity as well as evaporator length and condenser length of horizontally position HPs. The experimental investigations and the optimization results are analyzed and discussed and obtained results summarize as follow.

The HP is tested in horizontal, 45˚ orientation and vertical position and at different evaporator length (75 mm-300 mm). From the experimental analysis of the HP, it is found the orientation does not show a very significant effect on the thermal performance of screen mesh HPs while the evaporator length shows a significant influence. It is found that at the same operating conditions, as the evaporator length increases the thermal resistance decreases while there is an optimal evaporator length in which the device shows a highest thermal efficiency. Investigation of the effect of cooling temperature also shows the advantage of the use of hotter medium (here in water) for cooling the HP condenser when lower values of its thermal resistance are required.

This study suggests that an improved thermal performance can be attained by having a large effective thermal conductivity, but having a small permeability at lower heat transfer rates while at high heat transfer rate a small effective thermal conductivity, but a large permeability. In conclusion, the optimal wick thickness and wick permeability finds to be a strong function of the heat flux. However, the designer must always make trade-offs between these competing factors to obtain an optimal wick design. The results of the demonstrated optimization analysis in the present study serve as a useful designing tool for optimum thermal performance of screen mesh HPs for the mid-low operating temperature applications.

Appendix A. Mathematical treatment of conservation equations in the HP's wall, wick and vapor

Heat conduction in the wall

The two-dimensional heat conduction obtains by assuming linear temperature profile across the wick portion and constant saturation temperature at the liquid-vapor interface (Eq. 10) by employing the separation-of-variable method (Rohsenow et al., 1985)

$$\theta(r,x)=\sum_{m=0}^{\infty}\cos(A_m x)\{\omega_m[I_0(A_m r)+\eta_m K_0(A_m r)]\} \tag{A.1}$$

where I_0 and K_0 are modified Bessel functions of the first and second kind of order zero, respectively, ω_m is

unknowns which should be determined for every m and $A_m=m\pi L$ *proposing* the boundary condition (Eq. 7)

$$\omega_m = \frac{1}{-k_s \frac{L}{2}\{A_n[I_1(A_m r_o)-\eta_m K_1(A_m r_o)]\}}\left\{\int q_e \cos(A_m x)dx + h_\infty \sum_{i=0}^{\infty}\omega_i F_i + h_\infty (T_v - T_\infty)\int \cos(A_m x)dx\right\} \quad \text{(A. 2)}$$

where constants can be calculated for every given m. The system of m equations expressed in above equation is solved by use of the direct methods. When a sufficient number of ω_m are calculated, the temperature can be determined from Eq. A.1.

The liquid flow in the wick section

The axial liquid velocity is calculated by integrating Eq. 11 with respect to x and substituting v_l (Eq. 13) as

$$\frac{\partial u_l}{\partial x} = \frac{2q_e r_i}{\rho_l h_{fg}(r_i^2 - r_v^2)} \quad \text{(A.3)}$$

By Combining Darcy's law (Eq. 14) and Eq. A.3, the average velocity profile along the wick is calculated by obtaining the axial gradient of pressure

$$\frac{d^2 P_l}{dx^2} = -\frac{2r_i \mu q_e}{\rho_l h_{fg} K(r_i^2 - r_v^2)} \quad \text{(A.4)}$$

The liquid pressure can be obtained by considering $q=-k_{wall}\partial\theta/\partial r$ and Eq. 5 as

$$\begin{cases} \frac{dP_l}{dx} = -\frac{2r_i \mu k_s}{\rho_l h_{fg} K(r_i^2 - r_v^2)}\sum_{m=0}^{\infty}\sin(A_m x)\{\omega_m[I_1(A_m r_i)-\eta_m K_1(A_m r_i)]\} & \text{(A.5)} \\ P_l = -\frac{2r_i \mu k_s}{\rho_l h_{fg} K(r_i^2 - r_v^2)}\sum_{m=0}^{\infty}\frac{\cos(A_m x)}{A_m}\{\omega_m[I_1(A_m r_i)-\eta_m K_1(A_m r_i)]\} & \text{(A.6)} \end{cases}$$

The average liquid velocity can be obtained according Darcy's law when the axial gradient of pressure is calculated.

Vapor flow in the core

A parabolic velocity profile is considered for the vapor flow [18, 20, 21].

$$u_v(r,x) = U_v(x)(\xi_1 + \xi_2 r + \xi_3 r^2) \quad \text{(A.7)}$$

where U_v is the local average velocity of the vapor and the constants (ξ_1, ξ_2 and ξ_3) are verified by applying the

boundary conditions in Eq. 17 and Eq. 18 and the definition given in

$$U_v(x) = \frac{2}{r_v^2}\int_0^{r_v} r u_v dr \tag{A.8}$$

Thus, the vapor velocity profile define as

$$u_v(r,x) = 2U_v(x) - \frac{2U_v(x)r^2}{r_v^2} \tag{A.9}$$

By substituting Eq. A.9 in the continuity equation (Eq. 15) and integrating with respect to r, yields

$$r_v U_v'(x) + 2v_v = 0 \tag{A.10}$$

By considering this fact that at the interface, the vapor interfacial velocity is related to the liquid interfacial velocity by a mass balance ($\rho_v v_v = \rho_l v_l$) and using Eq. 13, the vapor interfacial velocity is verified as

$$v_v = \frac{q_e\big|_{r=r_i} r_i}{\rho_v h_{fg} r_v} \tag{A.11}$$

Considering $v_l = (q_e/\rho_l h_{fg})(r_i/r_v)$ *and* $v_v = (q_e/\rho_v h_{fg})(r_i/r_v)$ and integrating Eq. A.10 with respect to x the mean vapor velocity is calculated as follow

$$U_v(x) = -\frac{2r_i k_s}{\rho_v h_{fg} r_v^2}\sum_{m=1}^{\infty}\sin(A_m x)\left\{\omega_m\left[I_1(A_m r_i) - \eta_m K_1(A_m r_i)\right]\right\} \tag{A.12}$$

Finally, concerning boundary layer momentum equation along the vapor velocity profile, the axial distribution of the vapor pressure is obtained by neglecting the radial variation of the vapor pressure by

$$\nabla P = -\frac{16 r_i \mu k_s}{\rho_v h_{fg} r_v^4}\sum_{m=1}^{\infty}\left[1-\cos(A_m x)\right]\left\{\frac{\omega_m\left[I_1(A_m r_i) - \eta_m K_1(A_m r_i)\right]}{A_m}\right\} - \frac{8}{3\rho_v}\left\langle \frac{r_i k_s}{h_{fg} r_v^2}\sum_{m=1}^{\infty}\sin(A_m x)\left\{\omega_m\left[I_1(A_m r_i) - \eta_m K_1(A_m r_i)\right]\right\}\right\rangle^2 \tag{A.13}$$

References

[1] Incorparated BCS. Waste heat recovery: technology and opportunities in US industry. Department of Energy (US); 2008. [March].

[2] Faghri A. Heat Pipe Science and Technology. Philadelphia, PA: Taylor & Francis (1995).[3] Jafari D, Franco A, Filippeschi S, Di Marco P, Two-phase closed thermosyphons: A review of studies and solar applications, Renewable & Sustainable Energy Reviews 53 (2016) 575–93.

[4] Shabgard H, Allen MJ, Sharifi N, Benn SP, Faghri A, Bergman TL, Heat pipe heat exchangers and heat sinks: Opportunities, challenges, applications, analysis, and state of the art, International Journal of Heat and Mass Transfer 89 (2015) 138–58.

[5] Jadhav TS, Lele MM, Analysis of annual energy savings in air conditioning using different heat pipe heat exchanger configurations integrated with and without evaporative cooling, Energy 109 (2016) 876-85.

[6] Singh R, Mochizuki M, Nguyen T, Akbarzadeh A, Applications of heat pipes in thermal management and energy conservation, Front. Heat Pipes 2 (2011) 1–13.

[7] Gang P, Huide F, Huijuan Z, Jie L, Performance study and parametric analysis of a novel heat pipe PV/T system, Energy 37 (2012) 384-95.

[8] Robertson AS, Cady EC, Development and operational testing of a heat pipe dry cooling tower, American Society of Mechanical Engineers 80 (1980)22.

[9] Ayompe LM, Duffy A, Mc Keever M, Conlon M, McCormack SJ, Comparative field performance study of flat plate and heat pipe evacuated tube collectors (ETCs) for domestic water heating systems in a temperate climate, Energy 36 (2011) 3370-8.

[10] Azad E, Theoretical and experimental investigation of heat pipe solar collector, Experimental Thermal and Fluid Science 32 (2008) 1666–72.

[11] Amini A, Miller J, Jouhara H, An investigation into the use of the heat pipe technology in thermal energy storage heat exchangers, Energy (2016) 1-10.[12] Peterson GP, Heat Pipes, Modeling, Testing, and Applications, John Wiley and Sons (1994).

[13] Reay DA, Kew P, Heat Pipes, 5th ed. Oxford, UK: Butterworth-Heinemann, (2006).

[14] Zuo ZJ, Faghri A, A network thermodynamic analysis of the heat pipe, International Journal of Heat and

Mass Transfer 41 (1998) 1473-84.

[15] Tournier JM, El-Genk M S, A Heat Pipe Transient Analysis Model, International Journal of Heat and Mass Transfer 37(1994) 753-62.

[16] Faghri A, Buchko M, Experimental and numerical analysis of low-temperature heat pipe with multiple heat source, Journal of heat transfer 113 (1991) 728-34.

[17] Huang X Y, Liu CY, The pressure and velocity fields in the wick structure of a localized heated flat plate heat pipe, International Journal of Heat and Mass Transfer 39 (1996) 1325-30.

[18] Vafai K, Wang W, Analysis of flow and heat transfer characteristics of an asymmetrical flat plate heat pipe, International Journal of Heat and Mass Transfer 35 (1992) 2087-99.

[19] Vafai K, Zhu N, Wang W, Analysis of assymetrical disk-shaped and flat plate heat pipes, ASME Journal of Heat Transfer 117 (1995) 209-18.

[20] Zhu N, Vafai K, Analysis of cylindrical heat pipes incorporating the effects of liquid-vapor coupling and non-Darcian transport- a closed form solution, International Journal of Heat and Mass Transfer 42 (1999) 3405-18.

[21] Lefevre F, Lallemand M, Coupled thermal and hydrodynamic models of flat micro heat pipes for the cooling of multiple electronic components, International Journal of Heat and Mass Transfer 49 (2006) 1375–83.

[22] Rice J, Faghri A, Analysis of Screen Wick Heat Pipes, Including Capillary Dry-Out Limitations, Journal of Thermophysics and Heat Transfer 21 (2007) 475-86.

[23] Aghvami M, Faghri A, Analysis of Flat Heat Pipes with various Heating and Cooling Configurations, Applied Thermal Engineering 31(2011) 2645-55.

[24] Shabgard H, Faghri A, Performance characteristics of cylindrical heat pipes with multiple heat sources, Applied Thermal Engineering 31 (2011) 3410-9.

[25] Brautsch A, Kew PA, Examination and visualisation of heat transfer processes during evaporation in capillary porous structures, Applied Thermal Engineering 22 (2002) 815–24.

[26] Li C, Peterson GP, Wang Y, Evaporation/boiling in thin capillary wicks (I) – wick thickness effects, Journal of Heat Transfer 128 (2006) 1312– 9.

[27] Li C, Peterson GP, Evaporation/boiling in thin capillary wicks (II)-Effects of volumetric porosity and mesh size, Journal of Heat Transfer 128 (12) (2006) 1320–8.

[28] Kempers R, Ewing D, Ching CY, Effect of number of mesh layers and fluid loading on the performance of screen mesh wicked heat pipes, Applied Thermal Engineering 26 (2006) 589–95.

[29] Wang Y, Peterson GP, Investigation of a Novel Flat Heat Pipe, Journal of Heat Transfer 127 (2005) 165-70.

[30] Wong SC, Kao YH, Visualization and performance measurement of operating mesh-wicked heat pipes, International Journal of Heat and Mass Transfer 51 (2008) 4249–59.

[31] Weibel JA, Garimella SV, North MT, Characterization of evaporation and boiling from sintered powder wicks fed by capillary action, International Journal of Heat and Mass Transfer 53 (2010) 4204–15.

[32] Brahim T, Dhaou MH, Jemni A, Theoretical and experimental investigation of plate screen mesh heat pipe solar collector, Energy Conversion and Management 87 (2014) 428–38.

[33] Tsai YY, Lee CH, Effects of sintered structural parameters on reducing the superheat level in heat pipe evaporators, International Journal of Thermal Sciences 76 (2014) 225-34

[34] El-Genk MS, Huang L, An experimental investigation of the transient response of a water heat pipe, International Journal of Heat and Mass Transfer 36 (1993) 3823-30.

[35] Kempers R, Robinson AJ, Ewing D, Ching CY, Characterization of evaporator and condenser thermal resistances of a screen mesh wicked heat pipe, International Journal of Heat and Mass Transfer 51 (2008) 6039–46.

[36] Russel MK, Young C, Cotton JS, Ching CY, The effect of orientation on U-shaped grooved and sintered wick heat pipes, Applied Thermal Engineering 31 (2011) 69-76

[37] Loh CK, Harris E, Chou DJ, Comparative study of heat pipes performance in different orientations, 21st IEEE SEMI-THERM Symposium (2005) 191-5.

[38] Kumaresan G, Venkatachalapathy S, Asirvatham LG, Experimental investigation on enhancement in thermal characteristics of sintered wick heat pipe using CuO nanofluids, International Journal of Heat and Mass Transfer 72 (2014) 507–16.

[39] Sadeghinezhada E, Mehrali IM, Rosen MA, Akhiani AR, Latibari ST, Mehrali M, Metsela HSC, Experimental investigation of the effect of graphene nanofluids on heat pipe thermal performance, Applied Thermal Engineering 100 (2016) 775–87.

[40] Li J, Lv L, Experimental studies on a novel thin flat heat pipe heat spreader, Applied Thermal Engineering 93 (2016) 139–46.

[41] Wang SF, Chen JJ, Hu YX, Zhang W, Effect of evaporation section and condensation section length on thermal performance of flat plate heat pipe, Applied Thermal Engineering 31(2011) 2367–73.

[42] Liang TS, Hung YM, Experimental investigation on the thermal performance and optimization of heat sink with U-shape heat pipes, Energy Conversion and Management 51 (2010) 2109–16

[43] Chen JS, Chou JH, The length and bending angle effects on the cooling performance of flat plate heat pipes, International Journal of Heat and Mass Transfer 90 (2015) 848–56.

[44] Kim SJ, Seo JK, Do KH, Analytical and experimental investigation on the operational characteristics and the thermal optimization of a miniature heat pipe with a grooved wick structure, International Journal of Heat and Mass Transfer 46 (2003) 2051–63

[45] Sousa FL, Vlassov V, Ramos FM, Generalized extremal optimization: An application in heat pipe design, Applied Mathematical Modelling 28 (2004) 911–31.[46] Vlassov VV, de Sousa FL, Takahashi WK, Comprehensive optimization of a heat pipe radiator assembly filled with ammonia or acetone, International Journal of Heat and Mass Transfer 49 (2006) 4584–95.

[47] Rao RV, More KC, Optimal design of the heat pipe using TLBO (teachingelearning-based optimization) algorithm, Energy 80 (2015) 535-44.

[48] Zhang C, Chen Y, Shi M, Peterson GP, Optimization of heat pipe with axial ‘‘X”-shaped micro grooves based on a niched Pareto genetic algorithm (NPGA), Applied Thermal Engineering 29 (2009) 3340–5.

[49] Lips S, Lefèvre F, Bonjour J, Combined effects of the filling ratio and the vapour space thickness on the performance of a flat plate heat pipe, International Journal of Heat and Mass Transfer 53 (2010) 694–702.

[50] Rohsenow WM, Harnett JP, Ganic EN, Handbook of Heat Transfer Fundamentals. 2nd ed. New York: McGraw-Hill (1985).

[51] Deb K, Agrawal S, Pratap A, Meyarivan T, A Fast Elitist Non-Dominated Sorting Genetic Algorithm for Multi-Objective Optimization: NSGA-II, IEEE Transactions on Evolutionary Computation 6 (2002) 182-97.

[52] Lips S, Lefevre F, Bonjour J, Physical mechanisms involved in grooved flat heat pipes: experimental and numerical analyses, International Journal of Thermal Science 50 (2011) 1243–52.

Figures

Fig. 1 Schematic view of the HP.

Fig. 2 Schematic view of the proposed HP as well as sequence of modelling procedure.

Fig. 3 Experimental setup scheme and thermocouples locations.

Fig. 4 Flowchart of NSGA-II algorithm.

Fig. 5 Axial distribution of the wall temperatures of the HP: the analytical and the experimental results.

Fig. 6 Axial distribution of the obtained liquid pressure drops of the HP from the analytical results.

Fig. 7 Variation of vapor temperatures versus pressure drops to evaluate capillary limit (pressure drops obtaine from $\Delta P_c=2\sigma_l/r_c$ and analytical model).

Fig. 8 Steady state temperature profiles at the outer wall of the HP (Q=200 W and $T_{cooling}$=25 ˚C): (a) horizontal position, (b) 45° orientation and (c) vertical position.

Fig. 9 Thermal resistances at different evaporation section lengths and orientations (Q=200 W and cooling temperature of 25 °C).

Fig. 10 Thermal performance at different evaporator length sections and orientations.

Fig. 11 The total thermal resistance of the HP ($T_{cooling}$=25 °C, 55 °C and 85 ˚C and L_e=225 mm).

Fig. 12 Evaporator wall temperature dependence on heat transfer rate and cooling temperature of the HP at horizontal position.

Fig. 13 Initial and final population distribution.

Fig. 14 Relation between heat flux, optimal wire diameter and porosity.

Fig. 15 Relations between heat flux, optimal wick permeability and effective thermal conductivity.

Fig. 16 Relations between heat flux, optimal wick thickness and related pressure drop.

Fig. 17 Relation between heat flux, optimal L_e/L_c ration and function of optimal wick permeability (K) and wick thickness (t_{wick}).

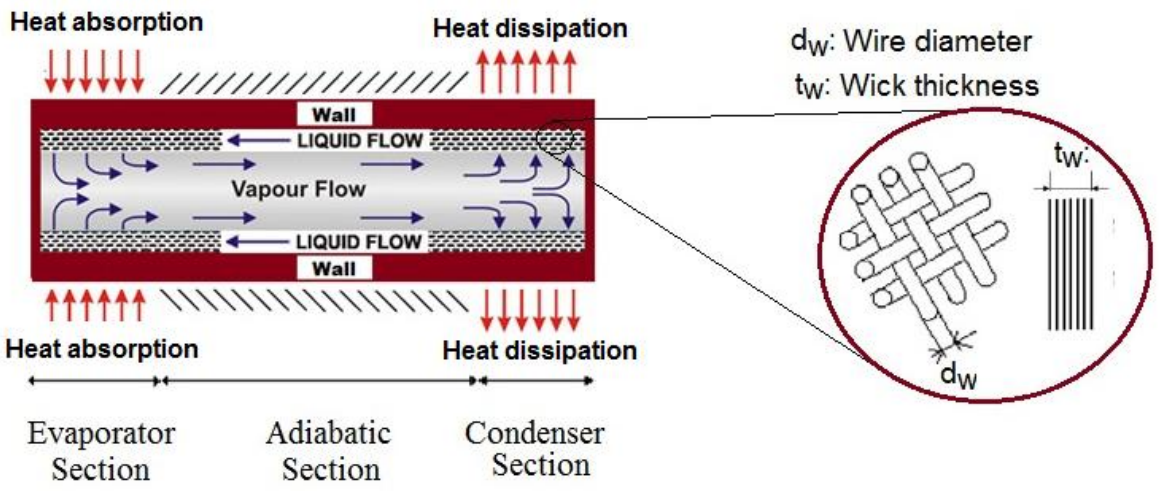

Fig. 1

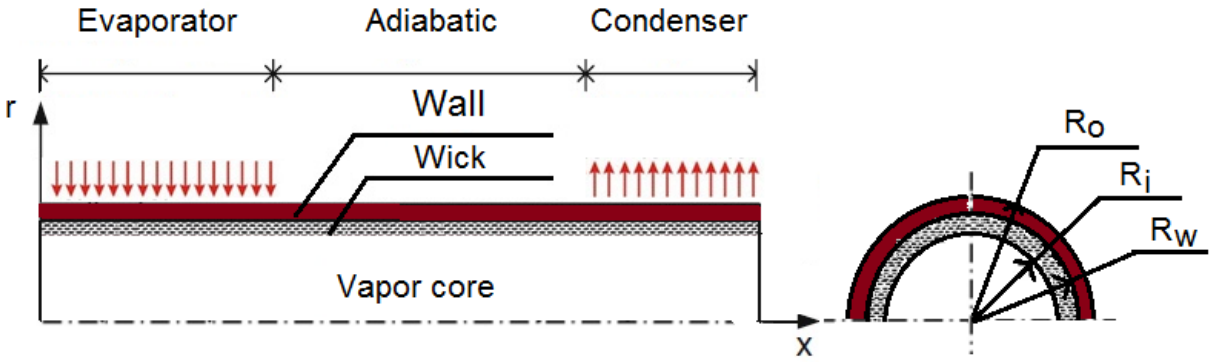

	1. Set the initial conditions (input heat flux, cooling, vapor temperature and etc.)
Heat Conduction	**2.** Obtaining temperature → Eq. A.5
Liquid flow in wick	**3.** Obtaining the axial gradient of liquid pressure along the wick → Eq. A.10 **4.** Obtaining the average liquid velocity along the wick → Eq. A.7
Liquid-vapor interface	**5.** Obtaining interfacial velocity → Eq. 23
Vapor flow in the core	**6.** Obtaining mean vapor velocity → Eq. A.12 **7.** Obtaining the axial vapor pressure →Eq. A.13

Fig.2

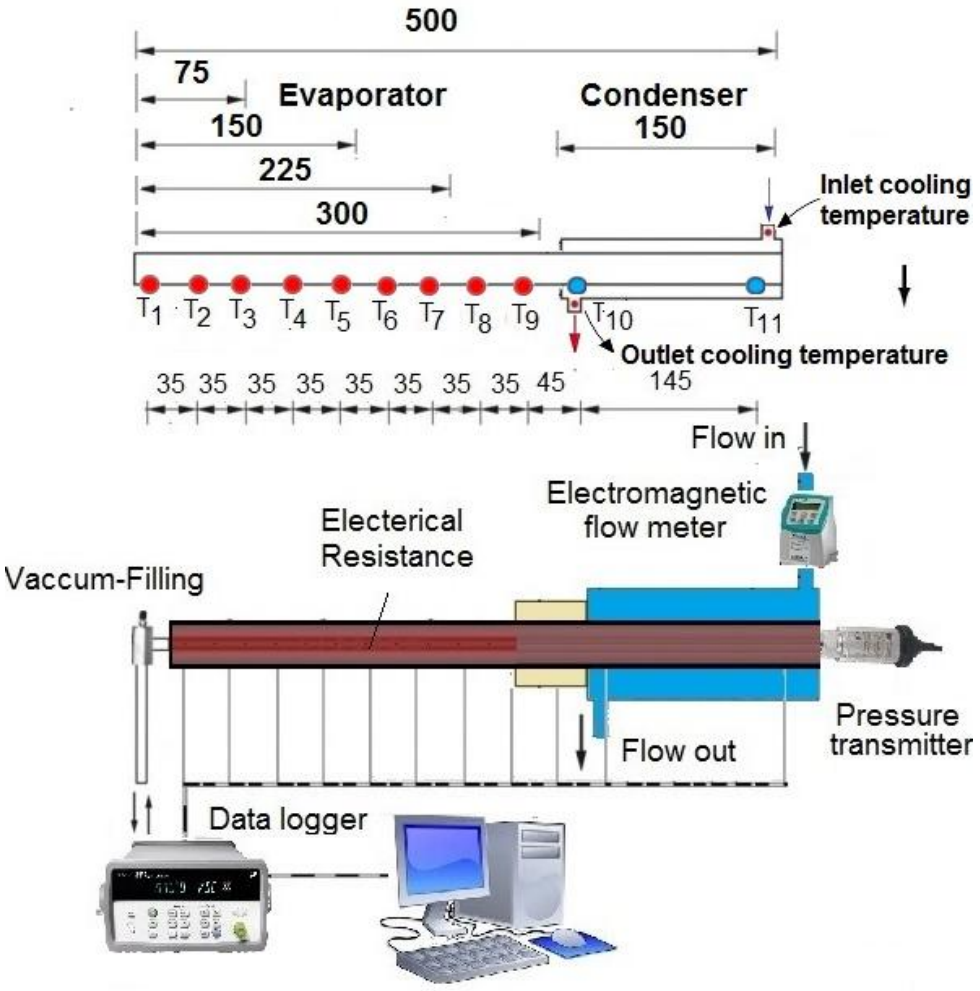
500
75
Evaporator
Condenser
150
150
225
300
Inlet cooling temperature
T1 T2 T3 T4 T5 T6 T7 T8 T9 T10 T11
Outlet cooling temperature
35 35 35 35 35 35 35 35 45 145
Flow in
Electromagnetic flow meter
Electerical Resistance
Vaccum-Filling
Pressure transmitter
Flow out
Data logger

Fig. 3

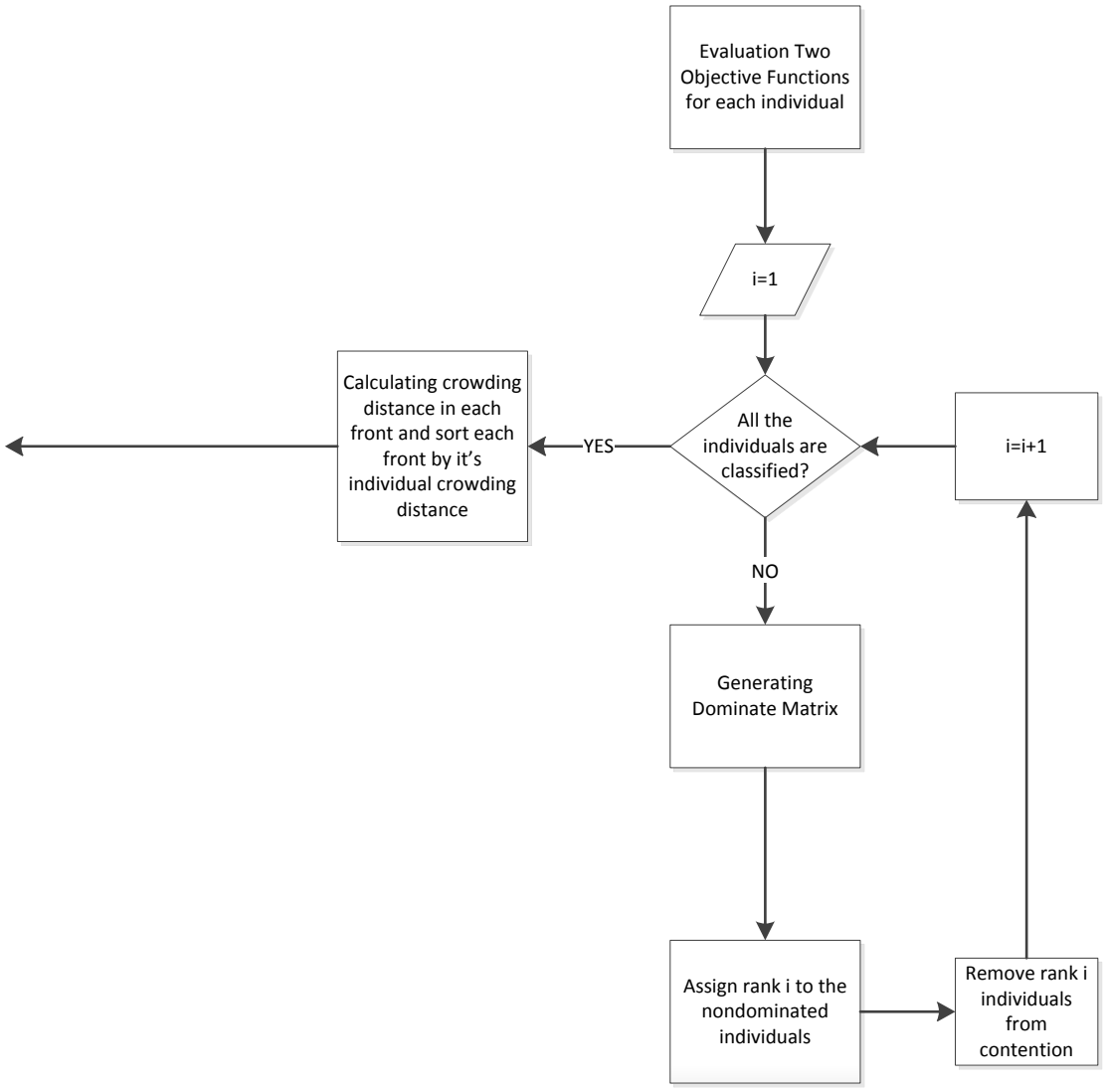
Evaluation Two Objective Functions for each individual
i=1
All the individuals are classified?
YES
Calculating crowding distance in each front and sort each front by it's individual crowding distance
i=i+1
NO
Generating Dominate Matrix
Assign rank i to the nondominated individuals
Remove rank i individuals from contention

Fig. 4

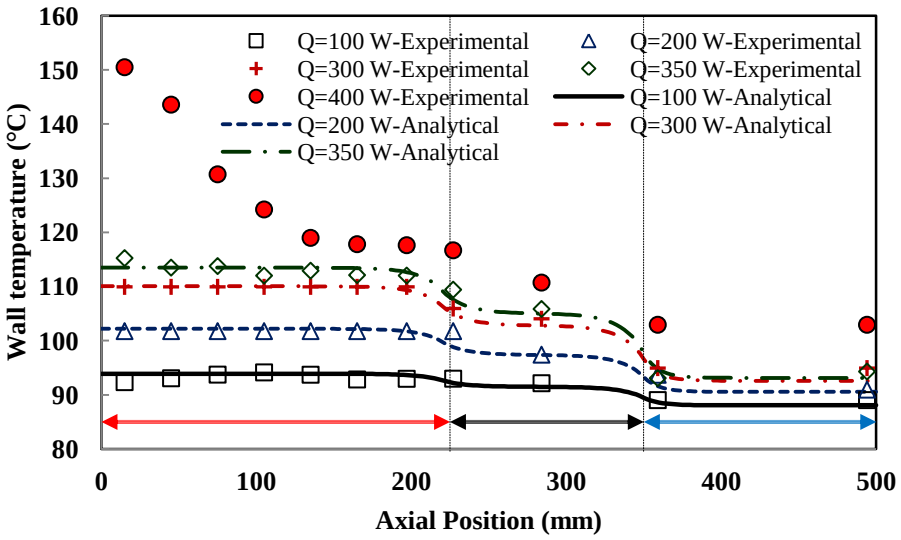

Fig. 5

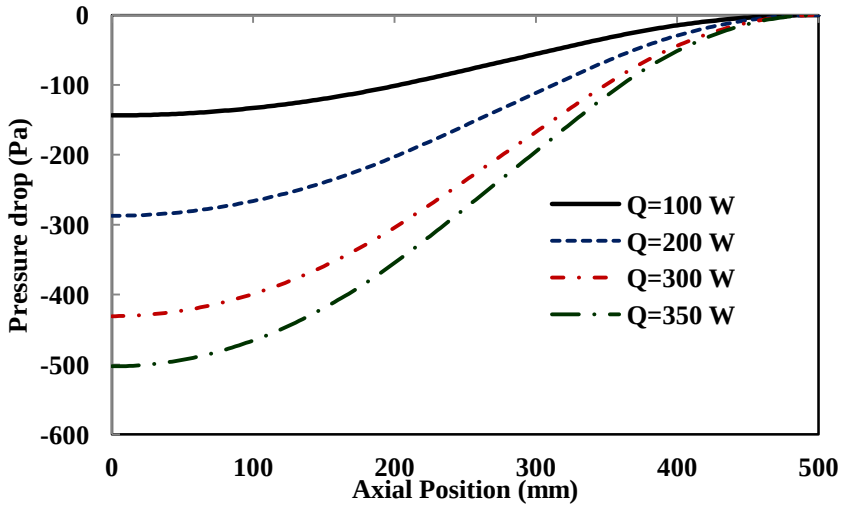

Fig. 6

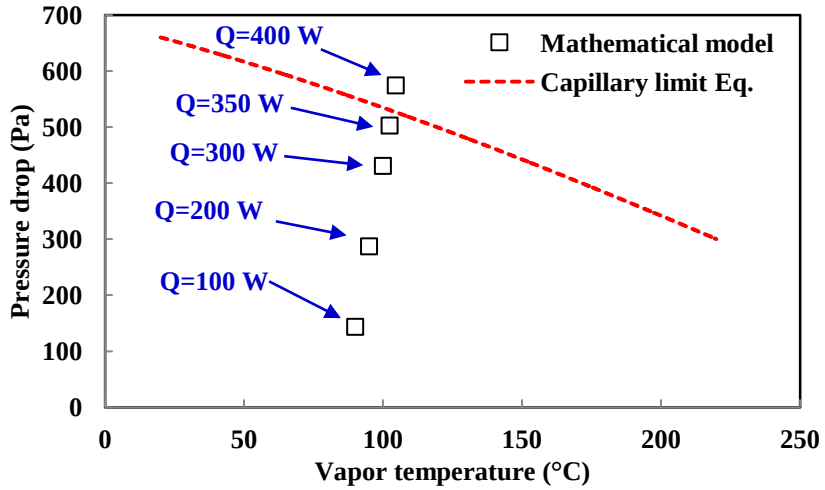

Fig. 7

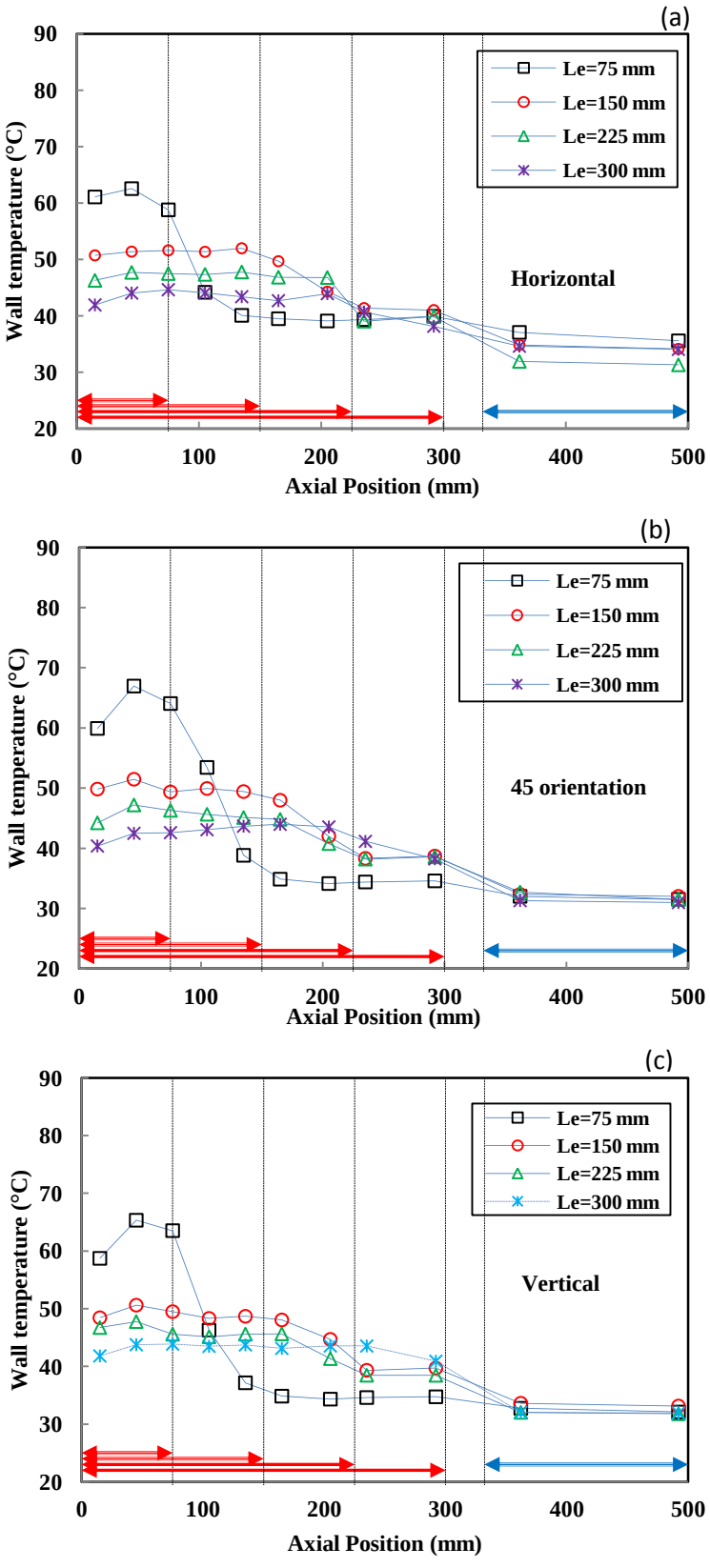
(a)
Le=75 mm
Le=150 mm
Le=225 mm
Le=300 mm
Horizontal
Wall temperature (°C)
Axial Position (mm)
(b)
45 orientation
(c)
Vertical

Fig. 8.

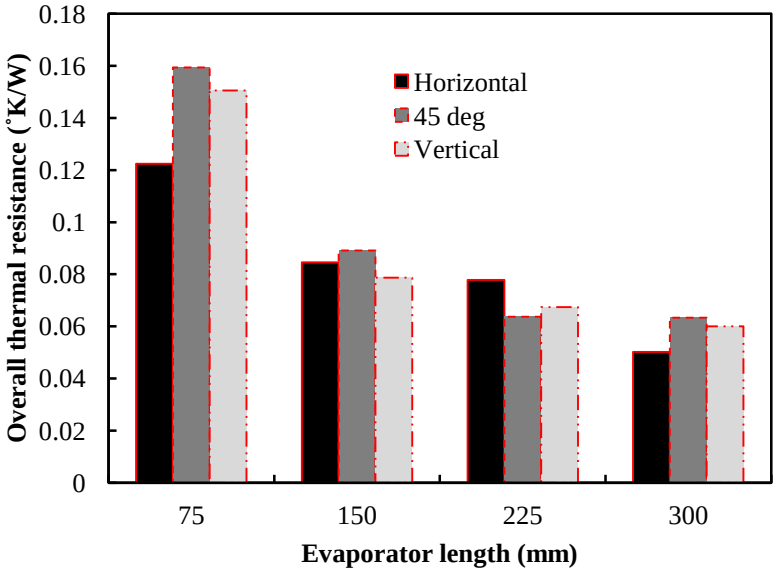
0.18
0.16
0.14
0.12
0.1
0.08
0.06
0.04
0.02
0
Overall thermal resistance (°K/W)
Horizontal
45 deg
Vertical
75
150
225
300
Evaporator length (mm)

Fig. 9

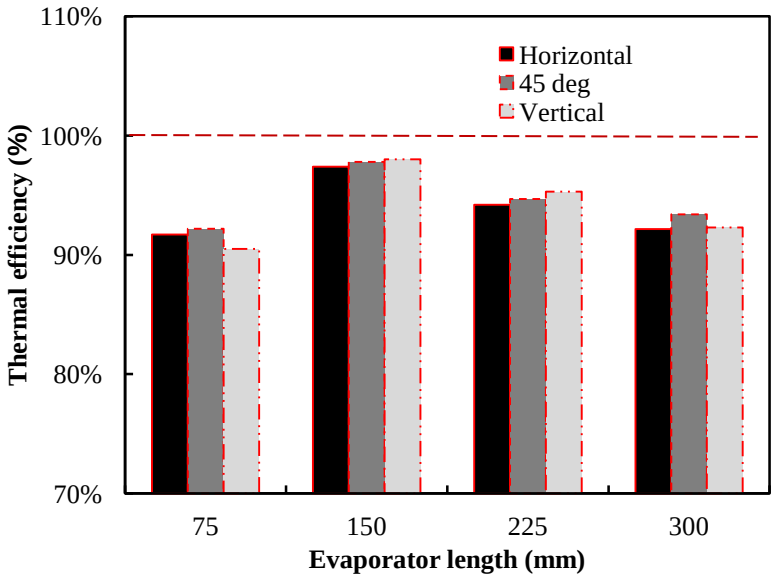
110%
100%
90%
80%
70%
Thermal efficiency (%)
Horizontal
45 deg
Vertical
75
150
225
300
Evaporator length (mm)

Fig. 10

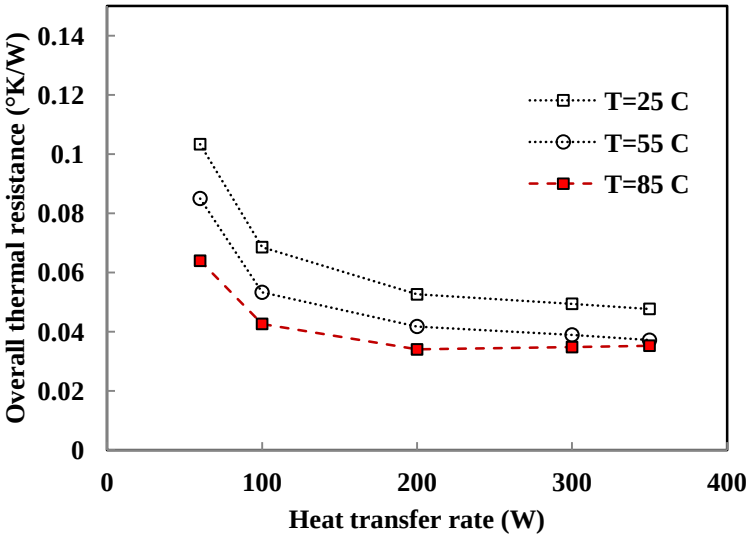
Overall thermal resistance (°K/W)
0.14
0.12
0.1
0.08
0.06
0.04
0.02
0
0
100
200
300
400
Heat transfer rate (W)
T=25 C
T=55 C
T=85 C

Fig. 11

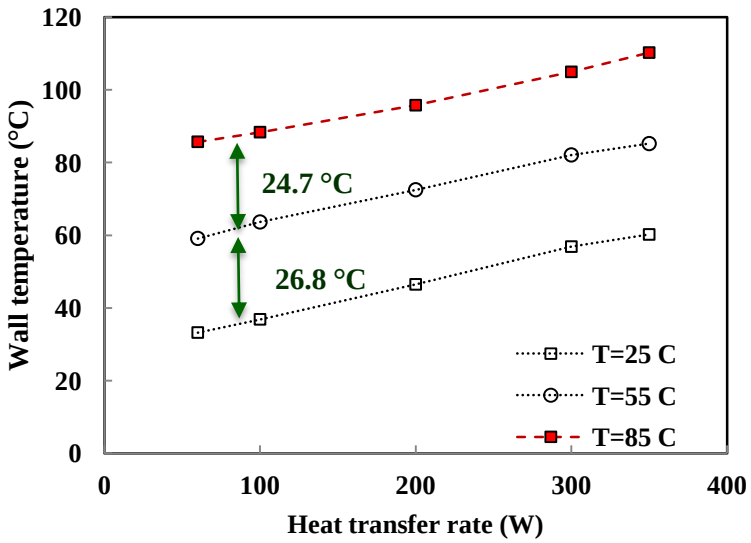
Wall temperature (°C)
120
100
80
60
40
20
0
0
100
200
300
400
Heat transfer rate (W)
24.7 °C
26.8 °C
T=25 C
T=55 C
T=85 C

Fig. 12

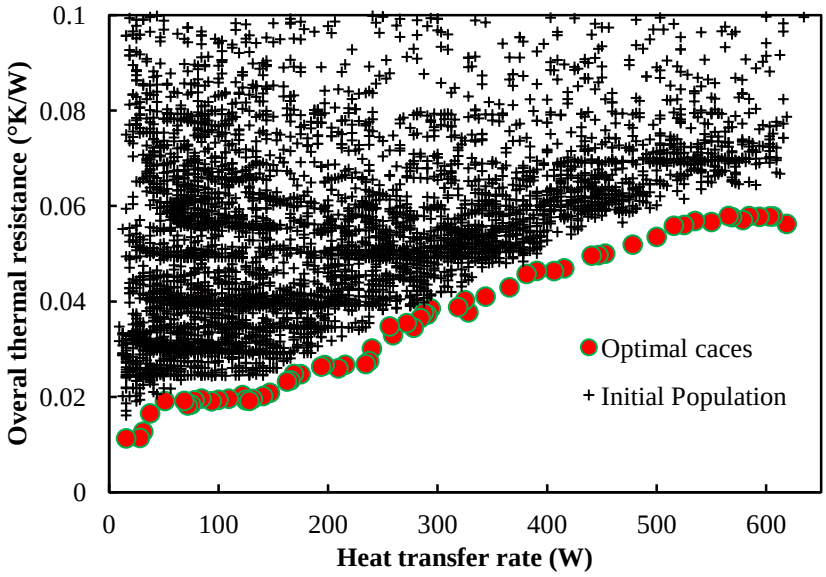
Overal thermal resistance (°K/W)
0.1
0.08
0.06
0.04
0.02
0
0
100
200
300
400
500
600
Heat transfer rate (W)
Optimal caces
Initial Population

Fig. 13

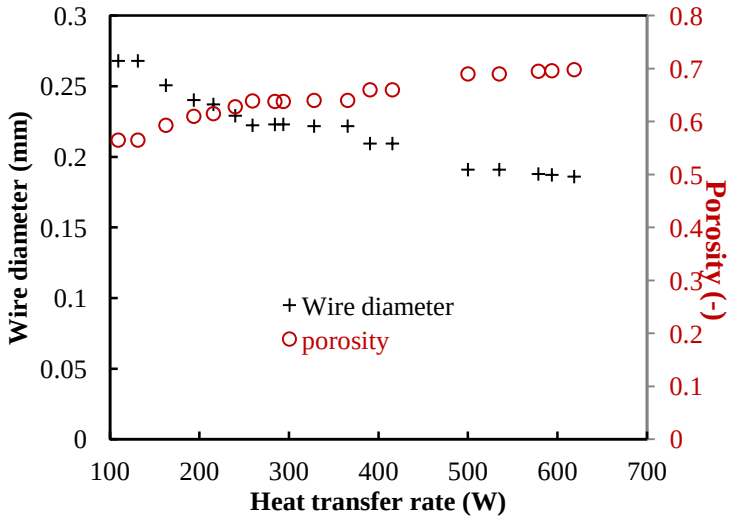
Wire diameter (mm)
0.3
0.25
0.2
0.15
0.1
0.05
0
Porosity (-)
0.8
0.7
0.6
0.5
0.4
0.3
0.2
0.1
0
100
200
300
400
500
600
700
Heat transfer rate (W)
Wire diameter
porosity

Fig. 14

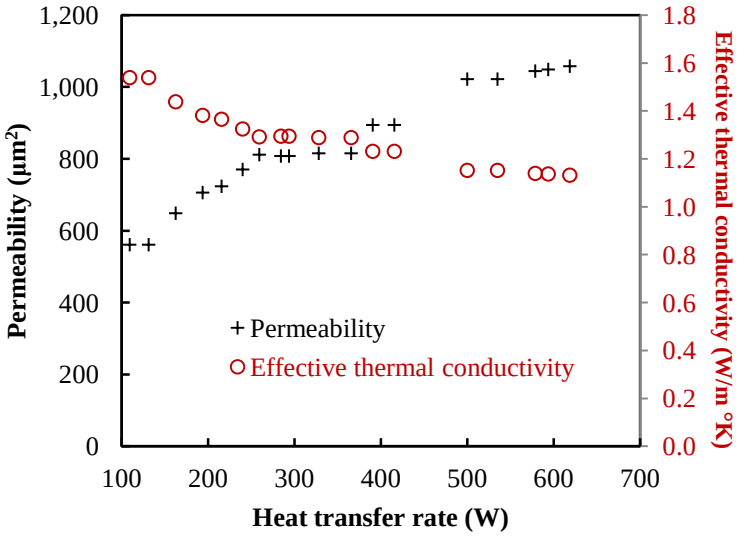
1,200
1,000
800
600
400
200
0
100
200
300
400
500
600
700
1.8
1.6
1.4
1.2
1.0
0.8
0.6
0.4
0.2
0.0
Permeability (μm²)
Effective thermal conductivity (W/m °K)
Heat transfer rate (W)
Permeability
Effective thermal conductivity

Fig. 15

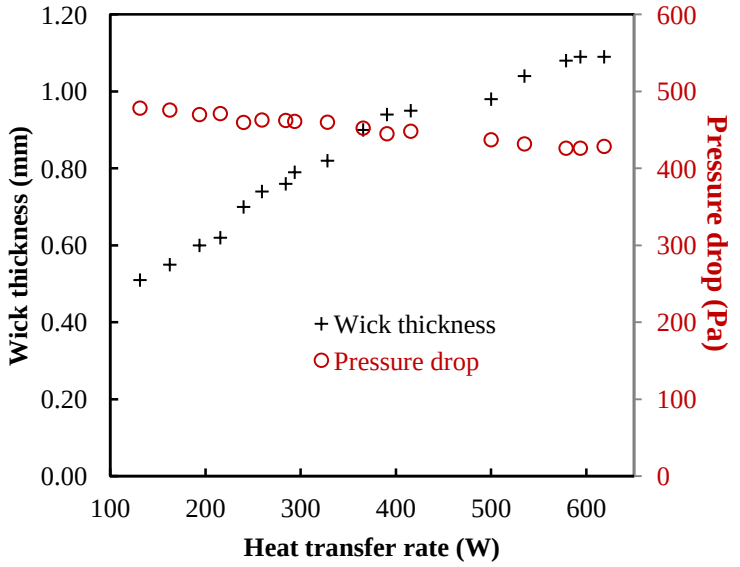
1.20
1.00
0.80
0.60
0.40
0.20
0.00
100
200
300
400
500
600
600
500
400
300
200
100
0
Wick thickness (mm)
Pressure drop (Pa)
Heat transfer rate (W)
Wick thickness
Pressure drop

Fig. 16

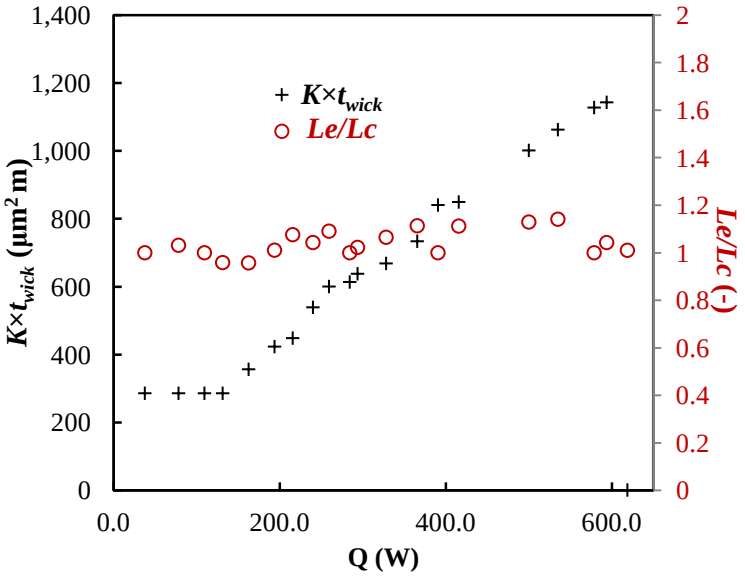
1,400
1,200
1,000
800
600
400
200
0
0.0
200.0
400.0
600.0
Q (W)
K×t_wick (µm² m)
Le/Lc (-)
2
1.8
1.6
1.4
1.2
1
0.8
0.6
0.4
0.2
0
K×t_wick
Le/Lc

Fig. 17

Tables

Table 1 Expressions for screen mesh HP wick design

Table 2 Governing equations and related boundary conditions.

Table 3 Fix parameters.

Table 4 Levels of the variable parameters.

Table 5 Parameters used for optimization calculation.

Table 6 Optimal solution sets to optimize the total thermal resistance depending heat transfer rates.

Table 1

Effective thermal conductivity	Effective capillary radius	Permeability	Porosity
$k_{eff} = \frac{k_l[(k_l + k_w) - (1-\varepsilon)(k_l - k_w)]}{(k_l + k_w) + (1-\varepsilon)(k_l - k_w)}$	$r_c = 1/2N$ $1968 < N < 13800$	$K = \frac{d_w^2 \varepsilon^3}{122(1-\varepsilon)^2}$	$\varepsilon = 1 - \frac{S\pi N d_w}{4}$
(Eq. 1)	(Eq. 2)	(Eq. 3)	(Eq. 4)

Table 2

Correlations		Boundary conditions	
Heat conduction in the wall		**End caps:**	
$\frac{\partial^2\theta}{\partial r^2}+\frac{1}{r}\frac{\partial\theta}{\partial r}+\frac{\partial^2\theta}{\partial x^2}=0$	(5)	$\frac{\partial\theta}{\partial x}=0, \quad (\mathrm{x}=0, \mathrm{L})$	(6)
		Outer wall:	
		$k_s\frac{\partial\theta}{\partial r}\Big\vert_{r=r_o}=q_e, \quad (\text{Evap.})$	(7)
		$\frac{\partial\theta}{\partial r}\Big\vert_{r=r_o}=0, \quad (\text{Adiabatic})$	(8)
		$-k_s\frac{\partial\theta}{\partial r}\Big\vert_{r=r_o}=h_\infty\theta(r_o,x), \quad (\text{Cond.})$	(9)
		Wall-wick interface:	
		$\frac{\partial\theta}{\partial r}=\frac{k_{eff}}{r_i k_s\ln(r_i/r_v)}\theta, \quad (r=r_i)$	(10)
Liquid flow in the wick		**Wick-vapor interface:**	
$r\frac{\partial u_l}{\partial x}+\frac{\partial}{\partial r}(rv_l)=0$	(11)	$v_l=\frac{q_e\vert_{r=r_i}r_i}{\rho_l h_{fg} r_v}$	(13)
$\frac{dP_l}{dx}=-\frac{\mu_l u_l}{K}$	(12)	**Wick-wall interface:**	
		$v_l=0$	(14)
Vapor flow in the core		**End caps:**	
$r\frac{\partial u_v}{\partial x}+\frac{\partial}{\partial r}(rv_v)=0$	(15)	$u_v=0, \quad \mathrm{x}=0, \mathrm{L}$	(17)
$\rho_v(u_v\frac{\partial u_v}{\partial x}+v_v\frac{\partial u_v}{\partial r})=-\frac{\partial P_v}{\partial z}+\mu_v(\frac{\partial u_v}{\partial r^2}+\frac{1}{r}\frac{\partial u_r}{\partial r})$	(16)	**Centerline:**	
		$\frac{\partial u_v}{\partial r}=0, \quad \mathrm{r}=0$	(18)
		vapor-wick interface:	
		$u_v=0, \quad \mathrm{r}=\mathrm{r}_v$	(19)

Table 3

Parameters	
Wall material	Copper
Wick material	Stainless steal
Wick type	Screen mesh
Mesh number	50 mesh/inch
Working fluid material	Water
Outer diameter, (mm)	25.4
Wall thickness, (mm)	1
Total length, (mm)	1000
Working temperature, (˚C)	85

Table 4

Parameters	Min	Max
Evaporator length, (mm)	0	1000
Condenser length, (mm)	0	1000
Wick porosity	0.5	0.9
Wick thickness, (mm)	0.2	2

Table 5

Mutation Rate	Population Size	Maximum Generation	Objective number	Variable number
0.05	160	120	2	4

Table 6

No.	Q	R_{tot}	L_e	L_c	t_{wick}	Porosity	T_v	Q_b	ΔP_l	ΔP_c	T_e	T_c
1	618.7	0.056	490	485	1.09	0.698	122.1	618.9	428.6	429.7	139.5	104.7
2	593.8	0.058	485	465	1.09	0.696	122.3	625.6	426.3	429.4	139.2	104.9
3	578.7	0.057	475	475	1.08	0.695	120.4	670.0	426.3	432.4	137.0	104.0
4	535.0	0.057	485	425	1.04	0.69	120.8	724.0	431.8	432.8	135.1	104.6
5	500.0	0.054	480	425	0.98	0.69	117.4	855.4	437.2	439.0	130.0	103.2
6	415.6	0.047	495	445	0.95	0.66	109.8	1150.5	448.3	449.0	119.1	99.6
7	390.6	0.046	440	440	0.94	0.66	108.1	1294.4	445.0	451.6	117.8	98.7
8	365.6	0.043	490	440	0.90	0.64	106.1	1432.5	452.4	454.8	113.5	97.8
9	328.1	0.038	490	460	0.82	0.64	102.4	1760.9	460.0	460.5	108.4	96.0
10	293.7	0.039	450	440	0.79	0.638	101.0	2034.1	461.1	462.6	106.6	95.3
11	284.3	0.037	455	455	0.76	0.638	100.0	2153.8	462.3	464.1	105.2	94.8
12	259.3	0.033	480	440	0.74	0.639	100.8	2074.8	462.9	466.4	105.8	95.3
13	240.0	0.030	485	465	0.70	0.628	96.8	2678.8	459.7	460.9	100.4	93.1
14	215.6	0.027	495	460	0.62	0.615	95.3	3138.5	471.2	475.1	98.1	92.3
15	193.7	0.026	465	460	0.60	0.61	94.1	3509.4	469.9	472.9	96.7	91.6
16	162.5	0.023	450	470	0.55	0.593	92.2	4280.7	475.8	476.3	94.1	90.4
17	131.2	0.020	465	485	0.51	0.565	90.5	5121.3	478.3	478.9	91.8	89.3
18	109.3	0.020	475	475	0.51	0.565	89.7	5259.4	399.9	479.5	90.8	88.6
19	78.1	0.019	490	475	0.51	0.565	88.3	5424.2	284.9	481.5	89.1	87.6
20	37.5	0.017	485	485	0.51	0.565	86.6	5743.5	138.8	484.1	86.9	86.2

DESTEC
UNIVERSITÀ DI PISA
Dipartimento di Ingegneria dell'Energia, dei Sistemi, del Territorio e delle Costruzioni
Largo Lucio Lazzarino - 56122 Pisa (Italy)
Tel. +39 050 2217300 Fax + 39 050 2217333
Partita IVA 00286820501 VAT No. IT00286820501
Codice fiscale 80003670504

Pisa 18 of November 2016

Object: Detailed respond to reviewers (**ETFS-D-16-00791**)

Reviewer #1

Thank you for your suggestions and constructive comments. Following your suggestions, we have considered your interesting comments. In the attached highlighted version of manuscript, you can find the added parts according to your comments and our modification with blue and deleted phrases with red. You can also find the detailed response to your comments and related added or deleted phrases as follow:

COMMENT 1:

The author chronologically listed several references in the second paragraph of Introductory section, what is the basis of the arrangement of these references? I recognized that references [14-19] mainly investigated the effects of various operating parameters on thermal performance of screen-mesh HPs in experimental approaches. But I could not found any logical relation and connection among these referenced articles. I guess the author might want to demonstrate several important factors, such as working fluids, filling ratios etc., that governs the performance of screen-mesh HP. However, you'd better to explicitly describe and summarize these important factors briefly at the beginning of the paragraph. On the other hand, the works and contributions of reference [11-13] should be introduced briefly in order to let readers know the development of screen-mesh HPs modeling approaches.

ANSWER:

Thank you for your comment. We consider your comments and deeply revise the second paragraph by deleting the old one and extending and describing the literature review. Firstly, we develop the development of modeling approaches and afterward the affecting parameter on thermal performance of heat pipes is described as well as numerous experimental investigations in the literature as follow.

DESTEC
UNIVERSITÀ DI PISA
Dipartimento di Ingegneria dell'Energia, dei Sistemi, del Territorio e delle Costruzioni
Largo Lucio Lazzarino - 56122 Pisa (Italy)
Tel. +39 050 2217300 Fax + 39 050 2217333
Partita IVA 00286820501 VAT No. IT00286820501
Codice fiscale 80003670504

Removed sentences:

The design of HPs needs of careful consideration. Several modeling approaches [11-13] and experimental analysis have been. Among the others, in 1991, Faghri and Buchko [14] experimentally and numerically investigated the dryout limit of cylindrical screen wick HPs by increasing heat load in several arrangements. In 1993, El-Genk and Huang [15] experimentally investigated the transient response of a HP (screen mesh) at different input powers and cooling rates. In 2008, Kempers et al. [16] experimentally investigated the heat transfer mechanisms in the condenser and evaporator sections of a screen-mesh HP. Wong and Kao [17] experimentally investigated screen mesh HPs using ether as working fluid. In 2010, Lips et al. [18] experimentally analyzed the effect of filling ratios, heat fluxes and vapor space thicknesses on a flat plate HP. In 2013, Sukchana and Jaiboonma [19] investigated the effect of the filling ratio on thermal performance of HP using R-134a as a working fluid.

Added and revised sentences:

The design of HPs for a particular application needs of careful consideration. Several modeling approaches have been reported from a simple lumped model [14] to a transient multi-dimensional simulation [15]. However, a steady state thermal performance prediction is of significant value in the design of HPs [16,17]. Among others, Vafai and Wang [18] developed a modeling approach for the heat and mass transfer analyses in a flat HP. They applied Darcy's law to verify the liquid flow in the wick and assumed a parabolic vapor velocity profile to obtain the axial vapor pressure distribution. With the same approach, Vafai et al. [19] presented a numerical simulation in a disk shaped HPs. Zhu and Vafai [20] extended the work of Vafai et al. [19] considering inertial effects on the liquid flow in the HP wick section. As the most commonly operating limitation to the performance of a HP for low to medium temperature application appears to be capillary limit [2,12,13], researchers investigated this problem. Among others, Lefevre and Lallemand [21] developed a steady state analytical model considering both liquid flow in the wick and vapor flow to analyze thermal behavior of a flat miniature HP as well as prediction of the maximum heat transfer capability. Rice and Faghri [22] developed a numerical model considering the liquid flow in the wick to investigate thermal performance of screen mesh HPs. They show that the capillary dryout limitations can be predicted for a

Largo Lucio Lazzarino - 56122 Pisa (Italy)
Tel. +39 050 2217300 Fax + 39 050 2217333
Partita IVA 00286820501 VAT No. IT00286820501
Codice fiscale 80003670504

given heating load in their simulations. Aghvami and Faghri [23] presented a steady state model including both liquid and vapor flows to investigate thermal and hydraulic behavior of flat HPs. They investigated capillary pressures for given heat inputs to determine the dryout limitations. Shabgard and Faghri [24] extended the above modeling approach to cylindrical HPs. They coupled two-dimensional heat conduction in the HP's wall with the liquid flow in the wick and the vapor hydrodynamics. Among above presented models Vafai and Wang [18], Vafai et al., [19] and Zhu and Vafai [20] did not considered axial heat conduction in the HP's wall while Shabgard and Faghri [24] found that neglecting the axial heat conduction through the wall resulting in overestimated pressure drops up to 10%.

In reviewing the recent experimental investigations on design variables and operating parameters of HPs, it is apparent that the geometric properties of the wick structure, such as the wick thickness and porosity should always be carefully considered [25-33]. Furthermore, operating parameters such as filling ratio, cooling temperature, input heat flux and orientating could be important factors affecting thermal performance of the HP [34-40] as well as its evaporation to condensation length ratio [41-43]. Brautsch and Kew [25] studied heat transfer process of stainless steel mesh HPs using water as working fluid. They showed that maximum heat flux increases with wick thickness but also increases thermal resistance. Li et al. [26] and Li and Peterson [27] investigated the influence of varying wick thicknesses, porosities, and pore sizes on thermal resistance and critical heat flux of a horizontal copper surface sintered with multiple layers of copper mesh. They illustrated that the evaporation/boiling is strongly dependent on the wick thickness, however, it is weakly dependent on porosity. Kempers et al. [28] investigated the effect of the wick thickness on the heat transfer performance of screen mesh wick HPs using water as the working fluid. They observed that there is a small increase in thermal resistance when increasing the wick thickness; however, the maximum heat transfer also increases. Wang and Peterson [29] investigated a sintered copper screen mesh flat HP to examine its maximum heat transport capacity. They concluded that increasing the structural thickness increased the thermal resistance, but it enhanced heat transfer capacity. Wong and Kao [30] investigated screen mesh HPs using ether as working fluid at different mesh wicks, fluid charges and heat loads. They found a partial dryout at small filling ratio and boiling in the larger water/wick thickness.

DESTEC
UNIVERSITÀ DI PISA
Dipartimento di Ingegneria dell'Energia, dei Sistemi, del Territorio e delle Costruzioni
Largo Lucio Lazzarino - 56122 Pisa (Italy)
Tel. +39 050 2217300 Fax + 39 050 2217333
Partita IVA 00286820501 VAT No. IT00286820501
Codice fiscale 80003670504

Weibel et al. [31] analyzed the dependence of thermal resistance on the thickness of sintered powder wicks surfaces. They showed a trade-off between the increased area for heat transfer and increased thermal resistance. Brahim et al. [32] investigated screen mesh HPs and showed that the mesh number is an important factor which affects the overall thermal performance of the system. Tsai and Lee [33] investigated the effects of structural parameters on the evaporation heat transfer in sintered wick HPs. They suggested thinner structural thickness to enhance evaporation heat transfer. Among operating parameters affection on thermal performance of HPs, the tilt angle have a considerable impact by assisting (the condenser section above the evaporator section, e.g. gravity-assisted) or suppressing (the evaporator section above the condenser section, e.g. gravity-opposed) the return of the working fluid. However, the sensitiveness to the orientation is much different for various wick structures [2]. A number of investigations have been shown that the thermal performance of groove type wick HPs significantly depend on the orientation [36] while a much smaller impact has found in sintered wick HPs [37]. Some other researchers [29] indicated that the maximum heat transport capacity of screen mesh wick is reduced by increasing the tilt angle while the performance of the sintered mesh wick is better than the screen mesh one because of the higher effective thermal conductivity. Kumaresan et al. [38] showed that the increasing of angle of inclination of the sintered wick HP improves the HP condensation heat transfer by 30% at 45° orientation in comparison of the horizontal position. However, tilt angles close to vertical position results in deterioration of performance. Sadeghinezhad et al. [39] recently showed the orientation of a sintered wick HP has a major influence on its thermal efficiency, in which gradually increases with the inclination angle up to 60° and then decreases, while Li and Lv [40] have not found a major influence of title angle on the thermal resistance of a flat HP from 45° to vertical position, however it was lower than horizontal position. With regard to impact of the ratio of the evaporator length to the condenser length on the thermal performance of HPs, Wang et al. [41] investigated the effect of evaporation and condensation length on thermal performance of flat HPs. They showed that dryout would occur at a lower heating power for a longer condensation section length and thermal performance is better at equal lengths of the condensation and evaporation sections. Liang and Hung [42] found that the optimal evaporator length to condenser length ratio of the sintered HP depends on

Largo Lucio Lazzarino - 56122 Pisa (Italy)
Tel. +39 050 2217300 Fax + 39 050 2217333
Partita IVA 00286820501 VAT No. IT00286820501
Codice fiscale 80003670504

other geometrical parameters such as its diameter. Chen and Chou [43] investigated the effects of length (80 mm-300 mm) on the thermal performance of flat HPs. They showed that an increasing of the length from 80 mm to 300 mm increases the overall thermal resistance of the HP while the maximum heat transport capability decreases.

COMMENT 2:

In the third paragraph of introductory section, the author intended to overview state-of-the-art HPs modeling methodologies. They listed several relevant papers. However, the author mainly discussed the optimal results, while the optimization method and character were not detailed. I think the optimization methodologies and characters should be introduced more specifically like you introduced reference [22].

ANSWER:

Thank you for your comment. We consider your comments and develop the following section accordingly.

Removed sentences:

Despite optimization of HPs is very useful for advancement in the heat transfer performance, the optimal design of HPs rarely studied. Thus, it is necessary to perform a methodology to improve the heat transfer capacity and to reduce the thermal resistance of HPs. To optimize the heat transfer performance of HPs, in 2003, Kim et al. [20] proposed a mathematical model in a grooved wick HP to maximum heat transport rate and the overall thermal resistance. They estimated that the maximum heat transport rate of outer diameter 3 and 4 mm HPs can be enhanced up to 48% and 73%, respectively by optimizing the groove wick structure. In 2004, Sousa et al. [21] proposed a method to optimize the thermal performance of a HP for a space engineering application by minimizing the total mass of the HP. In 2005, Rao and More [22] presented an optimization algorithm (Teachinge Learning-Based Optimization) to optimize Ω-shaped grooved HP. They considered the maximizing of the heat transfer rate and minimizing the resistance of a HP as objective functions. In 2009, Zhang et al. [23] utilized the niched Pareto genetic algorithm based approach to optimize an axial Ω-shaped micro grooves HP. They conclude that a larger groove number and vapor core diameter could be enhanced the heat transfer capability. In 2011, Liang and Hung [24] experimentally investigated

DESTEC
UNIVERSITÀ DI PISA
Dipartimento di Ingegneria dell'Energia, dei Sistemi, del Territorio e delle Costruzioni
Largo Lucio Lazzarino - 56122 Pisa (Italy)
Tel. +39 050 2217300 Fax + 39 050 2217333
Partita IVA 00286820501 VAT No. IT00286820501
Codice fiscale 80003670504

and optimized the thermal performance of a U-shape HP. They showed that the optimal evaporator to condenser length ratio dependents on the pipe diameter. To the best of authors' knowledge, although there are some papers presented on the optimization of grooved wick HPs, there is no study available in the literature on the optimal design of a screen mesh HP considering both the heat transfer capability and the total thermal resistance.

Added and revised sentences:

The above studies indicate that thermal performance and maximum heat transfer capacity of HPs strongly depending on the geometry and the capillary structure. A good HP is characterized by a low thermal resistance and a high dryout tolerance. Thus, optimization approaches help to better understand of optimal structural parameters in the design of HPs. To optimize the heat transfer performance of HPs, Kim et al. [44] proposed a one-dimensional mathematical model in a grooved wick HP to maximum heat transport rate and the overall thermal resistance. Their model included the effects of the liquid–vapor interfacial shear stress, the contact angle, and the amount of initial liquid charge. Sousa et al. [45] proposed generalized extremal optimization (GEO) approach to optimize the thermal performance of a HP for a space engineering application by minimizing its total mass. The method is a global search meta-heuristic, as the Genetic Algorithm (GA), but with a priori advantage of having only one free parameter to adjust. The results showed that the GEO algorithm is a good candidate to be incorporated to the designer's tools. With the same optimization approach (GEO), Vlassov et al. [46] optimized the mass characteristics for a grooved wick HP for space application for different operational modes. They concluded that the proposed optimization approach can be effectively applied to complex optimal design problems. Rao and More [47] presented an optimization algorithm, Teachinge Learning-Based Optimization (TLBO), to optimize Ω-shaped grooved HP. They considered the maximizing of the heat transfer rate and minimizing the resistance of a HP as objective functions. They compared results of application of TLBO algorithm for the design optimization of HPs with other optimization approaches (Niched Pareto Genetic Algorithm (NPGA), Grenade Explosion Method and GEO) and found that proposed algorithm produces better results in improvement of heat transfer rate and total thermal resistances. Zhang et al. [48] utilized the NPGA based approach to optimize an axial Ω-shaped

DESTEC
UNIVERSITÀ DI PISA
Dipartimento di Ingegneria dell'Energia, dei Sistemi, del Territorio e delle Costruzioni
Largo Lucio Lazzarino - 56122 Pisa (Italy)
Tel. +39 050 2217300 Fax + 39 050 2217333
Partita IVA 00286820501 VAT No. IT00286820501
Codice fiscale 80003670504

micro grooves HP. They performed the HP optimization design regarding the heat transfer capability and total thermal resistance as the objective function and the structure parameters as the decision variable. They concluded that the optimal set of solution can be used as an optimal design for a given application. . To the best of authors' knowledge, although there are some papers presented on the optimization of grooved wick HPs, there is no study available in the literature on the optimal design of a screen mesh HP considering both the heat transfer capability and the total thermal resistance.

COMMENT 3:

In Fig. 2, instead of using the words "heat in" and "heat out", I think the words "heat absorption" and "heat dissipation" seems much more proper for this figure.

ANSWER:

Thank you for indication. As you can see in Fig. 1 (Fig. 1 in the old manuscript is deleted), the figure modify based on your comment.

COMMENT 4:

All in all, the paper review with respect to the experimental and analytical studies on screen-mesh HPs, as well as relevant optimization methodologies is insufficient.

ANSWER:

This sentence is added in the last paragraph of introduction.

COMMENT 5:

In line 15, please mention the names of the researchers.

ANSWER:

The last paragraph of section 2 is moved and modified in the introduction.

DESTEC
UNIVERSITÀ DI PISA
Dipartimento di Ingegneria dell'Energia, dei Sistemi, del Territorio e delle Costruzioni
Largo Lucio Lazzarino - 56122 Pisa (Italy)
Tel. +39 050 2217300 Fax + 39 050 2217333
Partita IVA 00286820501 VAT No. IT00286820501
Codice fiscale 80003670504

Added and revised sentences:

Kempers et al. [28] investigated the effect of the wick thickness on the heat transfer performance of screen mesh wick HPs using water as the working fluid. They observed that there is a small increase in thermal resistance when increasing the wick thickness; however, the maximum heat transfer also increases.

COMMENT 6:

I do not find Eq. (5) in the manuscript.

ANSWER:

Thank you for your indication the number of equations is carefully checked and modified.

COMMENT 7:

The symbol Θ in Eq. (6-11) should be included in Nomenclature table.

ANSWER:

Thank you for your comment. It is added in Nomenclature table.

COMMENT 8:

lot of subscripts have been used in the manuscript, however, most of them are not defined explicitly in the Nomenclature. For example, the subscript "f" "v" and "i", their denotation should be described in Nomenclature.

ANSWER:

Thank you again for your indication. We add all the missed subscripts in Nomenclature table.

COMMENT 9:

In line 56 at page 6, the author claimed a series of assumptions for the simplification of the model. Please provide the relevant reasons or references to proof that these assumptions are valid in terms of present study.

DESTEC
UNIVERSITÀ DI PISA
Dipartimento di Ingegneria dell'Energia, dei Sistemi, del Territorio e delle Costruzioni
Largo Lucio Lazzarino - 56122 Pisa (Italy)
Tel. +39 050 2217300 Fax + 39 050 2217333
Partita IVA 00286820501 VAT No. IT00286820501
Codice fiscale 80003670504

ANSWER:

Thank you for your comment on assumptions of mathematical model. We consider relevant references of these assumptions.

Added and revised sentences:

[19-21, 23, 24]

COMMENT 10:

In line 57-60 at page 7, it is said that "A parabolic velocity profile is considered for the vapor flow and at the liquid-vapor interface a mass balance is applied for interfacial vapor and liquid velocities". Since we know that the liquid-vapor interaction in terms of heat, momentum and mass transfer is very complicate, what's the basis of this simplified treatment? Where's the relevant mathematical models for the implementation of this treatment?

ANSWER:

Thank you for your comments. As the model couples heat conduction in the heat pipe's wall with the liquid flow in the wick and the vapor hydrodynamics, the treatment of heat conduction should be firstly introduced. Therefore we add Appendix A and supported phrase at the end of section 3.1 as you can see as follow and revised manuscript to cover your questions.

Added and revised sentences:

At the centerline, the radial gradient of the axial velocity is equal to zero (Eq. 18). Details of using the method of separation of variables to solve the treatment of energy equations (Eq. 5) to verify the axial temperature distribution, the continuity equation (Eq. 11) and Darcy's law (Eq. 12) to obtain the axial gradient of pressure and the average liquid velocity along the wick portion and the conservation equations for mass (Eq. 15) and momentum (Eq. 16) to yield vapor velocity profile and the axial vapor pressure distribution describe in Appendix A.

Appendix A. Mathematical treatment of conservation equations in the HP's wall, wick and vapor

DESTEC
UNIVERSITÀ DI PISA
Dipartimento di Ingegneria dell'Energia, dei Sistemi, del Territorio e delle Costruzioni
Largo Lucio Lazzarino - 56122 Pisa (Italy)
Tel. +39 050 2217300 Fax + 39 050 2217333
Partita IVA 00286820501 VAT No. IT00286820501
Codice fiscale 80003670504

Heat conduction in the wall

The two-dimensional heat conduction obtains by assuming linear temperature profile across the wick portion and constant saturation temperature at the liquid-vapor interface (Eq. 10) by employing the separation-of-variable method (Rohsenow et al., 1985)

$$\theta(r,x)=\sum_{m=0}^{\infty}\cos(A_m x)\{\omega_m[I_0(A_m r)+\eta_m K_0(A_m r)]\} \qquad (A.1)$$

where I_0 and K_0 are modified Bessel functions of the first and second kind of order zero, respectively, ω_m is unknowns which should be determined for every m and $A_m=m\pi L$ proposing the boundary condition (Eq. 7)

$$\omega_m=\frac{1}{-k_s\frac{L}{2}\{A_n[I_1(A_m r_o)-\eta_m K_1(A_m r_o)]\}}\left\{\int q_e\cos(A_m x)dx+h_\infty\sum_{i=0}^{\infty}\omega_i F_i+h_\infty(T_v-T_\infty)\int\cos(A_m x)dx\right\} \qquad (A.2)$$

where constants can be calculated for every given m. The system of m equations expressed in above equation is solved by use of the direct methods. When a sufficient number of ω_m are calculated, the temperature can be determined from Eq. A.1.

The liquid flow in the wick section

The axial liquid velocity is calculated by integrating Eq. 11 with respect to x and substituting v_l (Eq. 13) as

$$\frac{\partial u_l}{\partial x}=\frac{2q_e r_i}{\rho_l h_{fg}(r_i^2-r_v^2)} \qquad (A.3)$$

By Combining Darcy's law (Eq. 14) and Eq. A.3, the average velocity profile along the wick is calculated by obtaining the axial gradient of pressure

$$\frac{d^2P_l}{dx^2}=-\frac{2r_i\mu q_e}{\rho_l h_{fg}K(r_i^2-r_v^2)} \qquad (A.4)$$

The liquid pressure can be obtained by considering $q=-k_{wall}\partial\theta/\partial r$ and Eq. 5 as

Largo Lucio Lazzarino - 56122 Pisa (Italy)
Tel. +39 050 2217300 Fax + 39 050 2217333
Partita IVA 00286820501 VAT No. IT00286820501
Codice fiscale 80003670504

$$\begin{cases} \dfrac{dP_l}{dx} = -\dfrac{2r_i\mu k_s}{\rho_l h_{fg} K(r_i^2 - r_v^2)} \displaystyle\sum_{m=0}^{\infty} \sin(A_m x)\{\omega_m [I_1(A_m r_i) - \eta_m K_1(A_m r_i)]\} & (A.5) \\ P_l = -\dfrac{2r_i\mu k_s}{\rho_l h_{fg} K(r_i^2 - r_v^2)} \displaystyle\sum_{m=0}^{\infty} \dfrac{\cos(A_m x)}{A_m} \{\omega_m [I_1(A_m r_i) - \eta_m K_1(A_m r_i)]\} & (A.6) \end{cases}$$

The average liquid velocity can be obtained according Darcy's law when the axial gradient of pressure is calculated.

Vapor flow in the core

A parabolic velocity profile is considered for the vapor flow [18, 20, 21].

$$u_v(r,x) = U_v(x)(\xi_1 + \xi_2 r + \xi_3 r^2) \quad (A.7)$$

where U_v is the local average velocity of the vapor and the constants (ξ_1, ξ_2 and ξ_3) are verified by applying the boundary conditions in Eq. 17 and Eq. 18 and the definition given in

$$U_v(x) = \frac{2}{r_v^2}\int_0^{r_v} r u_v dr \quad (A.8)$$

Thus, the vapor velocity profile define as

$$u_v(r,x) = 2U_v(x) - \frac{2U_v(x)r^2}{r_v^2} \quad (A.9)$$

By substituting Eq. A.9 in the continuity equation (Eq. 15) and integrating with respect to r, yields

$$r_v U_v'(x) + 2v_v = 0 \quad (A.10)$$

By considering this fact that at the interface, the vapor interfacial velocity is related to the liquid interfacial velocity by a mass balance ($\rho_v v_v = \rho_l v_l$) and using Eq. 13, the vapor interfacial velocity is verified as

$$v_v = \frac{q_e\big|_{r=r_i} r_i}{\rho_v h_{fg} r_v} \quad (A.11)$$

Considering $v_l = (q_e/\rho_l h_{fg})(r_i/r_v)$ and $v_v = (q_e/\rho_v h_{fg})(r_i/r_v)$ and integrating Eq. A.10 with respect to x the mean vapor velocity is calculated as follow

DESTEC
UNIVERSITÀ DI PISA
Dipartimento di Ingegneria dell'Energia, dei Sistemi, del Territorio e delle Costruzioni
Largo Lucio Lazzarino - 56122 Pisa (Italy)
Tel. +39 050 2217300 Fax + 39 050 2217333
Partita IVA 00286820501 VAT No. IT00286820501
Codice fiscale 80003670504

$$U_v(x) = -\frac{2r_i k_s}{\rho_v h_{fg} r_v^2} \sum_{m=1}^{\infty} \sin(A_m x)\{\omega_m [I_1(A_m r_i) - \eta_m K_1(A_m r_i)]\} \qquad (A.12)$$

Finally, concerning boundary layer momentum equation along the vapor velocity profile, the axial distribution of the vapor pressure is obtained by neglecting the radial variation of the vapor pressure by

$$\nabla P = -\frac{16 r_i \mu k_s}{\rho_v h_{fg} r_v^4} \sum_{m=1}^{\infty} [1 - \cos(A_m x)] \left\{ \frac{\omega_m [I_1(A_m r_i) - \eta_m K_1(A_m r_i)]}{A_m} \right\} - \frac{8}{3\rho_v} \left\langle \frac{r_i k_s}{h_{fg} r_v^2} \sum_{m=1}^{\infty} \sin(A_m x)\{\omega_m [I_1(A_m r_i) - \eta_m K_1(A_m r_i)]\} \right\rangle^2 \qquad (A.13)$$

COMMENT 11:

To my knowledge, analytical solution for a problem should be obtained by solving the equations directly without any numerical approximation. The author stated that they used an analytical method for the present study. But I also recognize the governing equations were discretized probably using some FEM methods. Such solution should not be called as an analytical solution while it is supposed to be a numerical solution. Therefore, I suggest the author replace the word "analytical" by "numerical" throughout the manuscript in order to avoid any misunderstanding.

ANSWER:

Thank you for your comment. As we introduced the mathematical model in Appendix A, it is clear that we have not performed any numerical simulation in our modeling and in author opinion the analytical model is applied. This approach also proposed in [21,23,24].

COMMENT 12:

In section 3.2, line 19, please specify that which part of the HP is made of Copper?

ANSWER:

Thank you for your comment. We clearly describe the material of the pipe and the wick structure.

DESTEC
UNIVERSITÀ DI PISA
Dipartimento di Ingegneria dell'Energia, dei Sistemi, del Territorio e delle Costruzioni
Largo Lucio Lazzarino - 56122 Pisa (Italy)
Tel. +39 050 2217300 Fax + 39 050 2217333
Partita IVA 00286820501 VAT No. IT00286820501
Codice fiscale 80003670504

Added and revised sentences:

The HP is made by smooth copper pipe where it is closed at the ends with two 3 mm thick copper caps consisting ofcontains three layers of stainless steel screen mesh (100 mesh/inch) with a wire diameter of 0.114 mm.

COMMENT 13:

Please check the tense in section 3.2, either use present tense or use past tense.

ANSWER:

Thank you for your comment. The section 3.2 and also other section carefully check accordingly.

COMMENT 14:

What kind of thermocouple are you used to measure the inlet and outlet temperature of the water in manifold? Please clearly mark the thermocouples in Fig. 3. Why only arranged two T-thermocouple in the condenser section?

ANSWER:

Thank you for your comment. We describe the kind of used thermocouples to measure inlet and outlet cooling temperatures and also marked the thermocouple positions in Fig. 3.

Added and revised sentences:

Two thermocouples *(K-type stainless steel probe)* in the manifold inlet and *the* outlet and *the* mass flow measurement allow to calculate the power output from *the* condenser section, and to compare it to the input electrical power.

COMMENT 15:

Were there any insulation measures designed for the adiabatic section? If not, the heat dissipation in this section may influence the result accuracy. If yes, please detail the insulation measures you applied.

DESTEC
UNIVERSITÀ DI PISA
Dipartimento di Ingegneria dell'Energia, dei Sistemi, del Territorio e delle Costruzioni
Largo Lucio Lazzarino - 56122 Pisa (Italy)
Tel. +39 050 2217300 Fax + 39 050 2217333
Partita IVA 00286820501 VAT No. IT00286820501
Codice fiscale 80003670504

ANSWER:

Thank you for your comment. We perform an insulation to avoid heat losses as described as follow in the manuscript to cover what you ask and also some other information.

Added and revised sentences:

During the tests, heaters and blocks as well as adiabatic and condenser sections are covered with several layers of polymer insulation to minimize heat losses. Energy balances between the heat input by the electrical heaters and the heat removed by the sinks is monitored to ensure an energy balance within 90 percent in the worst case. Prior to the recording of any test data, the test facility allows to reach the steady state, defined as the point at which the temperature reading for any thermocouple varied by less than 0.5°C over a period of fifteen minutes.

COMMENT 16:

Likewise, were there any insulation measures designed for the heater outer-surface?

ANSWER:

We answer this comment in COMMENT 15.

COMMENT 17:

In Fig. 5, a legend is needed to indicate which symbol (the line or the scatter) corresponds to the experimental data and which symbol (the line or the scatter) corresponds to the numerical results.

ANSWER:

Thank you for your indication. We modify the Fig. 5 to verify the experimental and analytical results.

COMMENT 18:

"Concerning the experimental capillary limit reported in Fig. 7"? Where is the experimental data in Fig. 7?

DESTEC
UNIVERSITÀ DI PISA
Dipartimento di Ingegneria dell'Energia, dei Sistemi, del Territorio e delle Costruzioni
Largo Lucio Lazzarino - 56122 Pisa (Italy)
Tel. +39 050 2217300 Fax + 39 050 2217333
Partita IVA 00286820501 VAT No. IT00286820501
Codice fiscale 80003670504

ANSWER:

Thank you for your comment. We wanted to compare the experimentally obtained limitation of Fig. 5 and analytically obtained limitation in Fig. 7. Therefore, this part is modified as follow.

Added and revised sentences:

*From the analysis of experimental data, it is observed that the reported maximum heat transfer capacity due to capillary limit (**Fig. 5)**, has good agreement with the analytical calculations (**Fig. 7**) in which the maximum heat transfer rate obtains (350 W). Therefore, it is evidenced that the analytical approach can predict the maximum heat transfer rate of the HP at mid-temperature operation (85°C).*

COMMENT 19:

When you discussed about the orientation, which section (condenser or evaporator) was on the upper side? This is very important and must be identified in the manuscript.

ANSWER:

Thank you for your note. We add a sentence in the section 4.2 (first paragraph line 4) to cover your comment. Also in the Introduction in the first of sixth paragraph we consider a phrase.

Added and revised sentences:

It would be noted that in the oriented position as well as vertical one the condenser section of the HP places at the top and the evaporator at its lower end (gravity assisted orientation).

Among operating parameters affection on thermal performance of HPs, the tilt angle have a considerable impact by assisting (the condenser section above the evaporator section, e.g. gravity-assisted) or suppressing (the evaporator section above the condenser section, e.g. gravity-opposed) the return of the working fluid.

COMMENT 20:

For Fig. 9, the author explained that the smaller thermal resistance for the case with higher condensation temperature is due to the reduced viscous of working fluid. Is this sufficient to explain the significant

DESTEC
UNIVERSITÀ DI PISA
Dipartimento di Ingegneria dell'Energia, dei Sistemi, del Territorio e delle Costruzioni
Largo Lucio Lazzarino - 56122 Pisa (Italy)
Tel. +39 050 2217300 Fax + 39 050 2217333
Partita IVA 00286820501 VAT No. IT00286820501
Codice fiscale 80003670504

decrease of thermal resistance (almost 50% decrease)? I think it may be also related to the higher operating pressure at higher condensation temperature that influence its performance? The author should give a more solid argumentation.

ANSWER:

Thank you for your indication. We develop this section to cover your comment and to clear the observation. The related modified section is as follow.

Added and revised sentences:

In order to investigate the effect of cooling temperature, a horizontal HP with evaporator length of 225 mm and cooling temperature of 25 *°C*, 55 *°C* and 85 °C *is tested*. **Fig. 11** shows the total thermal resistances under changes of the cooling temperatures in the range of heat loads from 60 W to 350 W. According to the *presented* results, the thermal resistance decreases with an increase in the condenser cooling temperature. *However, no significant difference is observed in the thermal resistance at higher heat transfer rate of cooling temperature of 55 °C and 85 °C. Such behavior could be explained by the fact that for a give heat flux, the vapor and liquid friction factor and simultaneously the vapor pressure drop and the liquid pressure drop along the wick portion decreases as the cooling temperature increases because of viscosity changes [52].*

Fig. 12 *also shows the related heat transfer rate dependences of the temperature of the evaporator wall. It is observed that a change in the condenser cooling temperature of a certain magnitude (30°C) does not always load to equivalent changes in the operating temperature of the HP. It means that temperature deference of evaporator walls are lower than temperature differences of cooling temperatures from 25 °C to 55 °C and to 85 °C. With an increase in the cooling temperature from 25°C to 55°C and from 55 °C to 85 °C the average HP wall temperature increases by 26.8 °C and 24.7 °C. Therefore, decreasing of the thermal resistance with an increase in the condenser cooling temperature (see* ***Fig. 11****) could be also explained by the fact that an increase in cooling temperature leads to a decrease in the temperature drop between the evaporator and the condenser, according to the presented results in* ***Fig. 12***. This shows the advantage of the use of hotter

DESTEC
UNIVERSITÀ DI PISA
Dipartimento di Ingegneria dell'Energia, dei Sistemi, del Territorio e delle Costruzioni
Largo Lucio Lazzarino - 56122 Pisa (Italy)
Tel. +39 050 2217300 Fax + 39 050 2217333
Partita IVA 00286820501 VAT No. IT00286820501
Codice fiscale 80003670504

medium water, air, etc.) for cooling the HP condenser when lower values of its thermal resistance are required in a practical application.

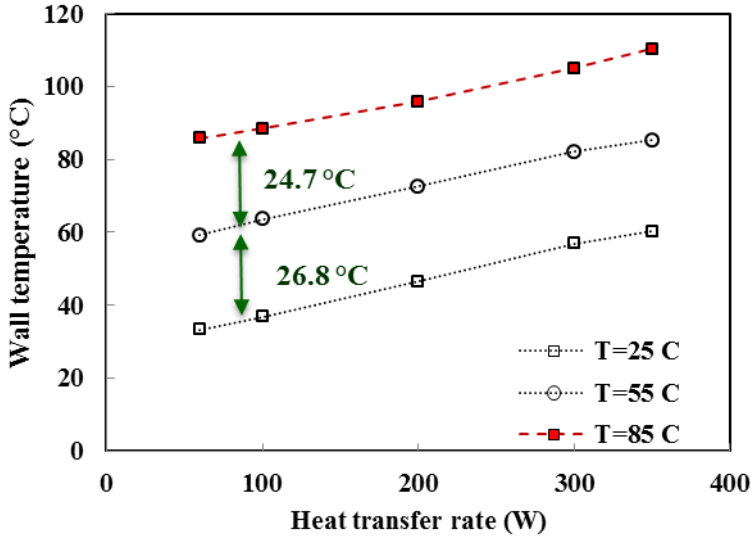

Fig. 12 *Evaporator wall temperature dependence on heat transfer rate and cooling temperature of the HP at horizontal position.*

COMMENT 21:

The caption for Table 6 should be more specific.

ANSWER:

Thank you for your indication. The capital for Table 6 is modified as follow.

Added and revised sentences:

Table 6 Optimal solution sets *to optimize the total thermal resistance depending heat transfer rates.*

COMMENT 22:

Please modify the last sentence of section 4.3, "It could be concluded that the wick thickness and wick permeability is a strong function of the heat flux." Add adjective word "optimal" before the "wick thickness and wick permeability", otherwise, it may mislead the readers.

DESTEC
UNIVERSITÀ DI PISA
Dipartimento di Ingegneria dell'Energia, dei Sistemi, del Territorio e delle Costruzioni
Largo Lucio Lazzarino - 56122 Pisa (Italy)
Tel. +39 050 2217300 Fax + 39 050 2217333
Partita IVA 00286820501 VAT No. IT00286820501
Codice fiscale 80003670504

ANSWER:

Thank you for your comment. The sentence is modified accordingly.

Added and revised sentences:

It could be concluded that the optimal wick thickness and wick permeability are a strong function of the heat flux.

COMMENT 23:

The permeability and wick thickness are supposed to be two independent parameters. But why did you multiply them together instead of investigate them independently during the optimization process? And you only found an optimal value for permeability times wick thickness while we want to know the independent optimal value when we design a HP.

ANSWER:

Thank you for your comment. Actually we consider optimal wick permeability and wick thickness as a function because both increase as pressure drop decreases. However, thanks to your comment we separately present and discuss all the optimally obtained structural wick parameters as follow.

Added and revised sentences:

Herein, a parametric study is presented based on obtained optimal set of solutions. It is know that variations in the wire diameter can change the size of the vapor space [2, 12, 13], which affects on the heat transfer capacity of the HP. As presented in ***Fig. 14****, the optimization results indicated that with increasing heat transfer rate the wire diameter decreases to have lower thermal resistance. In contrast, the porosity should be decreases with increasing heat transfer rate to have an optimal case depending heat transfer rate. These two parameters simultaneously change the conductive and permeability characteristics of the wick structure. For example, with increasing of the wick porosity, the effective thermal conductivity decreases while permeability increases. Moreover, increasing wire diameter leads to increase of permeability. Thus, the effective thermal conductivity and permeability of wick structure need to be analyzed in optimal cases.* ***Fig. 15*** *indicates the optimal permeability and effective thermal conductivity of the HP at various heating power.*

Largo Lucio Lazzarino - 56122 Pisa (Italy)
Tel. +39 050 2217300 Fax + 39 050 2217333
Partita IVA 00286820501 VAT No. IT00286820501
Codice fiscale 80003670504

Permeability is one of the important properties of a wick structure which is a measure of the wick resistance to axial liquid flow [2]. As it is observed in ***Fig. 15****, this parameter increases with increasing of heat transfer rate to have a small liquid pressure drop, and thus, avoiding capillary limit (see Table 6). Effective thermal conductivity is another important parameter in which its large value gives a small temperature drop across the wick, which is a favorable condition in the HP design. However, a high thermal conductivity and permeability are contradictory properties for designing wick structures. As it is evidenced in* ***Fig. 15*** *the optimal effective thermal conductivity decreases as heat transfer rate increases. Therefore, it is concluded that to have optimal case at lower heat fluxes for a screen mesh wick HP may have a large effective thermal conductivity, but have a small permeability. While at high heat transfer rate a small effective thermal conductivity, but a large permeability is recommended. The designer must always make trade-offs between these competing factors to obtain an optimal wick design.*

The wick thickness is also a parameter impact on the determination of the thermal resistance of the HP, thus an optimal thickness is important to reach maximum performance. ***Fig. 16*** *shows optimum wick thickness for an applied heat flux and related liquid pressure drop along the wick. It is indicated that the wick thickness values increase with increasing of heat transfer rate. An increase of the layer of the mesh wick can reduce the liquid frictional pressure drop proportionally by increasing the liquid flow area, resulting in improved heat transfer capacity. However, the increase in the layer of the screen mesh results in significant increases in superheat through the wick layer, and therefore, in premature boiling limitations [29]. On the other hand, decreasing the wick thickness decreases the radial thermal resistance of the wick while the working fluid cannot be supplied efficiently to the evaporator, which causes dryout.*

Finally, the thermal resistance of a HP as well as maximum heat transfer capacity depends on the evaporator length to the condenser length, L_e/L_c *ratio. The optimal* L_e/L_c *ratio and a function of wick permeability and wick thickness of the HP at various heating power are shown in* ***Fig. 17****. The motivation of presenting a function consisting both optimal wick permeability and wick thickness is that, as the wick thickness (See* ***Fig. 16****) and/or wick permeability (see* ***Fig. 15****) increase, the pressure drop decreases. Thus, an optimal relation of these two important parameters and given heat flux could be useful to design a screen*

DESTEC
UNIVERSITÀ DI PISA
Dipartimento di Ingegneria dell'Energia, dei Sistemi, del Territorio e delle Costruzioni
Largo Lucio Lazzarino - 56122 Pisa (Italy)
Tel. +39 050 2217300 Fax + 39 050 2217333
Partita IVA 00286820501 VAT No. IT00286820501
Codice fiscale 80003670504

mesh wick structure for a particular application. It is evidenced that the optimal L_e/L_c ratio for HPs is constant as about 1 while the function of wick permeability and wick thickness increase with increasing heat flux. It could be concluded that the optimal wick thickness and wick permeability are a strong function of the heat flux. The obtained optimal cases at equal lengths of the condensation and evaporation sections also affirms by experimental results in which highest thermal efficiency is obtained (see ***Fig. 10****).*

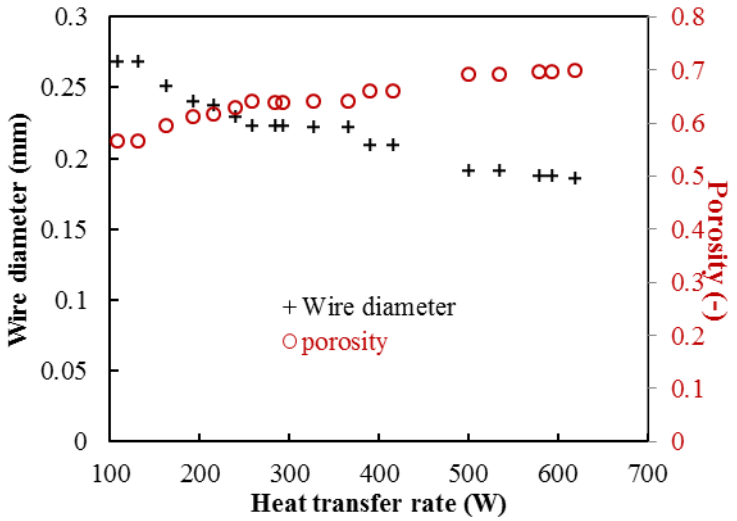

Fig. 14 *Relation between heat flux, optimal wire diameter and porosity.*

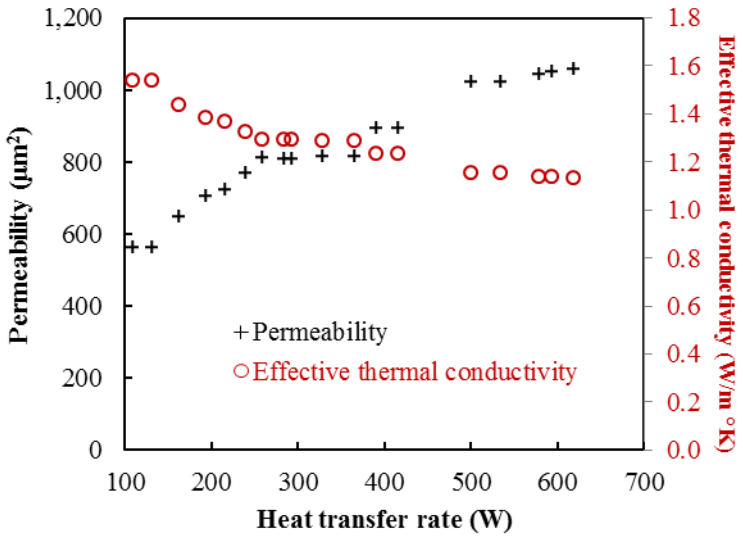

Fig. 15 *Relations between heat flux, optimal wick permeability and effective thermal conductivity.*

DESTEC
UNIVERSITÀ DI PISA
Dipartimento di Ingegneria dell'Energia, dei Sistemi, del Territorio e delle Costruzioni
Largo Lucio Lazzarino - 56122 Pisa (Italy)
Tel. +39 050 2217300 Fax + 39 050 2217333
Partita IVA 00286820501 VAT No. IT00286820501
Codice fiscale 80003670504

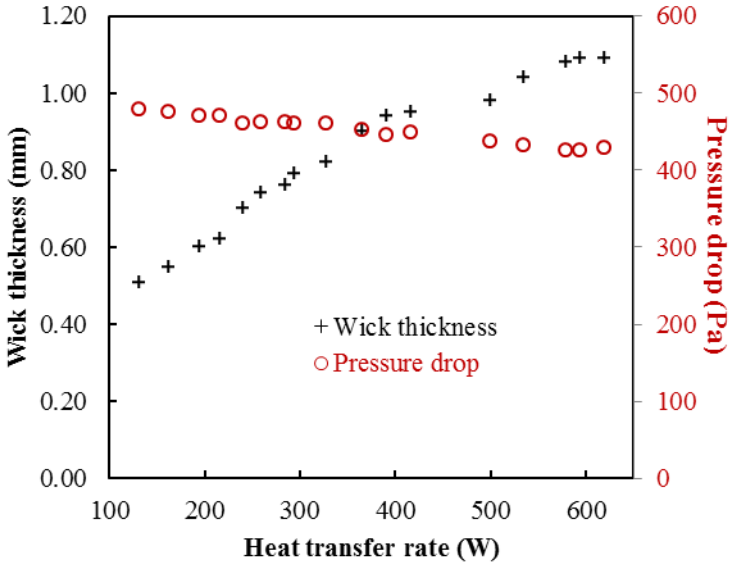

Fig. 16 *Relations between heat flux, optimal wick thickness and related pressure drop.*

COMMENT 22:

The conclusion section needs a major revise. On one hand, the first paragraph is out-of-order. You first developed your numerical model, then performed experimental study, and finally conducted parametric optimization. Therefore, the first paragraph of conclusion should be organized according to the order of your context. On the other hand, you concluded that "it is found the orientation is not affecting parameter on the thermal performance of screen mesh HPs". That was totally misleading. Your result showed some difference caused by the orientation (Fig. 8), through the difference is not very significant.

ANSWER:

Thank you for your comment. The conclusion totally re-write based on your comments.

Added and revised sentences:

For particular applications involving low to medium operating temperature, this study investigates the screen mesh wick HPs structural parameters as well as its operating parameters both analytically and experimentally. For this aim, a mathematical simulation, an experimental facility and optimization approach develop to measure and predict the maximum heat flux and thermal performance of HPs. A mathematical

DESTEC
UNIVERSITÀ DI PISA
Dipartimento di Ingegneria dell'Energia, dei Sistemi, del Territorio e delle Costruzioni
Largo Lucio Lazzarino - 56122 Pisa (Italy)
Tel. +39 050 2217300 Fax + 39 050 2217333
Partita IVA 00286820501 VAT No. IT00286820501
Codice fiscale 80003670504

model is presented to study the steady state performance of the horizontal HP and also to predict its operating limitation and to optimize its thermal performance. The model involves coupling two-dimensional heat conduction in the HP's wall with the liquid flow in the wick and the vapor hydrodynamics. A series of experiments performs to evaluate the heat transfer performance of the HP at different heat transfer rates, orientations, cooling temperatures and evaporator lengths as well as validation of analytical model in horizontal position at medium operating temperature. A NSGA-II optimization approach is introduced to maximize the heat transfer capability and to minimize the overall thermal resistance of screen mesh HPs. A modeling approach is conducted to optimize the structural parameters of screen mesh wick including wick thickness and porosity as well as evaporator length and condenser length of horizontally position HPs. The experimental investigations and the optimization results are analyzed and discussed and obtained results summarize as follow.

The HP is tested in horizontal, 45˚ orientation and vertical position and at different evaporator length (75 mm-300 mm). From the experimental analysis of the HP, it is found the orientation does not show a very significant effect on the thermal performance of screen mesh HPs while the evaporator length shows a significant influence. It is found that at the same operating conditions, as the evaporator length increases the thermal resistance decreases while there is an optimal evaporator length in which the device shows a highest thermal efficiency. Investigation of the effect of cooling temperature also shows the advantage of the use of hotter medium (here in water) for cooling the HP condenser when lower values of its thermal resistance are required.

This study suggests that an improved thermal performance can be attained by having a large effective thermal conductivity, but having a small permeability at lower heat transfer rates while at high heat transfer rate a small effective thermal conductivity, but a large permeability. In conclusion, the optimal wick thickness and wick permeability finds to be a strong function of the heat flux. However, the designer must always make trade-offs between these competing factors to obtain an optimal wick design. The results of the demonstrated optimization analysis in the present study serve as a useful designing tool for optimum thermal performance of screen mesh HPs for the mid-low operating temperature applications.

DESTEC
UNIVERSITÀ DI PISA
Dipartimento di Ingegneria dell'Energia, dei Sistemi, del Territorio e delle Costruzioni
Largo Lucio Lazzarino - 56122 Pisa (Italy)
Tel. +39 050 2217300 Fax + 39 050 2217333
Partita IVA 00286820501 VAT No. IT00286820501
Codice fiscale 80003670504

COMMENT 22:

There are some grammar errors in this paper, I have found some and highlight them with yellow background. Some inappropriate sentences are highlighted with green underline. I will upload my revised PDF file. Please download it and make modifications accordingly. The author need to revise their paper to correct those grammar errors.

ANSWER:

Thank you for your comment and your time. We deeply revise the manuscript and modify not only your highlighted phrases but also other modifications.

DESTEC
UNIVERSITÀ DI PISA
Dipartimento di Ingegneria dell'Energia, dei Sistemi, del Territorio e delle Costruzioni
Largo Lucio Lazzarino - 56122 Pisa (Italy)
Tel. +39 050 2217300 Fax + 39 050 2217333
Partita IVA 00286820501 VAT No. IT00286820501
Codice fiscale 80003670504

Reviewer #2

Thank you for your suggestions. Following your suggestions, we have considered your comments. In the attached highlighted version of manuscript, you can find the added parts according to your comments and our modification with blue and deleted phrases with red. You can also find the detailed response to your comments and related added or deleted phrases as follow:

COMMENT 1:

In heading it is mentioned energy recovering applications, as the paper deals with heat pipe only and since it can applied in many application therefore it is not necessary to mention energy recovery and no need for fig.1

ANSWER:

Thank you for your comment. We consider your comments and change the title of the manuscript as follow and Fig. 1 is deleted.

Added and revised sentences:

An experimental investigation and optimization of screen mesh heat pipes for low-mid temperature applications

COMMENT 2:

The effect of the cooling temperature, the orientation and the ratio of the evaporator length to the condenser length is investigated.

The effect of the cooling temperature was not investigated hence it can be omitted

ANSWER:

Thank you for your comment. We develop a section related the effect of cooling temperature as you can see in highlighted manuscript.

DESTEC
UNIVERSITÀ DI PISA
Dipartimento di Ingegneria dell'Energia, dei Sistemi, del Territorio e delle Costruzioni
Largo Lucio Lazzarino - 56122 Pisa (Italy)
Tel. +39 050 2217300 Fax + 39 050 2217333
Partita IVA 00286820501 VAT No. IT00286820501
Codice fiscale 80003670504

COMMENT 3:

Section 4.1 line 30 It is evidenced that at an input heat transfer rate of 400 W, the evaporator wall temperatures dramatically increase. This phenomenon can be explained by capillary limit.

I think it is burnout

As the heat flux is increased, the liquid in contact with the wall will become progressively superheated and bubbles will form at nucleation sites. These bubbles will transport some energy to the surface by latent heat of vapourisation and will also greatly increase convective heat transfer. With further increase of flux, a critical value will be reached, burnout, at which the wick will dry out and the heat pipe will cease to operate.

ANSWER:

Thank you very much for your interesting point of view. However, based on the results of mathematical model and comparison with experimental data, we consider this phenomena as capillary limitation and the capillary pressure needed in the wick to drive the flow, as the heat flux is not so much (400 W). Therefore, we consider the determined the dryout limitations of the heat pipe due to capillary limitation.

COMMENT 4:

A modeling approach to optimize the performance of the horizontal HP for heat exchanger application.

modify the sentence as follows:

A modeling approach to optimize the performance of the horizontal HP for several applications including heat exchanger

ANSWER:

Thank you for your comment. We consider your comment and modify the sentence accordingly.

Added and revised sentences:

For particular applications involving low to medium operating temperature, this study investigates the screen mesh wick HPs structural parameters as well as its operating parameters both analytically and experimentally.

An experimental investigation and optimization of screen mesh heat pipes for low-mid temperature ~~energy recovering~~ applications

Davoud Jafari[1,*], Hamidereza Shamsi[2], Sauro Filippeschi[1], Paolo Di Marco[1], Alessandro Franco[1]

[1]*Department of Energy, Systems, Territory and Constructions Engineering (DESTEC), University of Pisa, Italy*

[2]*Department of Energy Engineering, Sharif University of Technology, Tehran, Iran*

Abstract

The perspectives of utilization of a screen mesh heat pipe~~s~~ (HP) for low to medium operating temperature~~s in heat recovery~~ applications are studied in ~~the~~ *this* ~~present~~ study. A two-dimensional mathematical model for heat and mass transfer of HPs is presented to define its performances under steady state operations. The ~~thermal-fluid~~ model *couples heat conduction in* ~~includes~~ the wall~~,~~ *with* ~~and~~ both liquid *flow in the wick* and vapor flow *in the core~~s based on the physical and material properties of the pipe, wick and working fluid.~~* Experimental analysis has been developed to ~~determine the operating condition to~~ evaluate the *influence* ~~effect~~of ~~the~~ *operating parameters (the* orientation *and~~,~~* the cooling temperature*) as well as* ~~and~~ the evaporator section length on the performance of the HP. Furthermore, a modeling approach to optimize the HP performance from a thermal point of view is presented. Using the heat transfer capability and total thermal resistance as the objective function and the structure parameters as the decision variable, the optimization design for the HP is performed using the Non-Dominated Sorting in Genetic Algorithms-II (NSGA-II). *The results show* ~~It is found~~ that the optimal wick thickness and wick permeability to be a strong function of the heat flux. *It is concluded that to have lower thermal resistance at lower heat fluxes for a screen mesh wick HP may have a large effective thermal conductivity, but have a small permeability. While at high heat transfer rate a small effective thermal conductivity, but a large permeability is recommended. The designer must always make trade-offs between these competing factors to obtain an optimal wick design.* The investigations are aimed to determine working limits and thermal performance of HPs for low to medium *operating* temperature ~~heat recovery~~ applications.

Keywords:

Heat pipe~~, capillary limit~~, experimental analysis, optimization*, thermal resistance, maximum heat transport capability*

Nomenclature

C	Specific heat (J/kg K)	x	axial coordinate (m)
D	Diameter (m)	***Greek symbols***	
d_w	Wire diameter (m)	θ	*relative temperature (°C)*
F_k	*Nonempty front*	ε	Porosity
~~*H*~~*hfg*	*Heat of vaporization* ~~Heat transfer coefficient~~ (~~W~~J/~~m~~^{2}~~K~~*kg K*)	$\boldsymbol{\upsilon}$	Kinematic viscosity (m^2/s)
I	Individual	ρ	Density (kg/m^3)
I_e	*Current (A)*	μ	Dynamic viscosity (Pa s)
K	Permeability	σ	surface tension (N/m)
k	Thermal conductivity (W/mK)	α_c	*Crowded comparison operator*
L	Length (m)	η	*Thermal efficiency*
$\dot{m}$	Mass flow rate (kg/s)	***Subscripts***	
N	Mesh number	a	Adiabatic
n_o	*Number of objectives*	ave	Average
n_p	*Size of population*	*b*	*Boiling*
P	Pressure (Pa)	c	Condenser
P_c	Capillary pressure (Pa)	e	Evaporator
q	*Heat flux (W/m^2)*	eff	Effective
Q	Heat transfer rate (W)	i	Inner
R_{tot}	*Total thermal resistance (K/W)*	in	Inlet
R	*Radius (m)*	l	Liquid
r	radial coordinate (m)	out	Outlet
r_c	Effective capillary radius (m)	*s*	*Solid*
r_n	Critical nucleation site radius (m)	*tot*	*Total*

S	Crimping factor	v	Vapor
T	Temperature (K)	w	Wick
t	Thickness (m)		
u	Axial velocity (m/s)		
V	Voltage (V)		
v	Radial velocity (m/s)		

1. Introduction

Energy use has become a crucial concern in the last decades and *the* improvement of energy efficiency is very important in various sustainable renewable energy technologies. The majority of thermal energy in ~~heat recovery and~~*various* energy conversion system applications is at low to medium operating temperature (50-120°C)~~. Although low temperature heat recovery applications have less thermal value than high temperature applications, it is available in large quantities, as it was reported that the most unrecovered waste heat (about 60%) is at low to medium operating temperature~~ [1]. ~~Low temperature renewable heat resources, such as geothermal and solar energy, are also huge in quantity all over the world. Basing on~~*With regard to the* heat transfer point of view, the magnitude of the temperature difference between the heat source and *heat* sink is an important factor ~~of~~ *on the* thermal performance. The problems connected with the limitation~~s~~ on the maximum temperature, *the* temperature difference and the level of temperature uniformity must be solved for the thermal management of various heat exchanger systems. ~~To recover the waste heat, it is desirable to have a passive method to convert the thermal energy.~~ Heat pipes (HPs) as one of the excellent *two-phase* passive thermal transfer devices, ~~can~~ have effective thermal conductivities orders of magnitude higher than ~~that~~ *those* of *similarly-dimensioned* solid materials [2]. *Thus, their integration into heat exchangers has been shown to have strong potential for energy saving.* ~~The field of application of low to medium temperature HPs is wide enough. The integration of HPs into heat exchangers has been shown to have strong potential for energy savings which design goals are to maximize heat transfer rates while minimizing the overall thermal resistance~~. *The field of application of HPs in low to medium operating temperature is wide enough [3,4], including* ~~A HP for a heat exchanger application includes~~, but not limited, ~~to~~ heating, ventilation and air conditioning (HVAC) systems

[53], automotive cooling systems [64], photovoltaic/thermal systems [75], power plant cooling tower systems [86], solar water heating [79,108] and phase change material to store thermal energy *storage* systems [911]. In the proposed systems, as shown in Fig. 1, despite insertion of a device (HP) between heating and cooling external flows, a HP heat exchanger can provide higher heat transfer rates compared to a conventional heat exchanger. A factor contributing to the higher heat transfer rates of HP heat exchangers is due to the forced convection between the hot and cold streams and the evaporator sections of the HPs [10]. The advantage of using HPs in heat exchanger applications includes multiple redundancies (each pipe *HP* operates independently so unit is not vulnerable to a single pipe *HP* failure), low fouling, ease of cleaning and maintenance, isothermal operation (no hot or cold spots), low working pressure drop and highly scalable and configurable *[12,13]*.

The design of HPs *for a particular application* needs of careful consideration. Several modeling approaches [11-13] and experimental analysis have been. *have been reported from a simple lumped model [14] to a transient multi-dimensional simulation [15]. However, a steady state thermal performance prediction is of significant value in the design of HPs [16,17]. Among others, Vafai and Wang [18] developed a modeling approach for the heat and mass transfer analyses in a flat HP. They applied Darcy's law to verify the liquid flow in the wick and assumed a parabolic vapor velocity profile to obtain the axial vapor pressure distribution. With the same approach, Vafai et al. [19] presented a numerical simulation in a disk shaped HPs. Zhu and Vafai [20] extended the work of Vafai et al. [19] considering inertial effects on the liquid flow in the HP wick section. As the most commonly operating limitation to the performance of a HP for low to medium temperature application appears to be capillary limit [2,12,13], researchers investigated this problem. Among others, Lefevre and Lallemand [21] developed a steady state analytical model considering both liquid flow in the wick and vapor flow to analyze thermal behavior of a flat miniature HP as well as prediction of the maximum heat transfer capability. Rice and Faghri [22] developed a numerical model considering the liquid flow in the wick to investigate thermal performance of screen mesh HPs. They show that the capillary dryout limitations can be predicted for a given heating load in their simulations. Aghvami and Faghri [23] presented a steady state model including both liquid and vapor flows to investigate thermal and hydraulic behavior of flat HPs. They investigated capillary pressures for given heat inputs to determine the dryout limitations. Shabgard and Faghri*

[24] extended the above modeling approach to cylindrical HPs. They coupled two-dimensional heat conduction in the HP's wall with the liquid flow in the wick and the vapor hydrodynamics. Among above presented models Vafai and Wang [18], Vafai et al., [19] and Zhu and Vafai [20] did not considered axial heat conduction in the HP's wall while Shabgard and Faghri [24] found that neglecting the axial heat conduction through the wall resulting in overestimated pressure drops up to 10%.

In reviewing the recent experimental investigations on design variables and operating parameters of HPs, it is apparent that the geometric properties of the wick structure, such as the wick thickness and porosity should always be carefully considered [25-33]. Furthermore, operating parameters such as filling ratio, cooling temperature, input heat flux and orientating could be important factors affecting thermal performance of the HP [34-40] as well as its evaporation to condensation length ratio [41-43]. Brautsch and Kew [25] studied heat transfer process of stainless steel mesh HPs using water as working fluid. They showed that maximum heat flux increases with wick thickness but also increases thermal resistance. Li et al. [26] and Li and Peterson [27] investigated the influence of varying wick thicknesses, porosities, and pore sizes on thermal resistance and critical heat flux of a horizontal copper surface sintered with multiple layers of copper mesh. They illustrated that the evaporation/boiling is strongly dependent on the wick thickness, however, it is weakly dependent on porosity. Kempers et al. [28] investigated the effect of the wick thickness on the heat transfer performance of screen mesh wick HPs using water as the working fluid. They observed that there is a small increase in thermal resistance when increasing the wick thickness; however, the maximum heat transfer also increases. Wang and Peterson [29] investigated a sintered copper screen mesh flat HP to examine its maximum heat transport capacity. They concluded that increasing the structural thickness increased the thermal resistance, but it enhanced heat transfer capacity. Wong and Kao [30] investigated screen mesh HPs using ether as working fluid at different mesh wicks, fluid charges and heat loads. They found a partial dryout at small filling ratio and boiling in the larger water/wick thickness. Weibel et al. [31] analyzed the dependence of thermal resistance on the thickness of sintered powder wicks surfaces. They showed a trade-off between the increased area for heat transfer and increased thermal resistance. Brahim et al. [32] investigated screen mesh HPs and showed that the mesh number is an important factor which affects the overall thermal performance of the system. Tsai and Lee

[33] investigated the effects of structural parameters on the evaporation heat transfer in sintered wick HPs. They suggested thinner structural thickness to enhance evaporation heat transfer. Among operating parameters affection on thermal performance of HPs, the tilt angle have a considerable impact by assisting (the condenser section above the evaporator section, e.g. gravity-assisted) or suppressing (the evaporator section above the condenser section, e.g. gravity-opposed) the return of the working fluid. However, the sensitiveness to the orientation is much different for various wick structures [2]. A number of investigations have been shown that the thermal performance of groove type wick HPs significantly depend on the orientation [36] while a much smaller impact has found in sintered wick HPs [37]. Some other researchers [29] indicated that the maximum heat transport capacity of screen mesh wick is reduced by increasing the tilt angle while the performance of the sintered mesh wick is better than the screen mesh one because of the higher effective thermal conductivity. Kumaresan et al. [38] showed that the increasing of angle of inclination of the sintered wick HP improves the HP condensation heat transfer by 30% at 45° orientation in comparison of the horizontal position. However, tilt angles close to vertical position results in deterioration of performance. Sadeghinezhad et al. [39] recently showed the orientation of a sintered wick HP has a major influence on its thermal efficiency, in which gradually increases with the inclination angle up to 60° and then decreases, while Li and Lv [40] have not found a major influence of title angle on the thermal resistance of a flat HP from 45° to vertical position, however it was lower than horizontal position. With regard to impact of the ratio of the evaporator length to the condenser length on the thermal performance of HPs, Wang et al. [41] investigated the effect of evaporation and condensation length on thermal performance of flat HPs. They showed that dryout would occur at a lower heating power for a longer condensation section length and thermal performance is better at equal lengths of the condensation and evaporation sections. Liang and Hung [42] found that the optimal evaporator length to condenser length ratio of the sintered HP depends on other geometrical parameters such as its diameter. Chen and Chou [43] investigated the effects of length (80 mm-300 mm) on the thermal performance of flat HPs. They showed that an increasing of the length from 80 mm to 300 mm increases the overall thermal resistance of the HP while the maximum heat transport capability decreases.

The above studies indicate that thermal performance and maximum heat transfer capacity of HPs strongly depending on the geometry and the capillary structure. A good HP is characterized by a low thermal resistance and a high dryout tolerance. Thus, optimization approaches help to better understand of optimal structural parameters in the design of HPs. ~~Thus, it is necessary to perform a methodology to improve the heat transfer capacity and to reduce the thermal resistance of HPs.~~ To optimize the heat transfer performance of HPs, ~~in 2003,~~ Kim et al. [~~20~~*44*] proposed a *one-dimensional* mathematical model in a grooved wick HP to maximum heat transport rate and the overall thermal resistance. *Their model included the effects of the liquid–vapor interfacial shear stress, the contact angle, and the amount of initial liquid charge.* ~~They estimated that the maximum heat transport rate of outer diameter 3 and 4 mm HPs can be enhanced up to 48% and 73%, respectively by optimizing the groove wick structure. In 2004,~~ Sousa et al. [~~21~~*45*] proposed *generalized extremal optimization (GEO) approach*~~a method~~ to optimize the thermal performance of a HP for a space engineering application by minimizing *its*~~the~~ total mass~~ of the HP.~~ *The method is a global search meta-heuristic, as the Genetic Algorithm (GA), but with a priori advantage of having only one free parameter to adjust. The results showed that the GEO algorithm is a good candidate to be incorporated to the designer's tools. With the same optimization approach (GEO), Vlassov et al. [46] optimized the mass characteristics for a grooved wick HP for space application for different operational modes. They concluded that the proposed optimization approach can be effectively applied to complex optimal design problems.* ~~In 2005,~~ Rao and More [~~22~~*47*] presented an optimization algorithm, ~~(~~Teachinge Learning-Based Optimization *(TLBO),* ~~)~~to optimize Ω-shaped grooved HP. They considered the maximizing of the heat transfer rate and minimizing the resistance of a HP as objective functions. *They compared results of application of TLBO algorithm for the design optimization of HPs with other optimization approaches (Niched Pareto Genetic Algorithm (NPGA), Grenade Explosion Method and GEO) and found that proposed algorithm produces better results in improvement of heat transfer rate and total thermal resistances.* ~~In 2009,~~ Zhang et al. [~~23~~*48*] utilized the *NPGA*~~niched Pareto genetic algorithm~~ based approach to optimize an axial Ω-shaped micro grooves HP. *They performed the HP optimization design regarding the heat transfer capability and total thermal resistance as the objective function and the structure parameters as the decision variable. They concluded that the optimal set of solution can be used as an optimal*

design for a given application. ~~They conclude that a larger groove number and vapor core diameter could be enhanced the heat transfer capability. In 2011, Liang and Hung [24] experimentally investigated and optimized the thermal performance of a U-shape HP~~. ~~They showed that the optimal evaporator to condenser length ratio dependents on the pipe diameter.~~ To the best of authors' knowledge, although there are some papers presented on the optimization of grooved wick HPs, there is no study available in the literature on the optimal design of a screen mesh HP considering both the heat transfer capability and the total thermal resistance.

~~Among the others, in 1991, Faghri and Buchko [14] experimentally and numerically investigated the dryout limit of cylindrical screen wick HPs by increasing heat load in several arrangements. In 1993, El-Genk and Huang [15] experimentally investigated the transient response of a HP (screen mesh) at different input powers and cooling rates.~~ ~~In 2008, Wong and Kao [17] experimentally investigated screen mesh HPs using ether as working fluid. In 2010, Lips et al. [18] experimentally analyzed the effect of filling ratios, heat fluxes and vapor space thicknesses on a flat plate HP.~~

~~Despite optimization of HPs is very useful for advancement in the heat transfer performance, the optimal design of HPs rarely studied.~~ *All in all, the paper review with respect to the experimental and analytical studies on screen mesh HPs, as well as relevant optimization methodologies is insufficient.* The main concern of the proposed research is to verify the operation of a screen mesh HP under different operating conditions and design variables for a given wick size and to optimize its thermal performance by maximizing the heat transfer capability and minimizing the thermal resistance. In a first step, a steady state model of the HP is presented for a quick check on the estimated performance and to optimize ~~such devices~~*their heat transfer capacity* at horizontal position. In this model the ~~two~~ *two*-dimensional variations of the wall temperature and the Darcian effects for the liquid flow through the porous wick are *considered*~~taking into account~~. Additionally, as the mathematical modeling could not predict the thermal performance and operating limitation of HPs at all the operating conditions *(e.g. the orientation)*, a specific experimental setup has been designed~~, aimed~~ to not only validate the HP model at medium operating temperature, but also to understand the combined effect of the orientation and the evaporator length. In order to optimize the thermal performance of the HP, a Non-dominated ~~sorting~~ *Sorting* ~~genetic~~ *Genetic* ~~algorithm~~ *Algorithm* NSGA-II based is proposed. The *design*~~structure~~

parameters are selected as the decision variables including ~~(~~*the* evaporator length, *the* condenser length, *the* wick thickness and *the* porosity~~)~~. *The optimization results are evaluated to verify how the wick thickness and the porosity as well as the evaporation length to the condensation length ratio impact on the thermal performance of screen mesh HPs at a heat input to operate at the lowest thermal resistance.*

2. *Description of the* HP ~~operating principles~~ and design variables

As shown in **Fig. *1*~~2~~**, the components of a HP include pipe wall and end caps, a wick structure and a small amount of working fluid. The length of a HP is divided into three parts: the evaporator, *the* adiabatic and *the* condenser~~ sections~~. *A HP operates when heat externally is applied to the evaporator section, conducting through the wall, which causes vaporization of the working fluid.*~~Applying heat externally to the evaporator section, conducting through the wall causes to vaporizing the working fluid.~~ The vapor pressure drives the vapor through the adiabatic section to the condenser, and then the vapor condenses, releasing its latent heat of vaporization to the heat sink. In a HP, the capillary pressure created in the wick pumps the condensed liquid back to the evaporator section. Therefore, the HP can transfer the latent heat of vaporization from the evaporator to the condenser section as long as there is a sufficient capillary pressure to drive the condensate back to the evaporator *[2]*.~~The design of the HP is not an easy task as the most appropriate HPs needs to be selected for a particular application, and the following needs to be considered.~~ There are several important factors affecting HP performance: the working fluid, the wick structure, the material, the dimension, the orientation, the filling ratio, the operating temperature and the input heat flux. The diameter and the length need to be considered for designing HPs. *Larger diameter of the HP allows higher vapor volume to be moved from the evaporator to the condenser which is direct function of the heat pipe limits e.g. sonic and entrainment.* ~~as affect the rate of the vapor moves from evaporator to condenser due to vapor pressure differences.~~ The ratio of the evaporation section to the condensation section is one of the geometric characteristics which affects on the thermal performance of HPs with controlling the resistance. *The filling ratio, which defines as the ratio of the working fluid volume to the wick portion volume of the HP, also needs to be considered. Usually, the HP filling is over the optimum requirement (wick is completely saturated). A small filling ratio decreases the maximum heat*

transfer capacity while overfilling leads to a higher thermal resistance [12, 13]. A small filling ratio causes dryout at the evaporator while large filling ratios lead to flooding at the condenser [49]. Generally, it is better to overfill than to under-fill the HP [2].

The performance of a HP under specific orientations is directly related to its wick structure. The wick structure is the function of HPs as it is returned the condensate to the evaporator section. The appropriate ~~choice~~ *selection* of a screen mesh structure for a HP is based on material compatibility and performance. The effective capillary radius (r_c), *the* permeability (K_w), *the* effective thermal conductivity (k_{eff}) and the wick thickness are the most important parameters to select *the* wick structure and *to* determine the *thermal* performance of the HP. The relation of the screen mesh HP wick design is described in **Table 1.**

A screen mesh structure with a small effective capillary radius and a large effective thermal conductivity may have a small permeability. Therefore, the selection of these competing factors to obtain an optimal wick design is an important point of view. Another important parameter is the wick thickness. The thickness of the wick determines the cross sectional area for fluid transport from the condenser to the evaporator. A *HP containing* thicker wick *has* ~~results in~~ a lower pressure drop in the condensate flow, but ~~result in~~*has* a higher thermal resistance for *the* heat transfer between the wall and the pipe core. *Based on above discussion, for applications involving low to medium operating temperature, the investigation of the screen mesh wick structural parameters of HPs is important in its design.* ~~As not every HP is suitable for all applications, the combination of mentioned design variables need to be selected for designing HPs to have a high performance of system for a specific application, here in for low to medium temperature applications.~~

3. Methodology

~~Design goals for applying HPs in a thermal system are to maximize the heat transfer rates while minimizing the overall thermal resistance.~~ The methodology applied in this study is based on both mathematical modeling and experimental analysis, as described in following subsections.

3.1. Mathematical model of the HP

The geometry of the cylindrical HP is shown in Fig. 2. The proposed model includes thermal-fluid phenomena occurring within a HP: (1) heat conduction in the wall, (2) liquid flow in the wick, (3) vapor flow in the core region and (4) interaction between the liquid and vapor flows. *The wall of the HP has a material with thermal conductivity of k_s and its thickness is equal to t_w (r_o-r_i). The capillary structure is modeled by considering a porous medium of permeability K and heat conductivity k_w. The liquid along the porous medium has a dynamic viscosity μ_l, a heat conductivity k_l and a density ρ_l. The equivalent conductivity of both the liquid and the porous medium is equal to k_{eff}. The vapor space radius is equal to r_v, and kv and μ_v are the vapor heat conductivity and dynamic viscosity, respectively.* Two-dimensional heat conduction in the wall is coupled with the one-dimensional heat conduction in the wick (radial) based on approach used in [~~13~~*21, 23, 24*]. The assumptions in the analysis are steady state, incompressible and laminar flow, a saturated wick, constant properties and saturation temperature, and linear temperature profile across the thin wick structure *[19-21, 23, 24]*.

Table 2 summarizes the governing equations of different sections of the HP and related boundary conditions. The two-dimensional steady state heat conduction equation considering constant thermal conductivity is applied in the wall (Eq. ~~6~~*5*). Linear partial differential equations are solved for boundary condition *proposing*~~by applying~~ the separation-of-variable method [~~28~~*50*]. ~~by applying solution of modified Bessel functions~~. To introduce homogeneous wall-wick boundary condition θ is considered as T-T_v . The boundary conditions at the end caps (Eq. ~~7~~*6*) and at the outer wall *include* ~~depending on the sections:~~ constant heat fluxes in the evaporators (Eq. ~~8~~*7*), convection in the condenser (Eq. ~~9~~*8*) and the heat flux equal to zero in the adiabatic section (Eq. ~~10~~*9*) ~~are applied~~. Linear temperature profile across the wick structure and constant saturation temperature at the liquid-vapor interface is considered at wall-wick interface (Eq. ~~11~~*10*). Concerning the method of separation of variables, the Eq. ~~6~~ *5* is solved to determine the wall temperature *(see Appendix A)*. The continuity equation for the incompressible liquid flow (Eq. ~~12~~*11*) and Darcy's law (one-dimensional steady-state conservation of momentum, Eq. ~~13~~*12*) is used for the liquid flow in the porous wick. Where ~~μ is dynamic viscosity,~~ u_l is the average axial velocity of the liquid phase divided by the overall volume which is obtained by integrating the continuity equation with respect to r. One observation that can be made about this expression is that the pressure drop is inversely proportional to the product of the permeability and the wick thickness. If the permeability of

the wick is increased, then the thickness can be reduced, and this in turn will reduce the temperature drop across the wick. The interfacial velocity (v_l) at wall-wick interface equal to zero and v_l at the wick-vapor interface is define by the heat flux at liquid-vapor interface (Eq. ~~14~~*13*). The liquid pressure can be obtained by considering the solution obtained from heat conduction in the wall. The average liquid velocity can also be obtained according Darcy's law when the axial gradient of pressure is calculated. The governing equations for the continuity equation (Eq. ~~16~~*15*) and the momentum equations (~~17~~*16*) are described to determine vapor velocity and pressure in the vapor space of the HP. ~~For t~~*T*he boundary conditions *include~~,~~ the no-slip condition for velocity* at the end caps of the HP~~: the no-slip condition for velocity is applied~~ (Eq. ~~18~~*17*), ~~at the centerline: the radial gradient of the axial velocity is equal to zero (Eq. 19)~~ and at the vapor-wick interface the no-slip condition is in effect (Eq. ~~20~~*19*). *At the centerline, the radial gradient of the axial velocity is equal to zero (Eq. 18). Details of using the method of separation of variables to solve the treatment of energy equations (Eq. 5) to verify the axial temperature distribution, the continuity equation (Eq. 11) and Darcy's law (Eq. 12) to obtain the axial gradient of pressure and the average liquid velocity along the wick portion and the conservation equations for mass (Eq. 15) and momentum (Eq. 16) to yield vapor velocity profile and the axial vapor pressure distribution describe in Appendix A.* ~~A parabolic velocity profile is considered for the vapor flow and at the liquid-vapor interface a mass balance is applied for interfacial vapor and liquid velocities.~~

A MATLAB platform is used to discretize the governing equations, the number of terms to solve the problem is considered as 300 points and independency of the analytical results from the number of terms was tested.

3.2. Experimental setup

A specific experimental *setup* is developed to analyze the thermal behavior and operating limitation of the HP at horizontal orientation. The tested HP *is*~~were~~ characterized using the experimental facility shown in **Fig. 3**. The HP has the outer/inner diameter of 35/33 mm and the length of 500 mm (*the* evaporator length*s* of *75 mm, 150 mm,* 225 mm *and 300 mm* and *the* condenser length of 150 mm). The HP is made by *smooth* copper *pipe where it is closed at the ends with two 3 mm thick copper caps consisting of*~~contains~~ three layers of stainless steel screen mesh (100 mesh/inch) with a wire diameter of 0.114 mm. Experiments ~~were~~ *are* performed ~~for HPs~~*with a*

fluid charge ~~that included fluid charging~~ of 45 ml of degassed, ultra-pure water *which this corresponded to a filling ratio of 115%. The amount of charged water is enough in order to ensure that the wick completely saturated.* The evaporator section is uniformly heated using silicon type thermofoil heater (model MINCO HK5488R17.2L12A) clamped to the HP and the power input is supplied by a DC Power supply (Agilent DC6575A) which has an accuracy of ±1 percent of reading. In the condenser section, heat is convectively removed by water extracted from a cooling bath (HAKKE F-3C DIN 58966), by means of a 150 mm long copper manifold mounted around the HP. The constant-temperature bath is set to the required temperature and held at a constant-temperature (25 *°C*, 55 *°C* and 85 ˚C) through the tests. An electromagnetic flow meter (Siemens SITRANS F M MAGFLO5000) ~~allows~~ measure*s*~~ment~~ the mass flow rate of the cooling water with an accuracy of about 1%. ~~The~~ *Two* thermocouples *(K-type stainless steel probe)* in the manifold inlet and *the* outlet and *the* mass flow measurement allow to calculate the power output from *the* condenser section, and to compare it to the input electrical power. All the HP wall temperatures ~~were~~ *are* measured using eleven T-type thermocouples, which have been calibrated with an accuracy of ±0.2˚C. All the signals to monitor HP temperature*s* and cooling mass flow rate*s* are acquired by the Agilent HP32790 data acquisition system, and stored in a computer. *During the tests, heaters and blocks as well as adiabatic and condenser sections are covered with several layers of polymer insulation to minimize heat losses. Energy balances between the heat input by the electrical heaters and the heat removed by the sinks is monitored to ensure an energy balance within 90 percent in the worst case. Prior to the recording of any test data, the test facility allows to reach the steady state, defined as the point at which the temperature reading for any thermocouple varied by less than 0.5°C over a period of fifteen minutes.*

3.3. Optimization modeling approach

The maximization of heat transfer capability and the minimization of temperature difference between *the* evaporator and *the* condenser of the HP are selected as the objective functions in this study. The wick thickness (t_w), porosity (ε), evaporator length (L_e) and condenser length (L_c) are selected as decision variables in the

optimization process. **Table 3** and **Table 4** show the variable and fix design parameters chosen to perform the present analysis. Using these criteria, the optimization problem ~~can be~~ simply formulates~~d~~ as:

$Q=(t_w, \varepsilon, L_e, L_c)$ and $R_{tot}=(t_w, \varepsilon, L_e, L_c)$ (~~21~~*20*)

The first real problem for design*ing* a HP is to avoid operating limitation. HPs are very sensitive to their operational limitations such as capillary limit, boiling limit, entrainment limit, viscous limit and sonic limit. ~~In low to medium temperature applications, the screen mesh HP has very interesting features as a capillary structure.~~ The capillary limit consists in the fact that, for a HP to operate properly, the net pressure drop must be greater than the capillary pressure which is derived from the Laplace-Young equation ($\Delta P_c=2\sigma_l/r_c$), where σ_l is liquid surface tension and r_c is effective capillary radius of the evaporator wick. Therefore, the capillary pumping capability of the wick is based on some average effective pore radius for the wick. The boiling limit means the initiation of bubble generation inside the wick structure, and it may result in a locally burn out if the bubbles are trapped inside the wick. At higher applied heat flux, nucleate boiling may appear in the wick structure. At steady state operations, an expression for the heat flux beyond which bubble growth will occur may be developed by [~~29~~*12*]:

$$Q_b = \frac{2\pi L_{eff} k_{eff} T_v}{\rho_v h_{fg} \ln(r_i/r_v)}(2\sigma_l/r_n - \Delta P_c) \quad (~~22~~21)$$

where L_{eff} is the effective length, T_v is the vapor temperature, and r_v and r_i are *the* vapor core and *the* inner HP radius, and r_n is the critical nucleation site radius, which according to [~~30~~*13*] ranges from 0.1 to 25 μm for conventional metallic case materials. Therefore, to maximize heat transfer capability:

$$\begin{cases} Q < Q_b & (~~23~~22) \\ \Delta P_{l+v} < \Delta P_c & (23) \end{cases}$$

With regard to the fact that only one objective (maximum heat transfer capacity) is not sufficient to optimize performance of a HP. Therefore, multi-objective evolutionary algorithms (the maximization of the heat flux and the minimization of temperature difference) are ~~presented~~ *performed in* order to find the Pareto optimal set of individuals. In multi-objective ~~Pareto~~ optimal methodology, the set of all non-dominated solutions is considered as the Pareto optimal set, and the corresponding objective function values are named as the Pareto frontier. In

the present investigation, the Pareto optimal set and the corresponding Pareto frontier are achieved using the evolutionary algorithm based on the NSGA-II proposed by Deb et al. [~~31~~*51*]. Thanks to the fast HP mathematical model employed in this study, the large number of function evaluations usually required by the GA is not a limitation. The scheme of a NSGA-II ~~genetic algorithm~~*approach* is summarized in **Fig. 4**. The elements of the proposed approach includes: non-dominated sorting, crowding distance, selection and recombination and mating.

In this approach [~~31~~*51*], solutions of the first non-dominated front in a population ~~of~~ size (n_p) are defined by comparison of every other solution in the population to find if it is dominated. This requires ($n_p n_o$) comparisons for each solution, where n_o is the number of objectives. This process is continued to find all members of the first non-dominated level in the population which all individuals in the first non-dominated front are found. Here in n_p and n_o are 160 and 4, respectively (see **Table 5**). The individuals in the next non-dominated front can be found by discounting temporarily of the solutions of the first front and repeating the above procedure. The euclidian distance between each individual in a front based on their n_o objectives in the n_o dimensional space identifies by implementation of the crowing distance calculation. All the individuals in the population are assigned a crowding distance value as the individuals are selected based on rank and crowding distance. Crowding distance is assigned front wise as follow:

For all the individuals initialize the distance to be zero, $F_k(d_j) = 0$, where j corresponds to the j_{th} individual in k_{th} nonempty front (F_k). It should be noticed that for each objective function, sort the individuals in front based on objective and boundary values for each individual are assigned infinite value.

$$I(d_p) = I(d_p) + \frac{I(p+1)m - I(p-1)m}{f_m^{\max} - f_m^{\min}} \tag{24}$$

where $I(p)m$ is the value of the mth objective function of the pth individual in individuals *(I)*.

To do the selection and recombination, the selection is performed using a crowded comparison operator (α_c). The individuals in front F_k are firstly ranked as $p_{rank} = i$; afterward, from the crowding distance $F_k(dj)$, the ranks are compared using the comparison operator. The individuals are identified by using tournament selection with crowed comparison-operator. In applied method, a combination of an extrapolation method with a

crossover method is performed. It begins by randomly selecting a variable in the first pair of parents to be the crossover point.

4. Results and discussion

4.1. Results of analytical study

The experiments *are*~~were~~ performed with the HP in the horizontal position and the temperature measurements *are*~~were~~ taken in the axial length of HP at the steady state operation. In order to evaluate the thermal performance of the HP and validate the model at medium cooling temperature (85°C), the experiments are conducted for various heat loads (100 *W*, 200 *W*, 300 *W*, 350 *W* and 400 W). **Fig. 5** shows experimentally and analytically axial temperature distribution of *the* HP wall. The results indicate that the evaporator wall temperature rises with the increase of heat flux and the temperature distribution of the HP is uniform in the condenser and the evaporator sections. A comparison between the axial wall temperatures obtained from analytical model with the experimental data are in good agreement. It is evidenced that at an input heat transfer rate of 400 W, the evaporator wall temperatures dramatically increase. This phenomenon can be explained by capillary limit *[22]*. There is need to know the pressure drop in the wick to calculate the capillary limitations of a HP. For this deal the analytical methods used to determine the pressure drop, as presented in **Fig. 6**. It is evidenced that by increasing input heat transfer rate, the mass flow rate increases at the liquid-vapor interface by the increasing condensation of vapor*, resulting* ~~and causes to~~ *the* increase of pressure drop ~~considerably~~. **Fig. 7** shows the pressure drop predicted through HP by analytical model and the material properties of water which is substituted into ($\Delta P_c = 2\sigma_l / r_c$) for several vapor temperatures. ~~Concerning~~ *From the analysis of experimental data, it is observed that* ~~the experimental~~ *the reported maximum heat transfer capacity due to* capillary limit ~~reported in~~ ~~(~~**Fig.** ~~7~~***5)***, *has* ~~there is~~ good agreement with the analytical calculations ***(Fig. 7)*** *in which the maximum heat transfer rate obtains (350 W)*. Therefore, it is evidenced that the analytical approach can predict the maximum heat transfer rate of *the* HP ~~with good agreement in comparison of the experimental analysis~~ at mid-temperature operation (85°C).

4.2. Results of experimental analysis: effect of design variables

In this section, the effect of the evaporator length as well as operating parameters (the orientation and the cooling temperature) on thermal performance of the screen mesh HP is described. Several evaporation section lengths *(75 mm, 150 mm, 225 mm and 300 mm) and orientations (horizontal, 45° orientation and vertical)* are tested at the constant condenser length. *It would be noted that in the oriented position as well as vertical one the condenser section of the HP places at the top and the evaporator at its lower end (gravity assisted orientation).* **Figs. 8(a-c)** provide the axial wall temperature distributions of the HP for different evaporator lengths and orientations. As it is evidenced in all the orientations, the jumps in the maximum wall temperature ~~occurred~~ *occur* in shorter evaporator length and more effect observed for vertical position. *It is concluded that* ~~T~~*t*he ratio of the heat source length to the overall HP length is an important parameter controlling the resistance ~~to the spreading of heat from the evaporator to the condenser section~~.

The heat transfer behavior of a HP can be described by the overall thermal resistance analysis (R_{tot}) in which lower thermal resistance indicates better overall thermal performance. This is obtained by evaluating the temperature drop along the longitudinal direction of a HP for a heat transfer rate:

$$R_{tot} = \frac{T_{e,ave} - T_{c,ave}}{Q_{ave}} \qquad (25)$$

where $T_{,e,ave}$ and $T_{c,ave}$ are average evaporator wall temperature (depending on evaporator length) and average condenser wall temperature (T_{10} and T_{11}), respectively. The heat transport rate (Q_{av}) is calculated based on the principle of average of the heat dissipated from the condenser section (Q_{out}) and the input heat transfer rate by electrical heaters (Q_{in}):

$$Q_{out} = \dot{m} C_P (T_{out} - T_{in}) \qquad (26)$$

$$Q_{in} = VI \qquad (27)$$

where T_{in} , T_{out} and $\dot{m}$ denote the inlet and outlet water temperatures and the mass flow rate of the cooling jacket mounted surround the condenser section, respectively, V is the voltage and I is the current. The thermal resistance versus the evaporator length at heat transfer rate of 200 W is shown in ***Fig. 9*** *for different orientations (horizontal, oriented (45°) and vertical). It is clear that different orientations show a similar*

qualitative trend; the thermal resistance decrease as the evaporator length increases. Its major impact observes as the evaporator length increase from 75 mm to 150 mm at orientations of horizontal, oriented (45°) and vertical by decreasing of 31%, 44% and 48%, respectively. However, further increase of evaporator length has not significant effect on the thermal resistance of the HP at different orientations. Moreover, it is evidenced that effect of orientation is not significant at the same evaporator length. It could be concluded that the smaller ~~the~~ heat source has the higher maximum wall temperature (see ***Fig. 8****). As the heater size is reduced, the heat flux in the evaporator region increases and causes ~~to~~ a jump in the HP maximum wall temperature. It is because that the evaporation occurs in the evaporator section is more intense. This leads to increase the pressure difference between the evaporation and the condensation which is unbeneficial to assists the condensed liquid to flow back to the evaporation section. Thus, the temperature difference between evaporation and condensation increases and, therefore, the thermal resistance increases.*

The thermal efficiency (η) of the HP at different orientations and evaporator lengths is evidenced in ***Fig. 10****.*

$$\eta = \frac{Q_{out}}{Q_{in}} \times 1000 \qquad (28)$$

The lowest thermal efficiency observes for evaporator length of 75 mm (90.4%) and the highest thermal efficiency observes for evaporator length of 150 mm (98%). Based on experimental observations, it could be concluded that at the same operating condition (the cooling temperature, the orientation and the input heat transfer rate) with the increase of evaporation section length, the thermal resistance decreases while there is an optimal evaporator length in which the device shows a superior thermal efficiency.

~~Before introducing results of optimization of the HP, here in, the motivation of applying mid-temperature cooling temperature is presented.~~ *In order to investigate the effect of cooling temperature,* ~~A series of test has been performed on~~ a horizontal HP with evaporator length of 225 mm and cooling temperature of 25 *°C*, 55 *°C* and 85 °C *is tested*. **Fig. ~~9~~** ***11*** shows the total thermal resistances under changes of the cooling temperature*s* in the range of heat loads from 60 W to 350 W~~ at evaporator length of 225 mm and the fluid charge volume of 45 ml~~. According to the *presented* results~~ presented~~, the thermal resistance decreases with an increase in the condenser cooling temperature. *However, no significant difference is observed in the thermal resistance at*

higher heat transfer rate of cooling temperature of 55 °C and 85 °C. Such behavior could be explained by the fact that for a give heat flux, the vapor and liquid friction factor and simultaneously the vapor pressure drop and the liquid pressure drop along the wick portion decreases as the cooling temperature increases because of viscosity changes [~~32~~52].

~~Such behavior could be explained by the fact that the increase of cooling water temperature leads to the decrease of vapor and liquid friction factor which directly decreases the vapor pressure drop and the liquid pressure drop [32].~~ ***Fig. 12*** *also shows the related heat transfer rate dependences of the temperature of the evaporator wall. It is observed that a change in the condenser cooling temperature of a certain magnitude (30°C) does not always load to equivalent changes in the operating temperature of the HP. It means that temperature deference of evaporator walls are lower than temperature differences of cooling temperatures from 25 °C to 55 °C and to 85 °C. With an increase in the cooling temperature from 25°C to 55°C and from 55 °C to 85 °C the average HP wall temperature increases by 26.8 °C and 24.7 °C. Therefore, decreasing of the thermal resistance with an increase in the condenser cooling temperature (see* ***Fig. 11****) could be also explained by the fact that an increase in cooling temperature leads to a decrease in the temperature drop between the evaporator and the condenser, according to the presented results in* ***Fig. 12***. This shows the advantage of the use of hotter medium (water, air, etc.) for cooling the HP condenser when lower values of its thermal resistance are required in a practical application. ~~Therefore, in this study the cooling temperature of 85 °C is considered.~~

Bas*ed* ~~ing~~ on above experimental results, it is evidenced that the orientation has less effect on the thermal performance of the screen mesh HPs *while*~~and~~ the ratio of evaporator length and condenser length ~~is~~ *shows significant impact*~~effective parameter~~. ~~Also basing this fact that changing wick structure to investigate effect of wick thickness, porosity, etc. is difficult and time consuming following results would help to select the best design for a particular thermal control application.~~ *Therefore, in this study the effect of the evaporator length to condenser length ratio at cooling temperature of 85 °C is considered for optimization.*

4.3. Results of optimization approach

To find the best solution (the maximum heat transfer capability and the minimum temperature difference) for mid-*operating* temperature ~~heat recovery~~ applications (85˚C), A NSGA-II ~~based~~ approach ~~implemented~~ *performs* to solve the optimization problem of a screen mesh HP with the conditions shown in **Tables 4** and **5**. Based on the optimization method, the initial and final population distributions are illustrated in **Fig. ~~10~~*13***. The Pareto-optimal solution sets are given in **Table 6**. As shown in **Fig. ~~10~~*13***, the random initial population is distributed throughout the search space, and the ~~niched Pareto genetic algorithm~~ *NSGA-II* finds an apparent front after 120 generations. It is promising to see that in the final population there is a definite improvement. According to the different ~~heat recovery~~ application*s* at ~~low~~ mid-operating temperature, the designer must make a choice from the Pareto-optimal solution set as determined by the NSGA-II utilizing the requirements of the specific application. For example, as evidenced in **Table 6** for solution no. 12, there is no individual in the final population for which both Q>259.3W and R_{tot}<0.033 °K/W. It means that at selected heat flux, solution no. 12 represents the optimized design which it could be practical to design a HP heat exchanger for ~~low~~ mid-operating temperature.

Herein, a parametric study is presented based on obtained optimal set of solutions. ***Fig. 14*** *shows the optimal wire diameter and porosity of wick structure at different heating power. As it is evidenced, the optimization results indicated that with increasing heat transfer rate the wire diameter decreases to have lower thermal resistance. In contrast, the porosity should be decreases with increasing heat transfer rate to have an optimal case depending heat transfer rate. These two parameters simultaneously change the conductive and permeability characteristics of the wick structure. For example, with increasing of the wick porosity, the effective thermal conductivity decreases while permeability increases. Moreover, increasing wire diameter leads to increase of permeability. Thus, the effective thermal conductivity and permeability of wick structure need to be analyzed in optimal cases.* ***Fig. 15*** *indicates the optimal permeability and effective thermal conductivity of the HP at various heating power. As it is observed, the optimal permeability increase with increasing of heat transfer rate to have a small liquid pressure drop, and thus, avoiding capillary limit (see Table 6) while the optimal effective thermal conductivity decreases as heat transfer rate increases. Therefore, it is concluded that to have optimal case at lower heat fluxes for a screen mesh wick HP may have a large effective thermal*

conductivity, but have a small permeability. While at high heat transfer rate a small effective thermal conductivity, but a large permeability is recommended. The designer must always make trade-offs between these competing factors to obtain an optimal wick design.

The wick thickness is also a parameter impact on the determination of the thermal resistance of the HP, thus an optimal thickness is important to reach maximum performance. ***Fig. 16*** *shows optimum wick thickness for an applied heat flux and related liquid pressure drop along the wick. It is indicated that the wick thickness values increase with increasing of heat transfer rate. An increase of the layer of the mesh wick can reduce the liquid frictional pressure drop proportionally by increasing the liquid flow area, resulting in improved heat transfer capacity. However, the increase in the layer of the screen mesh results in significant increases in superheat through the wick layer, and therefore, in premature boiling limitations [29]. On the other hand, decreasing the wick thickness decreases the radial thermal resistance of the wick while the working fluid cannot be supplied efficiently to the evaporator, which causes dryout.*

Finally, the thermal resistance of a HP as well as maximum heat transfer capacity depends on the evaporator length to the condenser length, L_e/L_c *ratio. The* optimal L_e/L_c ratio and a function of wick permeability and wick thickness of the HP at various heating power ~~is~~ *are* shown in **Fig. ~~11~~*17***. *The motivation of presenting a function consisting both optimal wick permeability and wick thickness is that, as the wick thickness (See* ***Fig. 16****) and/or wick permeability (see* ***Fig. 15****) increase, the pressure drop decreases. Thus, an optimal relation of these two important parameters at a given heat flux could be useful to design a screen mesh wick structure for a particular application.* It is evidenced that the optimal L_e/L_c ratio for HPs is constant as about 1 while the function of wick permeability and wick thickness increase with increasing heat flux. It could be concluded that the *optimal* wick thickness and wick permeability ~~is~~ *are* a strong function of the heat flux. *The obtained optimal cases at equal lengths of the condensation and evaporation sections also affirms by experimental results in which highest thermal efficiency is obtained (see* ***Fig. 10****).*

5. Conclusions

For particular applications involving low to medium operating temperature, this study investigates the screen mesh wick HPs structural parameters as well as its operating parameters both analytically and experimentally. For this aim, a mathematical simulation, an experimental facility and optimization approach develop to measure and predict the maximum heat flux and thermal performance of HPs. A mathematical model is presented to study the steady state performance of *the* horizontal HP and also to predict *its* operating limitation and to optimize *its*~~the~~ thermal performance. *The model involves coupling two-dimensional heat conduction in the HP's wall with the liquid flow in the wick and the vapor hydrodynamics. A series of experiments performs to evaluate the heat transfer performance of the HP at different heat transfer rates, orientations, cooling temperatures and evaporator lengths as well as validation of analytical model in horizontal position at medium operating temperature. A NSGA-II optimization approach is introduced to maximize the heat transfer capability and to minimize the overall thermal resistance of screen mesh HPs. A modeling approach is conducted to optimize the structural parameters of screen mesh wick including wick thickness and porosity as well as evaporator length and condenser length of horizontally position HPs. The experimental investigations and the optimization results are analyzed and discussed and obtained results summarize as follow.*

The HP is tested in horizontal, 45˚ orientation and vertical position and at different evaporator length (75 mm-300 mm). From the experimental analysis of the HP, it is found the orientation does not show a very significant effect on the thermal performance of screen mesh HPs while the evaporator length shows a significant influence. It is found that at the same operating conditions, as the evaporator length increases the thermal resistance decreases while there is an optimal evaporator length in which the device shows a highest thermal efficiency. Investigation of the effect of cooling temperature also shows the advantage of the use of hotter medium (here in water) for cooling the HP condenser when lower values of its thermal resistance are required.

~~The optimal wick thickness and wick permeability is found to be a strong function of the heat flux. The results of the optimization analysis demonstrated in the present study serves as a useful designing tool for optimum thermal performance of HPs for the mid-low temperature heat exchanger applications.~~ *This study suggests that an improved thermal performance can be attained by having a large effective thermal conductivity, but having a small permeability at lower heat transfer rates while at high heat transfer rate a small effective thermal*

conductivity, but a large permeability. In conclusion, the optimal wick thickness and wick permeability finds to be a strong function of the heat flux. However, the designer must always make trade-offs between these competing factors to obtain an optimal wick design. The results of the demonstrated optimization analysis in the present study serve as a useful designing tool for optimum thermal performance of screen mesh HPs for the mid-low operating temperature applications.

~~A modeling approach to optimize the performance of the horizontal HP for heat exchanger application at mid-temperature operation is conducted. The heat transfer capability and total thermal resistance of screen mesh HPs are optimized and the effects of the design variables on the heat transfer capability and total thermal resistance are analyzed. To evaluate the heat transfer performance of the HP water used as a working fluid and the effect of the heat transfer rate, the orientation, the cooling water temperature and the evaporator length is experimentally investigated.~~

~~The HPs were tested in horizontal, 45˚ and vertical position. From the axial temperature distribution of the HP, it is found the orientation is not affecting parameter on the thermal performance of screen mesh HPs while the evaporator length shows a significant influence. Investigation of the effect of cooling temperature also shows the advantage of the use of hotter medium (water, air, etc.) for cooling the HP condenser when lower values of its thermal resistance are required.~~

~~A niched Pareto genetic algorithm is introduced to optimize the heat transfer performance. In the optimization, the design variables are selected as the decision variables and the optimization results are analyzed and discussed.~~

Appendix A. Mathematical treatment of conservation equations in the HP's wall, wick and vapor

Heat conduction in the wall

The two-dimensional heat conduction obtains by assuming linear temperature profile across the wick portion and constant saturation temperature at the liquid-vapor interface (Eq. 10) by employing the separation-of-variable method (Rohsenow et al., 1985)

$$\theta(r,x)=\sum_{m=0}^{\infty}\cos(A_m x)\{\omega_m[I_0(A_m r)+\eta_m K_0(A_m r)]\} \qquad (A.1)$$

where I_0 and K_0 are modified Bessel functions of the first and second kind of order zero, respectively, ω_m is unknowns which should be determined for every m and $A_m=m\pi L$ proposing the boundary condition (Eq. 7)

$$\omega_m=\frac{1}{-k_s\frac{L}{2}\{A_n[I_1(A_m r_o)-\eta_m K_1(A_m r_o)]\}}\left\{\int q_e\cos(A_m x)dx+h_\infty\sum_{i=0}^{\infty}\omega_i F_i+h_\infty(T_v-T_\infty)\int\cos(A_m x)dx\right\} \qquad (A.2)$$

where constants can be calculated for every given m. The system of m equations expressed in above equation is solved by use of the direct methods. When a sufficient number of ω_m are calculated, the temperature can be determined from Eq. A.1.

The liquid flow in the wick section

The axial liquid velocity is calculated by integrating Eq. 11 with respect to x and substituting v_l (Eq. 13) as

$$\frac{\partial u_l}{\partial x}=\frac{2q_e r_i}{\rho_l h_{fg}(r_i^2-r_v^2)} \qquad (A.3)$$

By Combining Darcy's law (Eq. 14) and Eq. A.3, the average velocity profile along the wick is calculated by obtaining the axial gradient of pressure

$$\frac{d^2P_l}{dx^2}=-\frac{2r_i\mu q_e}{\rho_l h_{fg}K(r_i^2-r_v^2)} \qquad (A.4)$$

The liquid pressure can be obtained by considering $q=-k_{wall}\partial\theta/\partial r$ and Eq. 5 as

$$\begin{cases}\dfrac{dP_l}{dx}=-\dfrac{2r_i\mu k_s}{\rho_l h_{fg}K(r_i^2-r_v^2)}\displaystyle\sum_{m=0}^{\infty}\sin(A_m x)\{\omega_m[I_1(A_m r_i)-\eta_m K_1(A_m r_i)]\} & (A.5)\\ P_l=-\dfrac{2r_i\mu k_s}{\rho_l h_{fg}K(r_i^2-r_v^2)}\displaystyle\sum_{m=0}^{\infty}\frac{\cos(A_m x)}{A_m}\{\omega_m[I_1(A_m r_i)-\eta_m K_1(A_m r_i)]\} & (A.6)\end{cases}$$

The average liquid velocity can be obtained according Darcy's law when the axial gradient of pressure is calculated.

Vapor flow in the core

A parabolic velocity profile is considered for the vapor flow [18, 20, 21].

$$u_v(r,x) = U_v(x)(\xi_1 + \xi_2 r + \xi_3 r^2) \tag{A.7}$$

where U_v is the local average velocity of the vapor and the constants (ξ_1, ξ_2 and ξ_3) are verified by applying the boundary conditions in Eq. 17 and Eq. 18 and the definition given in

$$U_v(x) = \frac{2}{r_v^2}\int_0^{r_v} r u_v dr \tag{A.8}$$

Thus, the vapor velocity profile define as

$$u_v(r,x) = 2U_v(x) - \frac{2U_v(x)r^2}{r_v^2} \tag{A.9}$$

By substituting Eq. A.9 in the continuity equation (Eq. 15) and integrating with respect to r, yields

$$r_v U_v'(x) + 2v_v = 0 \tag{A.10}$$

By considering this fact that at the interface, the vapor interfacial velocity is related to the liquid interfacial velocity by a mass balance ($\rho_v v_v = \rho_l v_l$) and using Eq. 13, the vapor interfacial velocity is verified as

$$v_v = \frac{q_e\big|_{r=r_i} r_i}{\rho_v h_{fg} r_v} \tag{A.11}$$

Considering $v_l = (q_e/\rho_l h_{fg})(r_i/r_v)$ and $v_v = (q_e/\rho_v h_{fg})(r_i/r_v)$ and integrating Eq. A.10 with respect to x the mean vapor velocity is calculated as follow

$$U_v(x) = -\frac{2r_i k_s}{\rho_v h_{fg} r_v^2}\sum_{m=1}^{\infty}\sin(A_m x)\{\omega_m[I_1(A_m r_i) - \eta_m K_1(A_m r_i)]\} \tag{A.12}$$

Finally, concerning boundary layer momentum equation along the vapor velocity profile, the axial distribution of the vapor pressure is obtained by neglecting the radial variation of the vapor pressure by

$$\nabla P = -\frac{16 r_i \mu k_s}{\rho_v h_{fg} r_v^4}\sum_{m=1}^{\infty}[1-\cos(A_m x)]\left\{\frac{\omega_m[I_1(A_m r_i) - \eta_m K_1(A_m r_i)]}{A_m}\right\} - \frac{8}{3\rho_v}\left\langle \frac{r_i k_s}{h_{fg} r_v^2}\sum_{m=1}^{\infty}\sin(A_m x)\{\omega_m[I_1(A_m r_i) - \eta_m K_1(A_m r_i)]\}\right\rangle^2 \tag{A.13}$$

References

[1] Incorparated BCS. Waste heat recovery: technology and opportunities in US industry. Department of Energy (US); 2008. [March].

[2] Faghri A. Heat Pipe Science and Technology. Philadelphia, PA: Taylor & Francis~~,~~ (1995).

[3] Jafari D, Franco A, Filippeschi S, Di Marco P, Two-phase closed thermosyphons: A review of studies and solar applications, Renewable & Sustainable Energy Reviews 53 (2016) 575–93.

[4] Shabgard H, Allen MJ, Sharifi N, Benn SP, Faghri A, Bergman TL, Heat pipe heat exchangers and heat sinks: Opportunities, challenges, applications, analysis, and state of the art, International Journal of Heat and Mass Transfer 89 (2015) 138–58.

[~~3~~*5*] Jadhav TS, Lele MM,~~.~~ Analysis of annual energy savings in air conditioning using different heat pipe heat exchanger configurations integrated with and without evaporative cooling,~~.~~ Energy 109 (2016) 876-~~8~~85.

[*6*~~4~~] Singh R, Mochizuki M, Nguyen T, Akbarzadeh A,~~.~~ Applications of heat pipes in thermal management and energy conservation, Front. Heat Pipes 2 (2011) 1–13.

[*7*~~5~~] Gang P, Huide F, Huijuan Z, Jie L,~~.~~ Performance study and parametric analysis of a novel heat pipe PV/T system,~~.~~ Energy 37 (2012) 384-~~3~~95.

[*8*~~6~~] Robertson AS, Cady EC,. Development and operational testing of a heat pipe dry cooling tower, *American Society of Mechanical Engineers*~~Am. Soc. Mech. Eng.~~ *80* (1980)~~. 80-JPGC/Pwr~~ 22.

[*9*~~7~~] Ayompe L~~.~~M~~.~~, Duffy A~~.~~, Mc Keever M~~.~~, Conlon M~~.~~, McCormack S~~.~~ J,~~.~~ Comparative field performance study of flat plate and heat pipe evacuated tube collectors (ETCs) for domestic water heating systems in a temperate climate,~~.~~ Energy 36 (2011) 3370~~e33-7~~8.

[*10*~~8~~] Azad E,~~.~~ Theoretical and experimental investigation of heat pipe solar collector,~~.~~ Experimental Thermal and Fluid Science 32 (2008) 1666–~~16~~72.

[11~~9~~] Amini A, Miller J, Jouhara H~~.~~, An investigation into the use of the heat pipe technology in thermal energy storage heat exchangers,~~.~~ Energy ~~xxx~~ (2016) 1-10.

[12] Peterson GP, Heat Pipes, Modeling, Testing, and Applications, John Wiley and Sons (1994).

[13] Reay DA, Kew P, Heat Pipes, 5th ed. Oxford, UK: Butterworth-Heinemann, (2006).

~~[10] Shabgard H, Allen MJ, Sharifi N, Benn SP, Faghri A, Bergman TL. Heat pipe heat exchangers and heat sinks: Opportunities, challenges, applications, analysis, and state of the art. International Journal of Heat and Mass Transfer 89 (2015) 138–158~~

[14] Zuo ZJ, Faghri A, A network thermodynamic analysis of the heat pipe, International Journal of Heat and Mass Transfer 41 (1998) 1473-84.

[15] Tournier JM, El-Genk M S, A Heat Pipe Transient Analysis Model, International Journal of Heat and Mass Transfer 37(1994) 753-62.

[~~14~~*16*] Faghri A, Buchko M,~~.~~ Experimental and numerical analysis of low-temperature heat pipe with multiple heat source,~~.~~ Journal of heat transfer 113 (1991) 728-34.

[17] Huang X Y, Liu CY, The pressure and velocity fields in the wick structure of a localized heated flat plate heat pipe, International Journal of Heat and Mass Transfer 39 (1996) 1325-30.

[18] Vafai K, Wang W, Analysis of flow and heat transfer characteristics of an asymmetrical flat plate heat pipe, International Journal of Heat and Mass Transfer 35 (1992) 2087-99.

[19] Vafai K, Zhu N, Wang W, Analysis of assymetrical disk-shaped and flat plate heat pipes, ASME Journal of Heat Transfer 117 (1995) 209-18.

[~~12~~*20*] Zhu N, Vafai K,~~.~~ Analysis of cylindrical heat pipes incorporating the effects of liquid-vapor coupling and non-Darcian transport- a closed form solution,~~.~~ International Journal of Heat and Mass Transfer 42 (1999) 3405-18.

[21] Lefevre F, Lallemand M, Coupled thermal and hydrodynamic models of flat micro heat pipes for the cooling of multiple electronic components, International Journal of Heat and Mass Transfer 49 (2006) 1375–83.

[22] Rice J, Faghri A, Analysis of Screen Wick Heat Pipes, Including Capillary Dry-Out Limitations, Journal of Thermophysics and Heat Transfer 21 (2007) 475-86.

[23] Aghvami M, Faghri A, Analysis of Flat Heat Pipes with various Heating and Cooling Configurations, Applied Thermal Engineering 31(2011) 2645-55.

[~~13~~*24*] Shabgard H, Faghri A,~~.~~ Performance characteristics of cylindrical heat pipes with multiple heat sources,~~.~~ Applied Thermal Engineering 31 (2011) 3410-9.

[25] Brautsch A, Kew PA, Examination and visualisation of heat transfer processes during evaporation in capillary porous structures, Applied Thermal Engineering 22 (2002) 815–24.

[26] Li C, Peterson GP, Wang Y, Evaporation/boiling in thin capillary wicks (I) – wick thickness effects, Journal of Heat Transfer 128 (2006) 1312– 9.

[27] Li C, Peterson GP, Evaporation/boiling in thin capillary wicks (II)-Effects of volumetric porosity and mesh size, Journal of Heat Transfer 128 (12) (2006) 1320–8.

[~~25~~*28*] Kempers R, Ewing D, Ching CY,~~.~~ Effect of number of mesh layers and fluid loading on the performance of screen mesh wicked heat pipes,~~.~~ Applied Thermal Engineering 26 (2006) 589–95.

[~~26~~*29*] Wang Y, Peterson GP,~~.~~ Investigation of a Novel Flat Heat Pipe,~~.~~ Journal of Heat Transfer 127 (2005) 165-70.

[~~17~~*30*] Wong SC, Kao YH,~~.~~ Visualization and performance measurement of operating mesh-wicked heat pipes,~~.~~ International Journal of Heat and Mass Transfer 51 (2008) 4249–59.

[31] Weibel JA, Garimella SV, North MT, Characterization of evaporation and boiling from sintered powder wicks fed by capillary action, International Journal of Heat and Mass Transfer 53 (2010) 4204–15.

[~~27~~*32*] Brahim T, Dhaou MH, Jemni A,~~.~~ Theoretical and experimental investigation of plate screen mesh heat pipe solar collector,~~.~~ Energy Conversion and Management 87 (2014) 428–~~4~~38.

[33] Tsai YY, Lee CH, Effects of sintered structural parameters on reducing the superheat level in heat pipe evaporators, International Journal of Thermal Sciences 76 (2014) 225-34

[~~15~~*34*] El-Genk MS, Huang L,~~.~~ An experimental investigation of the transient response of a water heat pipe,~~.~~ International Journal of Heat and Mass Transfer 36 (1993) 3823-30.

[3516] Kempers R, Robinson AJ, Ewing D, Ching CY,. Characterization of evaporator and condenser thermal resistances of a screen mesh wicked heat pipe,. International Journal of Heat and Mass Transfer 51 (2008) 6039–46.

[36] Russel MK, Young C, Cotton JS, Ching CY, The effect of orientation on U-shaped grooved and sintered wick heat pipes, Applied Thermal Engineering 31 (2011) 69-76

[37] Loh CK, Harris E, Chou DJ, Comparative study of heat pipes performance in different orientations, 21st IEEE SEMI-THERM Symposium (2005) 191-5.

[38] Kumaresan G, Venkatachalapathy S, Asirvatham LG, Experimental investigation on enhancement in thermal characteristics of sintered wick heat pipe using CuO nanofluids, International Journal of Heat and Mass Transfer 72 (2014) 507–16.

[39] Sadeghinezhada E, Mehrali IM, Rosen MA, Akhiani AR, Latibari ST, Mehrali M, Metsela HSC, Experimental investigation of the effect of graphene nanofluids on heat pipe thermal performance, Applied Thermal Engineering 100 (2016) 775–87.

[40] Li J, Lv L, Experimental studies on a novel thin flat heat pipe heat spreader, Applied Thermal Engineering 93 (2016) 139–46.

[41] Wang SF, Chen JJ, Hu YX, Zhang W, Effect of evaporation section and condensation section length on thermal performance of flat plate heat pipe, Applied Thermal Engineering 31(2011) 2367–73.

[2442] Liang TS, Hung YM,. Experimental investigation on the thermal performance and optimization of heat sink with U-shape heat pipes,. Energy Conversion and Management 51 (2010) 2109–2116

~~[19] Sukchana T, Jaiboonma C. Effect of Filling Ratios and Adiabatic Length on Thermal Efficiency of Long Heat Pipe Filled with R-134a. Energy Procedia 34 (2013) 298–306.~~

[43] Chen JS, Chou JH, The length and bending angle effects on the cooling performance of flat plate heat pipes, International Journal of Heat and Mass Transfer 90 (2015) 848–56.

[2044] Kim SJ, Seo JK, Do KH,. Analytical and experimental investigation on the operational characteristics and the thermal optimization of a miniature heat pipe with a grooved wick structure,. International Journal of Heat and Mass Transfer 46 (2003) 2051–2063

[2145] Sousa FL, Vlassov V, Ramos FM,. Generalized extremal optimization: An application in heat pipe design,. *Applied Mathematical Modelling*Appl. Math. Modelling 28 (2004) 911–931.

[46] Vlassov VV, de Sousa FL, Takahashi WK, Comprehensive optimization of a heat pipe radiator assembly filled with ammonia or acetone, International Journal of Heat and Mass Transfer 49 (2006) 4584–95.

[2247] Rao RV, More KC,. Optimal design of the heat pipe using TLBO (teachingelearning-based optimization) algorithm,. Energy 80 (2015) 535-544.

[2348] Zhang C, Chen Y, Shi M, Peterson GP,. Optimization of heat pipe with axial ‘‘X”-shaped micro grooves based on a niched Pareto genetic algorithm (NPGA),. Applied Thermal Engineering 29 (2009) 3340–3345.

[49] Lips S, Lefèvre F, Bonjour J, Combined effects of the filling ratio and the vapour space thickness on the performance of a flat plate heat pipe, International Journal of Heat and Mass Transfer 53 (2010) 694–702.

[2850] Rohsenow WM, Harnett JP, Ganic EN,. Handbook of Heat Transfer Fundamentals. 2nd ed. New York: McGraw-Hill (;1985).

[3151] Deb K, Agrawal S, Pratap A, Meyarivan T,. A Fast Elitist Non-Dominated Sorting Genetic Algorithm for Multi-Objective Optimization: NSGA-II,. IEEE Transactions on Evolutionary Computation 6 (2002) 182-197.

[52] Lips S, Lefevre F, Bonjour J, Physical mechanisms involved in grooved flat heat pipes: experimental and numerical analyses, International Journal of Thermal Science 50 (2011) 1243–52.

[11] Huang X Y, Liu CY. The pressure and velocity fields in the wick structure of a localized heated flat plate heat pipe. International Journal of Heat and Mass Transfer 39 (1996) 1325-30.

[18] Lips S, Lefèvre F, Bonjour J. Combined effects of the filling ratio and the vapour space thickness on the performance of a flat plate heat pipe. International Journal of Heat and Mass Transfer 53 (2010) 694–702.

[29] Peterson GP. Heat Pipes, Modeling, Testing, and Applications. John Wiley and Sons; 1994.

[30] Reay DA, Kew P. Heat Pipes, 5th ed. Oxford, UK: Butterworth-Heinemann;2006.

[32] Lips S, Lefevre F, Bonjour J. Physical mechanisms involved in grooved flat heat pipes: experimental and numerical analyses. International Journal of Thermal Science 50 (2011) 1243–1252.

Figures

Fig. 1 *Schematic view of the HP.*Schematic view of application of HPs in heat exchanger applications

Fig. 2 *Schematic view of the proposed HP as well as sequence of modelling procedure.*Schematic view of the HP

Fig. 2 *3* Experimental setup scheme and thermocouples locations.

Fig. 4 Flowchart of NSGA-II algorithm.

Fig. 5 Axial distribution of the wall temperatures of *the* HP: the analytical and *the* experimental result*s.*

Fig. 6 Axial distribution of the *obtained* liquid pressure drop*s* of *the* HP obtained from the analytical result*s.*

Fig. 7 Variation of vapor temperature*s* versus pressure drop*s* to evaluate capillary limit (pressure drop*s* obtained *from*by $\Delta P_c=2\sigma_l/r_c$ and analytical model).

Fig. 8 Steady state temperature profiles at the outer wall of the HP (Q=200 W and $T_{cooling}$=25 ˚C): (a) horizontal position, (b) 45° orientation and (c) vertical position.

Fig. 9 *Thermal resistances at different evaporation section lengths and orientations (Q=200 W and cooling temperature of 25 °C).*

Fig. 10 *Thermal performance at different evaporator length sections and orientations.*

Fig. 9 *11* The total thermal resistance of the HP *(*: $T_{cooling}$=25 *°C*, 55 *°C* and 85 ˚C and L_e=225 mm*).*

Fig. 12 *Evaporator wall temperature dependence on heat transfer rate and cooling temperature of the HP at horizontal position.*

Fig. 10 *13* Initial and final population distribution.

Fig. 14 *Relation between heat flux, optimal wire diameter and porosity.*

Fig. 15 *Relations between heat flux, optimal wick permeability and effective thermal conductivity.*

Fig. 16 *Relations between heat flux, optimal wick thickness and related pressure drop.*

Fig. ~~11~~ ***17*** Relation between heat flux, optimal L_e/L_c ration and function of optimal wick permeability (K) and wick thickness (t_{wick}).

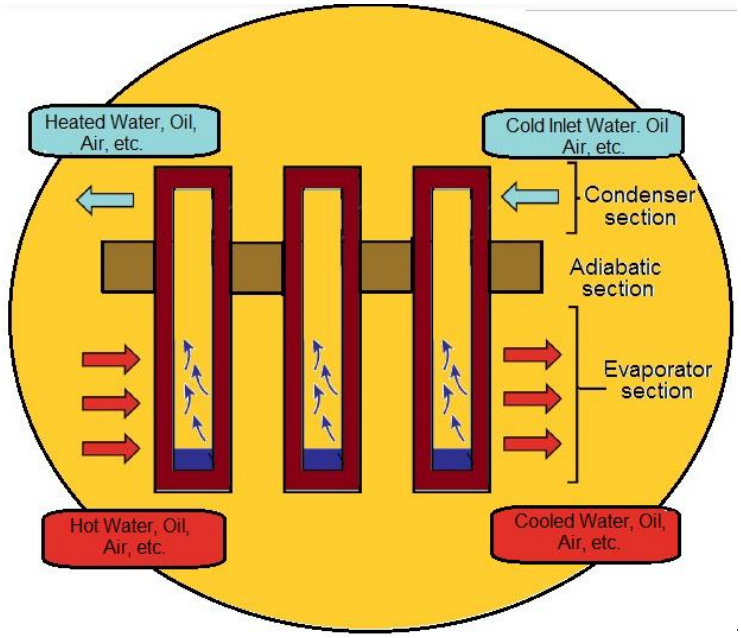

~~**Fig. 1** Schematic view of application of HPs/TPCTs in heat exchanger applications~~

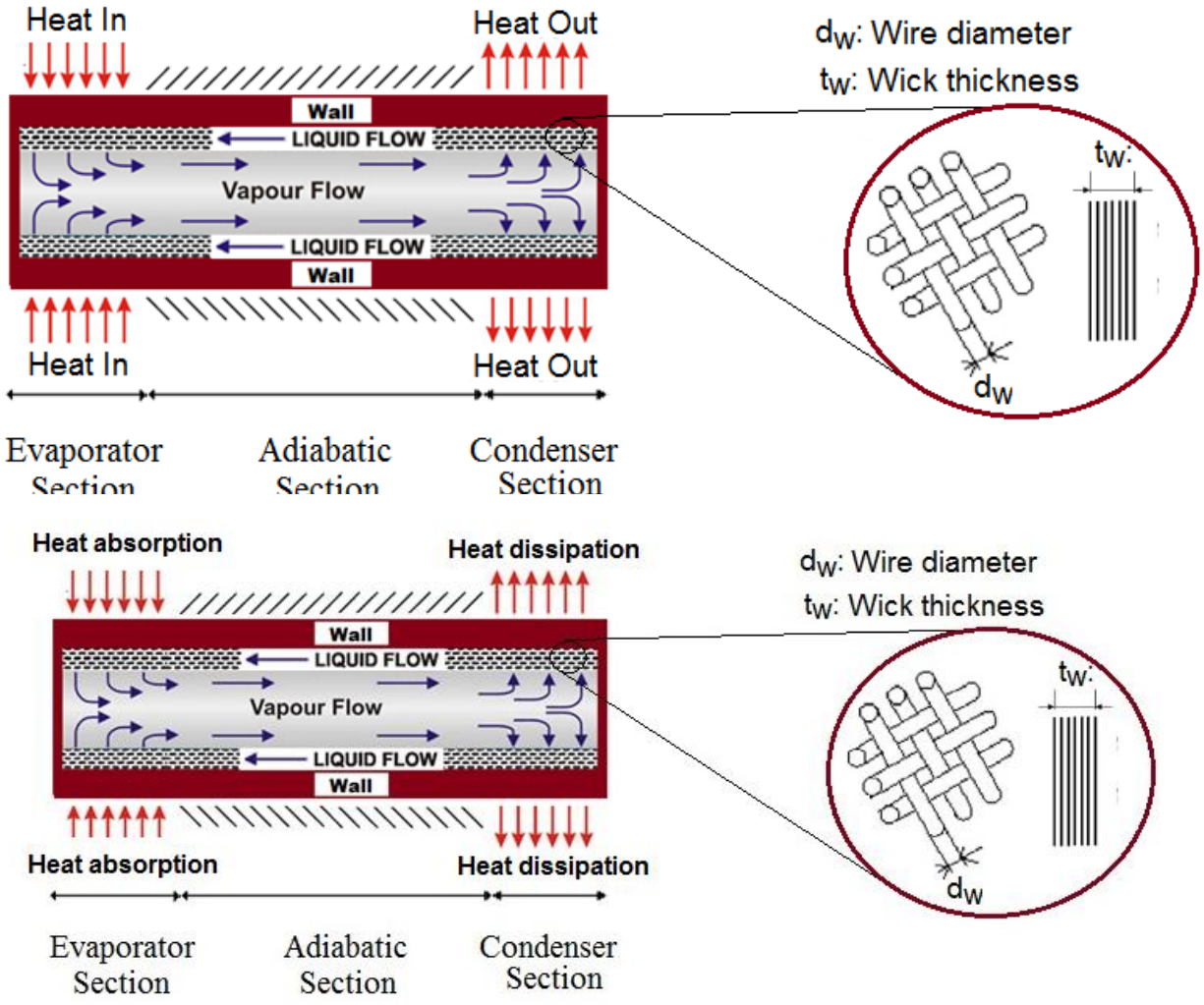

Fig. ~~2~~ *1* ~~Schematic view of the HP.~~

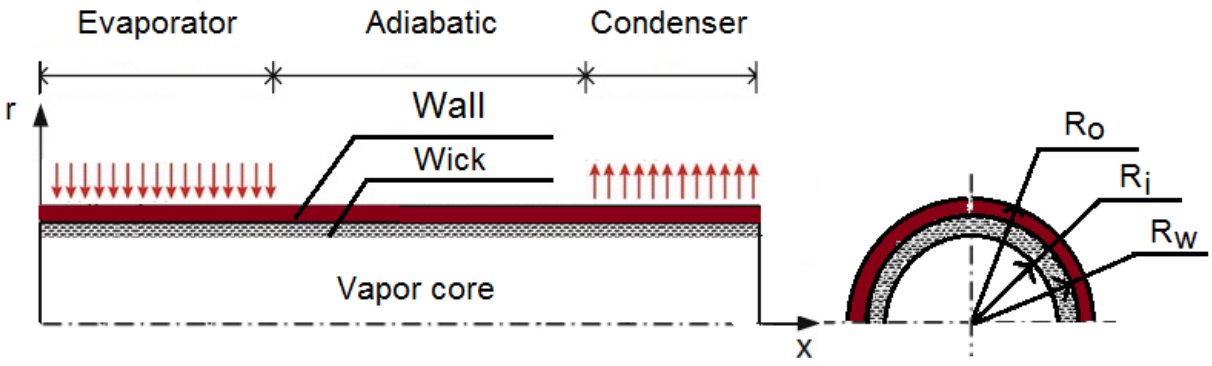

	1. *Set the initial conditions* *(input heat flux, cooling, vapor temperature and etc.)*
Heat Conduction	***2.*** *Obtaining temperature → Eq. A.5*

Liquid flow in wick	***3.*** *Obtaining the axial gradient of liquid pressure along the wick → Eq. A.10* ***4.*** *Obtaining the average liquid velocity along the wick → Eq. A.7*
Liquid-vapor interface	***5.*** *Obtaining interfacial velocity → Eq. 23*
Vapor flow in the core	***6.*** *Obtaining mean vapor velocity → Eq. A.12* ***7.*** *Obtaining the axial vapor pressure →Eq. A.13*

Fig.2

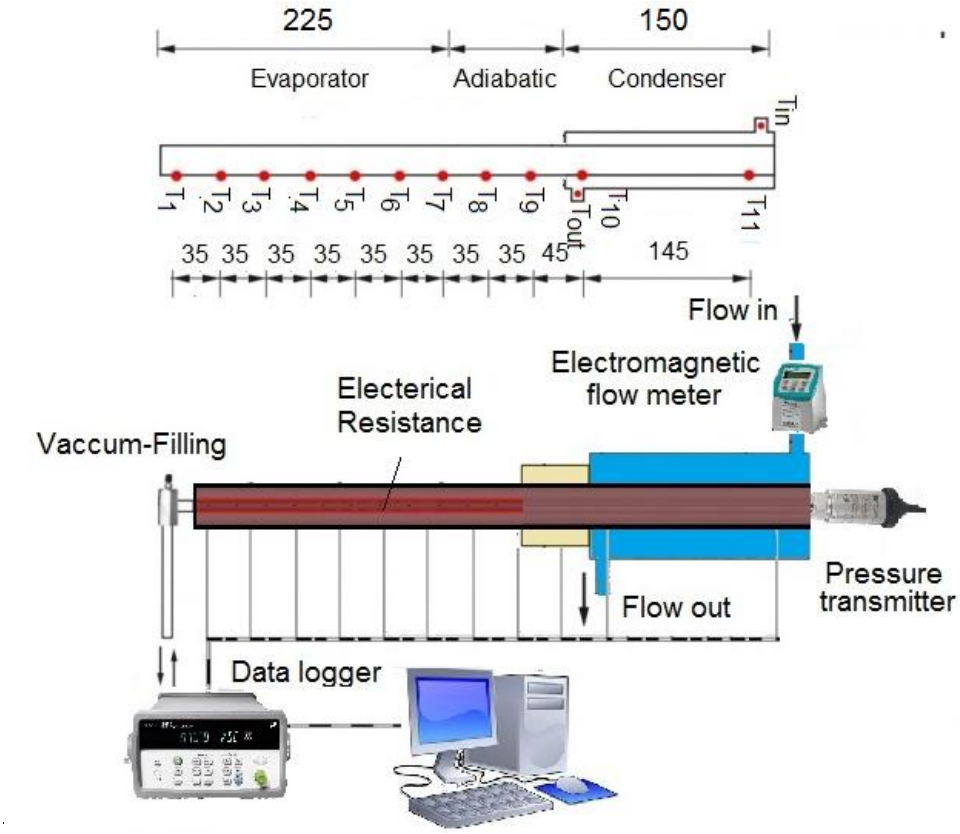

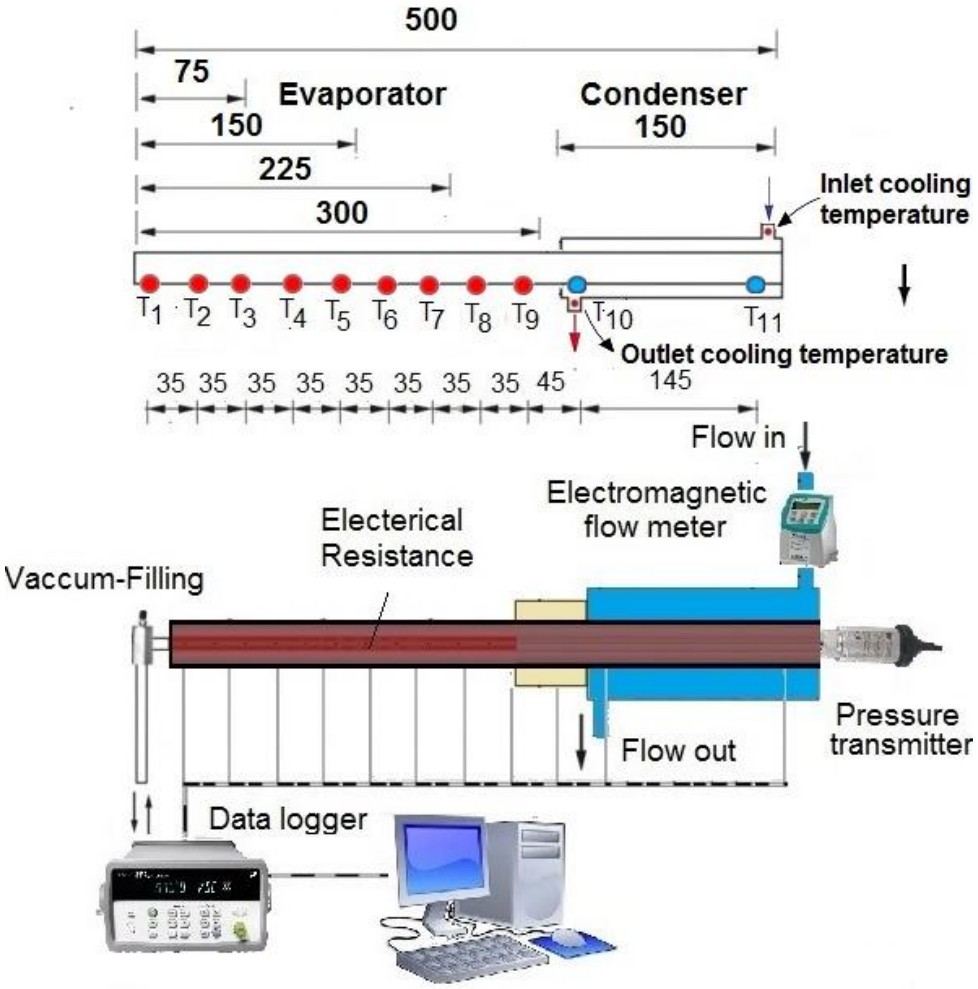

Fig. 3 ~~Experimental setup scheme and thermocouples locations.~~

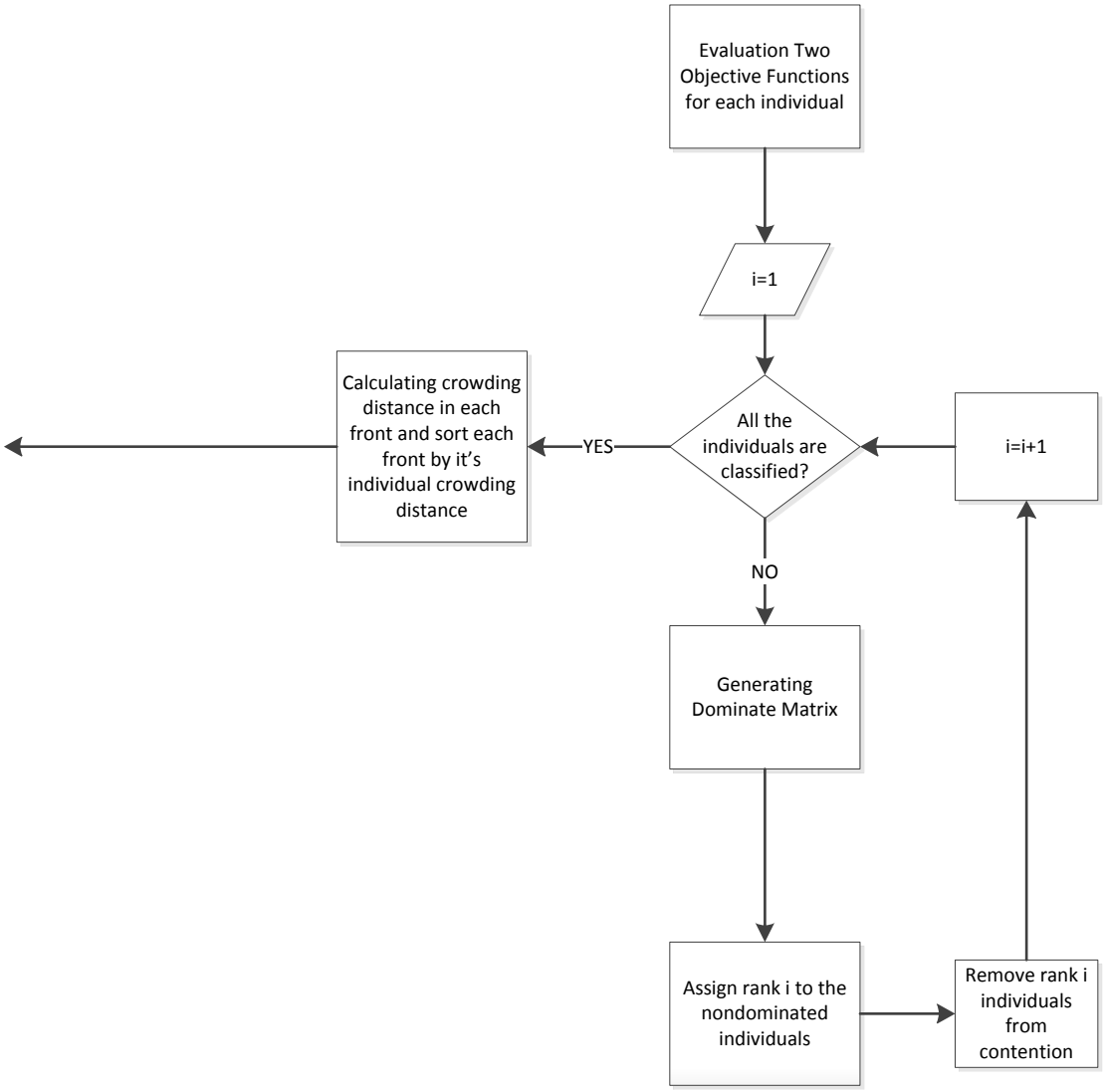

Fig. 4 ~~Flowchart of NSGA-II algorithm~~

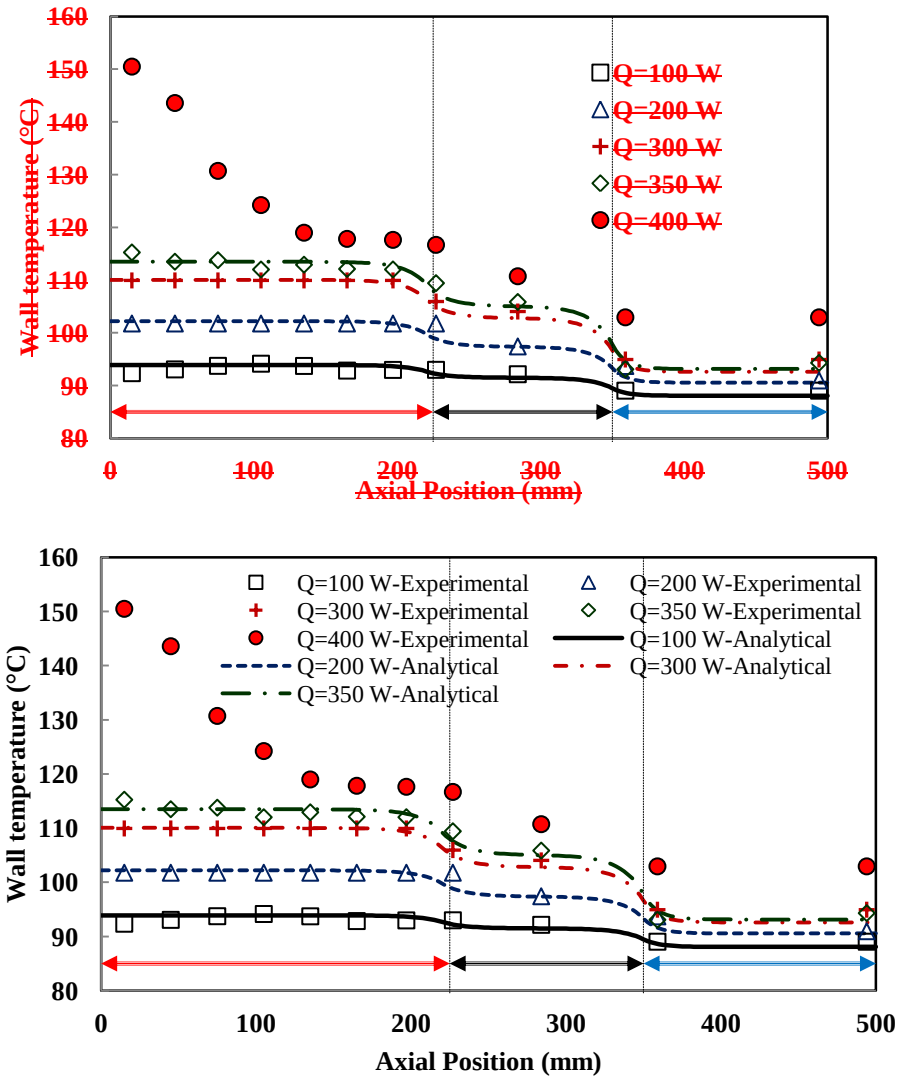

Fig. 5 Axial distribution of the wall temperatures of HP: the analytical and experimental result.

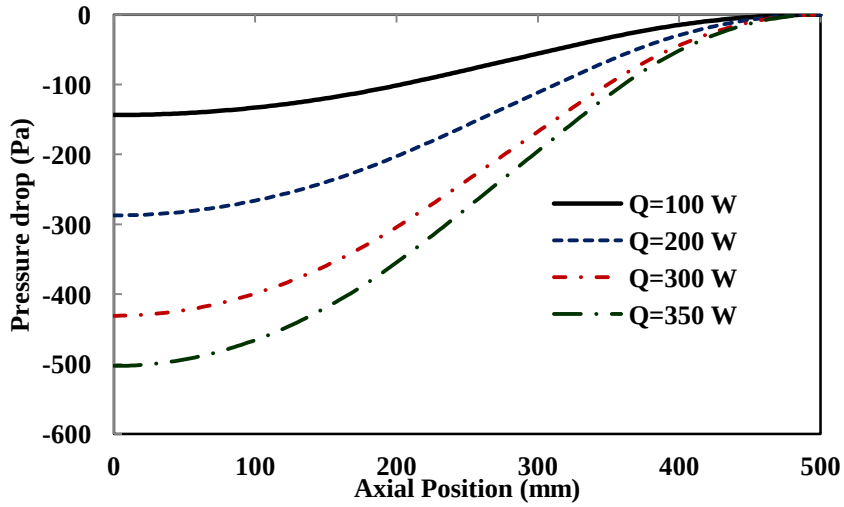

Fig. 6 Axial distribution of the liquid pressure drop of HP obtained from the analytical result.

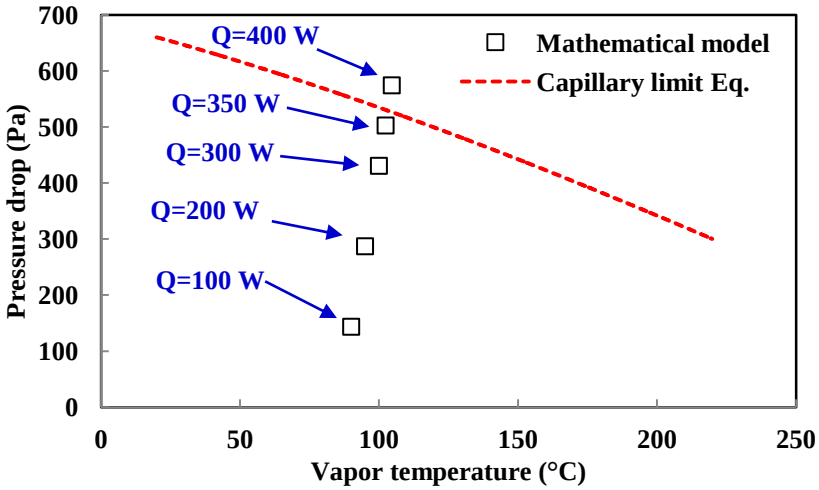

Fig. 7 ~~Variation of vapor temperature versus pressure drop to evaluate capillary limit (pressure drop obtained by $\Delta P_c = 2\sigma_l / r_c$ and analytical model).~~

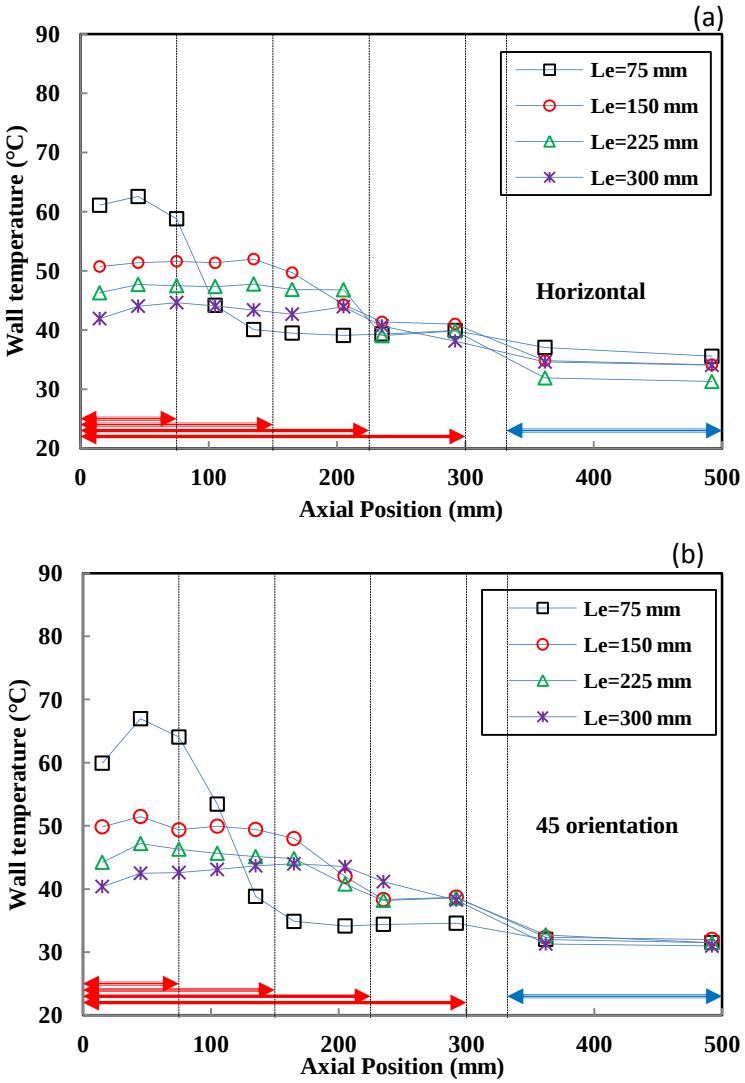

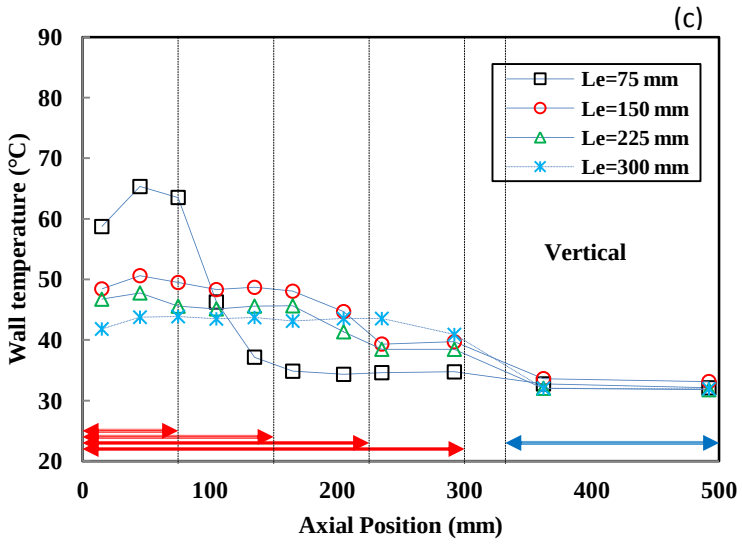

Fig. 8. ~~Steady state temperature profiles at the outer wall of the HP (Q=200 W and $T_{cooling}$=25 ˚C): (a) horizontal position, (b) 45° orientation and (c) vertical position (H=75 mm).~~

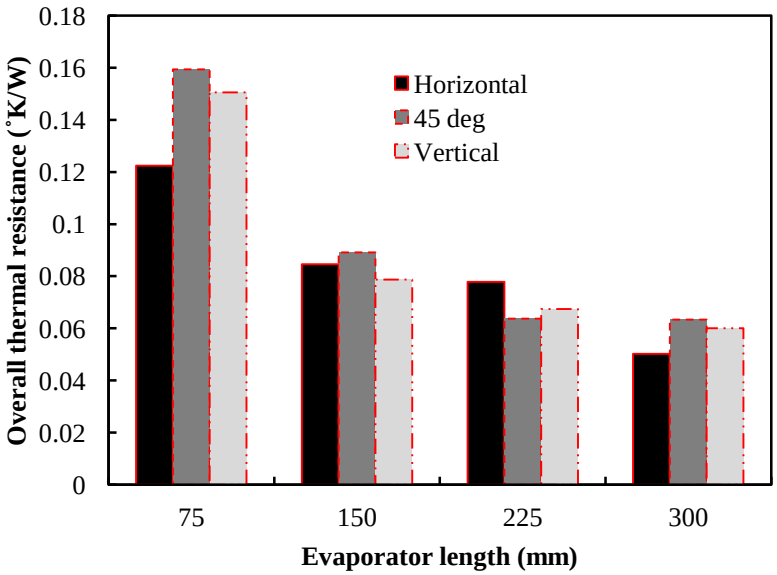

Fig. 9

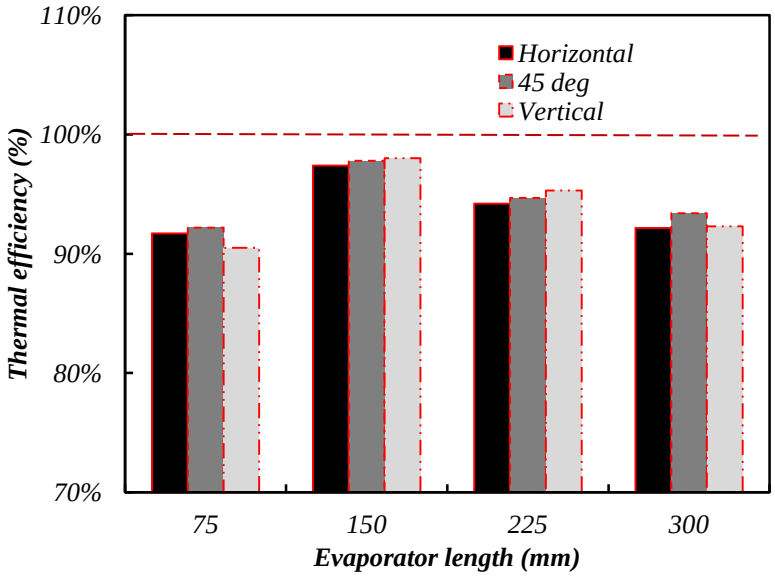

Fig. 10

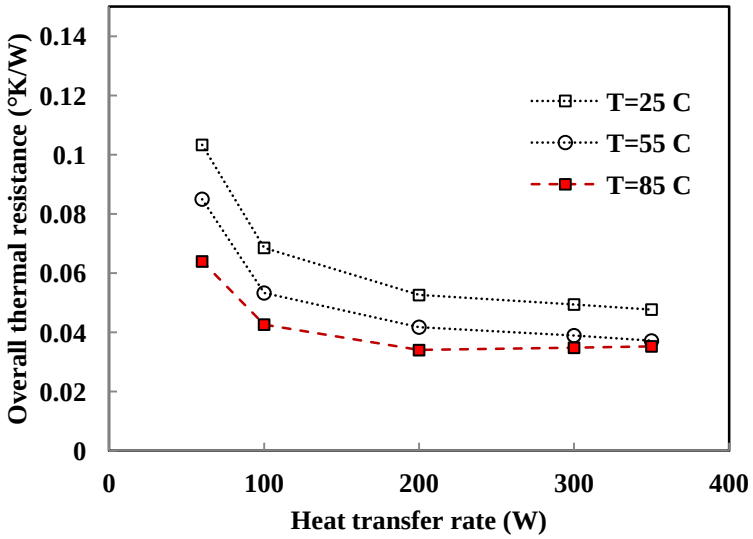

Fig. ~~9~~ *11* ~~The total thermal resistance of the HP: $T_{cooling}$=25, 55 and 85 °C and L_e=225 mm.~~

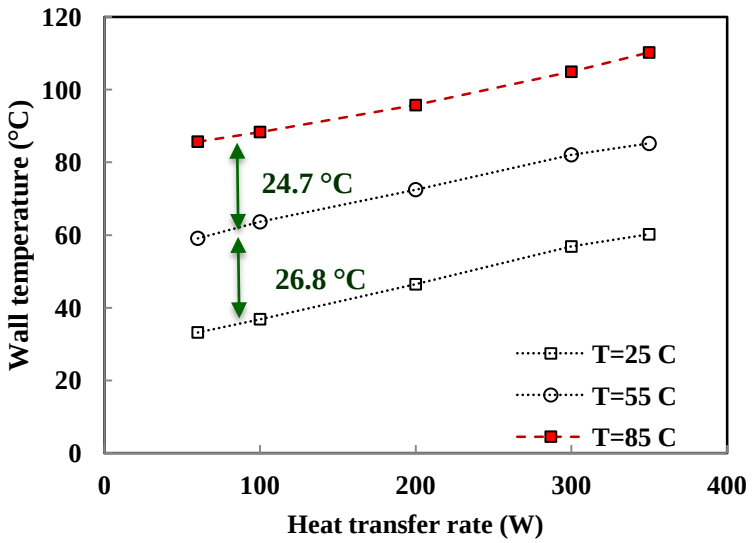

Fig. 12

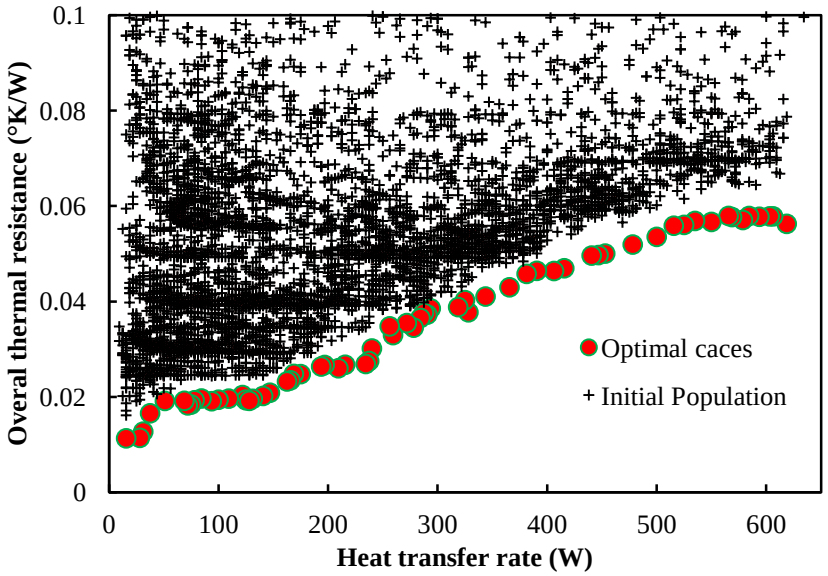

Fig. 13~~0 Initial and final population distribution.~~

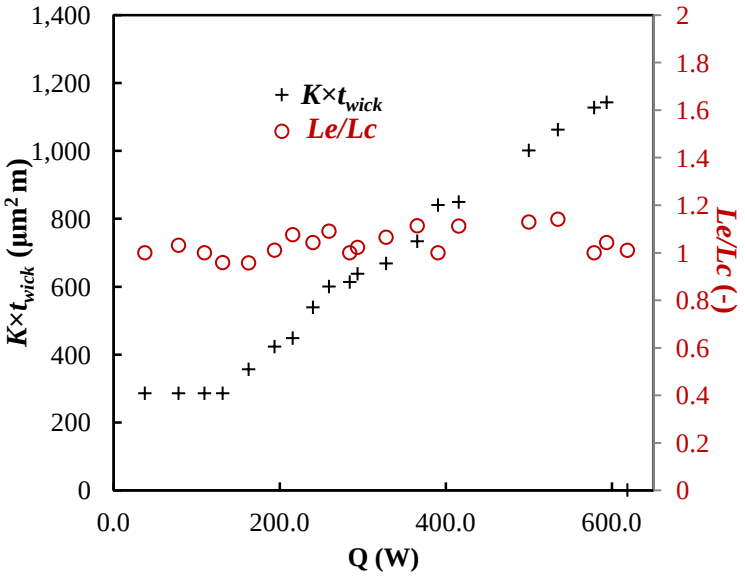

Fig. ~~11~~ *17* ~~Relation between heat flux, optimal L_e/L_e ration and function of optimal wick permeability (K) and wick thickness (t_{wick}).~~

Tables

Table 1 Expressions for screen mesh HP wick design

Table 2 Governing equations and related boundary conditions.

Table 3 Fix parameters.

Table 4 Levels of the variable parameters.

Table 5 Parameters used for optimization calculation.

Table 6 Optimal solution sets *to optimize the total thermal resistance depending heat transfer rates.*

Table 1

Effective thermal conductivity	Effective capillary radius	Permeability	Porosity
$k_{eff} = \frac{k_l[(k_l + k_w) - (1-\varepsilon)(k_l - k_w)]}{(k_l + k_w) + (1-\varepsilon)(k_l - k_w)}$	r_c=1/2N 1968<N<13800	$K = \frac{d_w^2 \varepsilon^3}{122(1-\varepsilon)^2}$	$\varepsilon = 1 - \frac{S\pi N d_w}{4}$
(Eq. 1)	(Eq. 2)	(Eq. 3)	(Eq. 4)

Table 2

Correlations		Boundary conditions	
Heat conduction in the wall $\frac{\partial^2\theta}{\partial r^2}+\frac{1}{r}\frac{\partial\theta}{\partial r}+\frac{\partial^2\theta}{\partial x^2}=0$	(~~6~~5)	**End caps:** $\frac{\partial\theta}{\partial x}=0, \quad (x=0, L)$ **Outer wall:** $\begin{cases} k_s\frac{\partial\theta}{\partial r}\Big\|_{r=r_o}=q_e, & \text{(Evap.)} \\ \frac{\partial\theta}{\partial r}\Big\|_{r=r_o}=0, & \text{(Adiabatic)} \\ -k_s\frac{\partial\theta}{\partial r}\Big\|_{r=r_o}=h_\infty\theta(r_o,x), & \text{(Cond.)} \end{cases}$ **Wall-wick interface:** $\frac{\partial\theta}{\partial r}=\frac{k_{eff}}{r_i k_s \ln(r_i/r_v)}\theta, \quad (r=r_i)$	(~~7~~6) (~~8~~7) (~~9~~8) (~~10~~9) (~~11~~10)
Liquid flow in the wick $r\frac{\partial u_l}{\partial x}+\frac{\partial}{\partial r}(rv_l)=0$ $\frac{dP_l}{dx}=-\frac{\mu_l u_l}{K}$	(~~12~~11) (~~13~~12)	**Wick-vapor interface:** $v_l=\frac{q_e\Big\|_{r=r_i} r_i}{\rho_l h_{fg} r_v}$ **Wick-wall interface:** $v_l=0$	(~~14~~13) (~~15~~14)
Vapor flow in the core $r\frac{\partial u_v}{\partial x}+\frac{\partial}{\partial r}(rv_v)=0$ $\rho_v(u_v\frac{\partial u_v}{\partial x}+v_v\frac{\partial u_v}{\partial r})=-\frac{\partial P_v}{\partial z}+\mu_v(\frac{\partial u_v}{\partial r^2}+\frac{1}{r}\frac{\partial u_r}{\partial r})$	(~~16~~15) (~~17~~16)	**End caps:** $u_v=0, \quad x=0, L$ **Centerline:** $\frac{\partial u_v}{\partial r}=0, \quad r=0$ **vapor-wick interface:** $u_v=0, \quad r=r_v$	(~~18~~17) (~~19~~18) (~~20~~19)

Table 3

Parameters	
Wall material	Copper
Wick material	Stainless steal
Wick type	Screen mesh
Mesh number	50 mesh/inch
Working fluid material	Water
Outer diameter, (mm)	25.4

Wall thickness, (mm)	1
Total length, (mm)	1000
Working temperature, (˚C)	85

Table 4

Parameters	Min	Max
Evaporator length, (mm)	0	1000
Condenser length, (mm)	0	1000
Wick porosity	0.5	0.9
Wick thickness, (mm)	0.2	2

Table 5

Mutation Rate	Population Size	Maximum Generation	Objective number	Variable number
0.05	160	120	2	4

Table 6

No.	Q	R_{tot}	L_e	L_c	t_{wick}	Porosity	T_v	Q_b	ΔP_l	ΔP_c	T_e	T_c
1	618.7	0.056	490	485	1.09	0.698	122.1	618.9	428.6	429.7	139.5	104.7
2	593.8	0.058	485	465	1.09	0.696	122.3	625.6	426.3	429.4	139.2	104.9
3	578.7	0.057	475	475	1.08	0.695	120.4	670.0	426.3	432.4	137.0	104.0
4	535.0	0.057	485	425	1.04	0.69	120.8	724.0	431.8	432.8	135.1	104.6
5	500.0	0.054	480	425	0.98	0.69	117.4	855.4	437.2	439.0	130.0	103.2
6	415.6	0.047	495	445	0.95	0.66	109.8	1150.5	448.3	449.0	119.1	99.6
7	390.6	0.046	440	440	0.94	0.66	108.1	1294.4	445.0	451.6	117.8	98.7
8	365.6	0.043	490	440	0.90	0.64	106.1	1432.5	452.4	454.8	113.5	97.8
9	328.1	0.038	490	460	0.82	0.64	102.4	1760.9	460.0	460.5	108.4	96.0
10	293.7	0.039	450	440	0.79	0.638	101.0	2034.1	461.1	462.6	106.6	95.3
11	284.3	0.037	455	455	0.76	0.638	100.0	2153.8	462.3	464.1	105.2	94.8
12	259.3	0.033	480	440	0.74	0.639	100.8	2074.8	462.9	466.4	105.8	95.3
13	240.0	0.030	485	465	0.70	0.628	96.8	2678.8	459.7	460.9	100.4	93.1
14	215.6	0.027	495	460	0.62	0.615	95.3	3138.5	471.2	475.1	98.1	92.3
15	193.7	0.026	465	460	0.60	0.61	94.1	3509.4	469.9	472.9	96.7	91.6
16	162.5	0.023	450	470	0.55	0.593	92.2	4280.7	475.8	476.3	94.1	90.4
17	131.2	0.020	465	485	0.51	0.565	90.5	5121.3	478.3	478.9	91.8	89.3
18	109.3	0.020	475	475	0.51	0.565	89.7	5259.4	399.9	479.5	90.8	88.6

19	78.1	0.019	490	475	0.51	0.565	88.3	5424.2	284.9	481.5	89.1	87.6
20	37.5	0.017	485	485	0.51	0.565	86.6	5743.5	138.8	484.1	86.9	86.2